



NASA
CR
1539
v.2
c.1

**NASA CONTRACTOR
REPORT**

NASA CR-154

NASA CR-1540



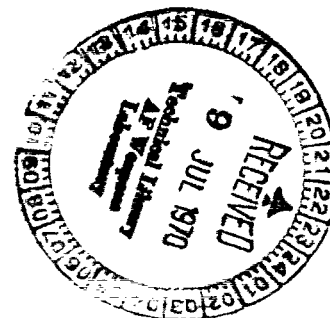
LOAN COPY: RETURN TO
AFWL (WL0L)
KIRTLAND AFB, N MEX

ADVANCEMENTS IN STRUCTURAL DYNAMIC TECHNOLOGY RESULTING FROM SATURN V PROGRAMS

VOLUME II

*by P. J. Grimes, L. D. McTigue, G. F. Riley,
and D. I. Tilden*

Prepared by
THE BOEING COMPANY
Huntsville, Ala.
for Langley Research Center



NATIONAL AERONAUTICS AND SPACE ADMINISTRATION • WASHINGTON, D. C. • JUNE 1970



0060846

1. Report No. NASA CR-1540		2. Government Accession No.		3	
4. Title and Subtitle ADVANCEMENTS IN STRUCTURAL DYNAMIC TECHNOLOGY RESULTING FROM SATURN V PROGRAMS - VOLUME II				5. Report Date June 1970	
				6. Performing Organization Code	
7. Author(s) P. J. Grimes, L. D. McTigue, G. F. Riley, and D. I. Tilden				8. Performing Organization Report No. D5-17015	
9. Performing Organization Name and Address The Boeing Company Huntsville, Alabama				10. Work Unit No. 124-08-13-04-23	
				11. Contract or Grant No. NAS1-8531	
12. Sponsoring Agency Name and Address National Aeronautics and Space Administration Washington, D.C. 20546				13. Type of Report and Period Covered Contractor Report	
				14. Sponsoring Agency Code	
15. Supplementary Notes					
16. Abstract Saturn V structural dynamic experience in replica modeling, math modeling and dynamic testing was assessed. Major problems encountered in each of these areas and their solutions are discussed. The material is presented in two volumes. Volume I (NASA CR-1539) contains a summary of the material presented in Volume II and is oriented toward the program managers of future structural dynamic programs. Volume II contains the methods and procedures used in the Apollo Saturn V structural dynamics programs. The major problems encountered and their solutions are discussed. Volume II is oriented toward the technical leaders of future structural dynamics programs.					
17. Key Words (Suggested by Author(s)) Saturn V structural dynamics 1/10 scale Saturn V replica models Saturn V math models Dynamic testing and data reduction				18. Distribution Statement Unclassified - unlimited	
19. Security Classif. (of this report) Unclassified		20. Security Classif. (of this page) Unclassified		21. No. of Pages 163	22. Price* \$3.00

PREFACE

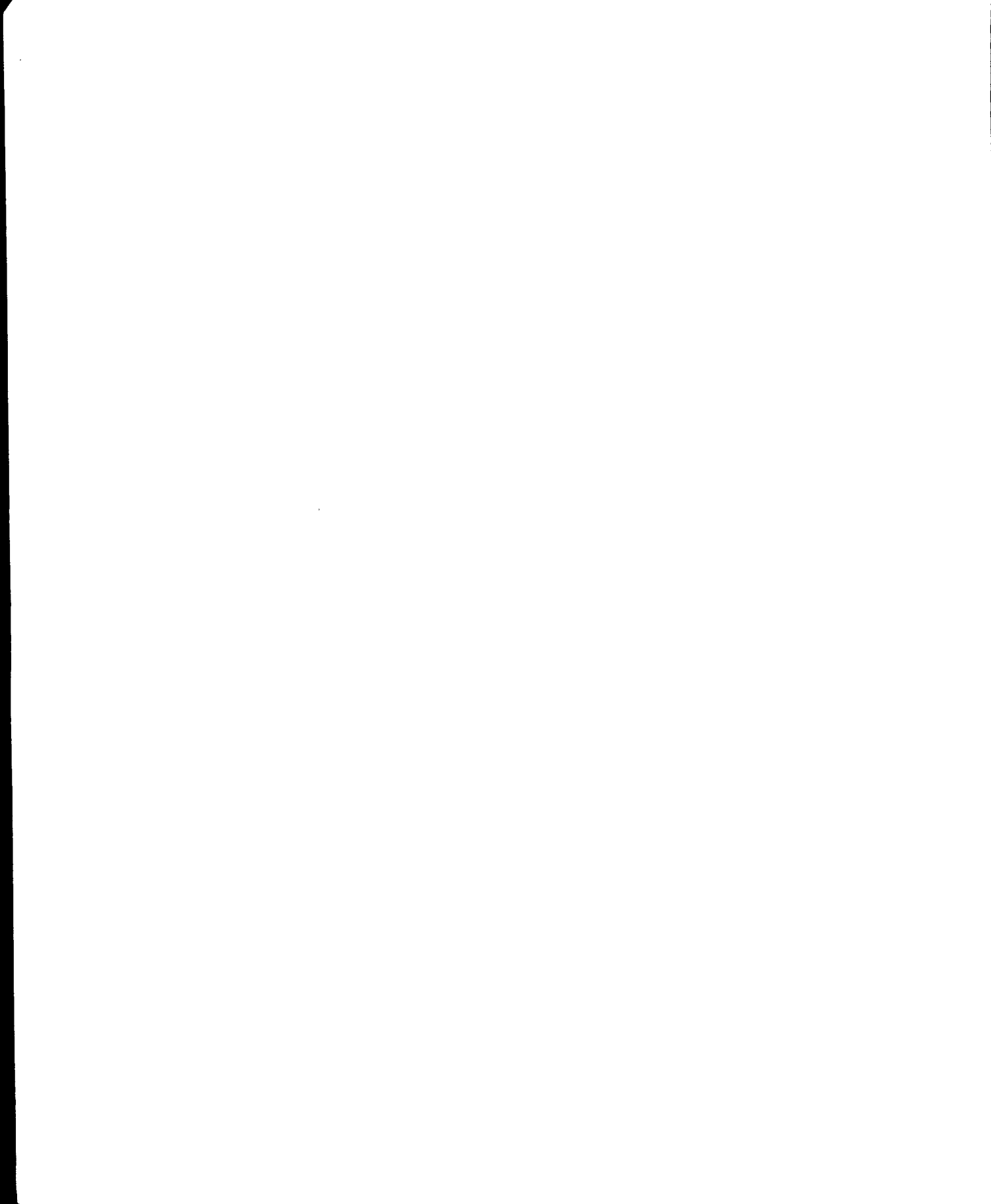
This document was produced under NASA-Langley Research Center Contract NAS1-8531. The contents are intended to carry forward to future programs the structural dynamics experience gained during the Saturn V programs.

The valuable contributions of S. A. Leadbetter, H. W. Leonard, and L. D. Pinson, Structural Vibration Section, Langley Research Center, are gratefully acknowledged.

The major contributors to this document include:

M. L. Biggart
P. J. Grimes
J. E. Henry
N. L. Hudson
W. H. Lawler
L. D. McTigue
G. F. Riley
D. I. Tilden

Questions on the contents of this document should be addressed to L. D. McTigue, The Boeing Company, P. O. Box 1680, Mail Stop AG-36, Huntsville, Alabama 35807.



CONTENTS OF VOLUME I

PARAGRAPH	PAGE
PREFACE	iii
CONTENTS	v
ILLUSTRATIONS AND TABLES	viii
LIST OF SYMBOLS	ix
ABBREVIATIONS	xi
 SECTION 1 - SUMMARY STRUCTURAL DYNAMIC TECHNOLOGY DEVELOPMENT	 1
1.0 INTRODUCTION	1
1.1 DEFINITION OF SATURN V	1
1.2 PROGRAM DESCRIPTION AND HISTORY	3
1.3 SUMMARY OF 1/10 SCALE MODEL TECHNOLOGY	5
1.3.1 Introduction	5
1.3.2 Description and History	5
1.3.3 Scale Model Cost and Accuracy	8
1.3.4 1/10 Scale Model Contributions and Areas of Improvement	8
1.4 SUMMARY OF MATHEMATICAL MODEL TECHNOLOGY	12
1.4.1 Introduction	12
1.4.2 Technical Approach	15
1.4.3 Math Model Analysis Guidelines	17
1.4.4 Math Model Cost and Accuracy	28
1.5 SUMMARY OF DYNAMIC TEST TECHNOLOGY	30
1.5.1 Introduction	30
1.5.2 Dynamic Test Program Guidelines	36
1.6 CONCLUSIONS	43
 REFERENCES	 44

CONTENTS OF VOLUME II

PREFACE	iii
CONTENTS	v
ILLUSTRATIONS AND TABLES	viii
LIST OF SYMBOLS	xi
ABBREVIATIONS	xiii
 SECTION 2 - INTRODUCTION	 1
2.0 GENERAL	1
2.1 DESCRIPTION OF SATURN V VEHICLE	2
2.2 HISTORY OF SATURN V STRUCTURAL DYNAMIC PROGRAMS	5
2.2.1 1/10 Scale Model Program	6

CONTENTS OF VOLUME II (Continued)

PARAGRAPH	PAGE
2.2.2 Full Scale Math Modeling	7
2.2.3 Full Scale Dynamic Test and Correlation	10
2.2.4 Saturn V Flight	11
REFERENCES	12
SECTION 3 - 1/10 SCALE MODEL TECHNOLOGY	13
3.0 GENERAL	13
3.1 THE SCALE MODEL TEST PROGRAM	14
3.1.1 Scale Model Description	14
3.1.2 Scale Model Test	18
3.2 CONTRIBUTIONS TO FULL SCALE TEST	18
3.3 CONTRIBUTIONS TO SATURN V MATH MODELING	20
3.3.1 Mathematical Analysis of the 1/10 Scale Model	21
3.3.2 Scale Model Test and Analysis Correlation	21
3.4 CONTRIBUTIONS TO SATURN V ANOMALY RESOLUTION	24
3.5 COST AND ACCURACY	24
3.5.1 Cost	24
3.5.2 Accuracy	24
3.5.3 Scale Model Joint Flexibility	31
REFERENCES	33
SECTION 4 - MATH MODEL TECHNOLOGY	35
4.0 GENERAL	35
4.1 TECHNICAL APPROACH	35
4.1.1 Stiffness Analysis	37
4.1.2 Inertia Analysis	40
4.1.3 Eigenvalue Solution	40
4.2 MODELING PHILOSOPHY	40
4.3 STIFFNESS MATRIX DEVELOPMENT	43
4.3.1 General Guidelines	43
4.3.2 Idealization Examples	57
4.3.3 Shell Idealizations	59
4.3.4 Major Component Idealization	67
4.4 INERTIA MATRIX DEVELOPMENT	71
4.4.1 General Guidelines	71
4.4.2 Inertia Examples	72
4.4.3 Shell Inertia Matrices	72
4.4.4 Propellant Tank Inertia Matrices	75
4.4.5 Rigid Subsection Inertia Matrix	81
4.4.6 Major Component Inertia Matrices	85

CONTENTS OF VOLUME II (Continued)

PARAGRAPH	PAGE	
4.5	VIBRATION ANALYSIS AND MODAL SYNTHESIS	87
4.5.1	General	87
4.5.2	Eigenfunction Solutions and Modal Orthogonality	87
4.5.3	Modal Synthesis	90
4.5.4	Evaluation	94
4.5.5	Establish Tolerance	95
4.5.6	Damping Considerations	95
4.6	SATURN V MODEL EVOLUTION	96
4.7	COST AND ACCURACY	97
4.7.1	Cost	97
4.7.2	Accuracy	101
	REFERENCES	107
	SECTION 5 - DYNAMIC TEST TECHNOLOGY	109
5.0	GENERAL	109
5.1	TEST REQUIREMENTS	109
5.1.1	Test Objectives	111
5.1.2	Vehicle Configuration	113
5.1.3	Test Facilities Requirements	116
5.1.4	Data Acquisition and Reduction System	124
5.1.5	Test Conduct	131
5.2	DIGITAL DATA REDUCTION TECHNIQUES	133
5.2.1	Fourier Analysis	136
5.2.2	Point Transfer Functions	137
5.2.3	Transfer Function Equations	137
5.2.4	Computation of Modal Parameters	141
5.3	TEST DATA EVALUATION PROCEDURES	146
5.3.1	On-Site Data Evaluation	146
5.3.2	Test Data Validation	147
5.3.3	Test Data Evaluation	148
5.3.4	Test Data Reporting	148
	REFERENCES	149
	SECTION 6 - CONCLUSIONS	151

ILLUSTRATIONS

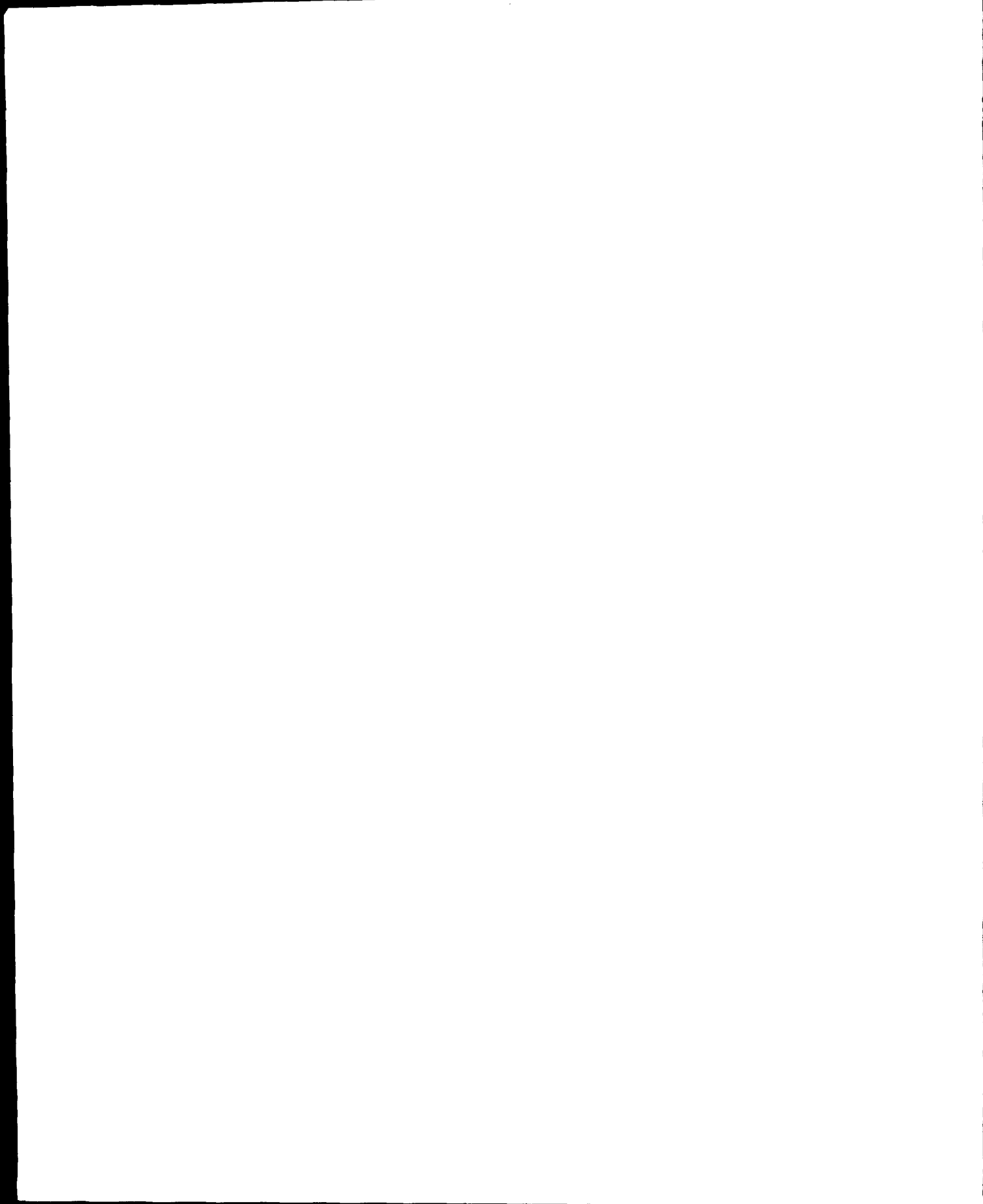
FIGURE		PAGE
2-1	Apollo Saturn V Configuration	3
2-2	Math Model Evolution	8
3-1	Schematic of 1/10 Scale Apollo Saturn V Model	15
3-2	1/10 Scale Model in Test Stand	16
3-3	Illustration of Detail Achieved in Modeling	17
3-4	Comparison of 1/10 Scale Model and Full Scale- Vehicle Bending Stiffness	19
3-5	Comparison of 1/10 Scale Longitudinal Test and Analysis Results - 100 Percent Propellant	22
3-6	Comparison of 1/10 Scale Pitch Test and Analysis Results - 100 Percent Propellant	23
3-7	Comparison of 1/10 Scale and Full Scale Pitch Test Results - Modes 1 and 2 - 100 Percent Propellant	27
3-8	Comparison of 1/10 Scale and Full Scale Pitch Test Results - Modes 3 and 4 - 100 Percent Propellant	28
3-9	Comparison of 1/10 Scale and Full Scale Longitudinal Test Results - Modes 1 and 2 - 100 Percent Propellant	29
3-10	Comparison of 1/10 Scale and Full Scale Longitudinal Test Results - Modes 3 and 4 - 100 Percent Propellant	30
3-11	Load Path Through 1/10 Scale Model and Full Scale Joints	32
4-1	Typical Saturn V Nodal Breakdown	36
4-2	Math Model Structural Elements	44
4-3	Transition Technique - Large to Small Plate Elements	46
4-4	Redundant Degree of Freedom Example	46
4-5	Structural Symmetry Example	50
4-6	Quarter Shell Analysis Coordinate System	53
4-7	Beam Elements for Ring Modeling	53
4-8	Merge-Reduce Error Accumulation	56
4-9	Classes of Modules for Saturn V Models	58
4-10	S-IVB Forward Skirt Nodal Breakdown	60
4-11	Short Stack Nodal Breakdown	60
4-12	Instrument Unit Model	62
4-13	Honeycomb Geometry	64
4-14	Bulkhead/Cable Analogy	64
4-15	S-IC Thrust Structure	66
4-16	S-II Thrust Structure	66
4-17	S-IVB Thrust Structure	66
4-18	LM Asymmetry Example	68
4-19	Influence of Major Components on Vehicle Dynamics	68
4-20	Service Module Tanks	70
4-21	Ring Shape of the 181th Order (Baseline Model)	74
4-22	Ring Shape of the 78th Order (Guyan Consistent Mass Model)	74
4-23	Ring Shape of the 78th Order (Relumped Mass Model)	74
4-24	Propellant Tank Liquid Idealization	76
4-25	Liquid Motion Due to Tank Expansion	76
4-26	Geometry of Deformed Bulkhead	82

ILLUSTRATIONS (Continued)

FIGURE		PAGE
4-27	Beam-Shell Interface	82
4-28	Warped Section of Cylindrical Model	86
4-29	S-IVB Engine Model	86
4-30	Control Gyro Location	91
4-31	Illustration of Modal Stacking Technique	93
4-32	Math Model Evolution	98
4-33	Comparison of Full Scale Pitch Test and Analysis Results - Modes 1 and 2 - 100 Percent Propellant	102
4-34	Comparison of Full Scale Pitch Test and Analysis Results - Modes 3 and 4 - 100 Percent Propellant	103
4-35	Comparison of Full Scale Longitudinal Test and Analysis Results - Modes 1 and 2 - 100 Percent Propellant	104
4-36	Comparison of Full Scale Longitudinal Test and Analysis Results - Modes 3 and 4 - 100 Percent Propellant	105
4-37	Longitudinal Frequency Response of Outboard Gimbal- 100 Percent Propellant	106
5-1	Test-Analysis Philosophy	110
5-2	Hydrodynamic Support	119
5-3	Stabilization System	121
5-4	Full Scale Data Acquisition and Reduction System Signal Train	130
5-5	Full Scale Accelerometer Data Error	132
5-6	Full Scale Test Data Reduction Flow Chart	135
5-7	Typical Curve Fit of Full Scale Test Data	140
5-8	Typical Curve Fit of Double Peak Response	142
5-9	Typical Effect of Force Level on Frequency Response	145

TABLES

TABLE		PAGE
3-I	Correlation of 1/10 Scale Model and Full Scale Response Data	25
4-I	Assessment of Saturn V Models	99
4-II	Math Model Development Planning Estimate	100
5-I	Saturn V Sensitive Parameters	112



LIST OF SYMBOLS

A	Area (Cross Sectional)
C	Damping Coefficient
E	Modulus of Elasticity
e	Error
F	Force
G	Gain or Transfer Function
GT	Gain Tolerance
g	Gravitational Constant
h	Height
I	Moment of Inertia
[I]	Identity Matrix
j	$\sqrt{-1}$
K	Stiffness Coefficient
L	Length
M, m	Mass Coefficient
\bar{m}	Generalized Mass
q	Generalized Coordinate
R _x	Rotation about X Axis
R _y	Rotation about Y Axis
R _z	Rotation about Z Axis
r	Radius
S	Prestress Force for Bulkhead
[T]	Coordinate Transformation Matrix
t	Time

V	Volume
W	Work
X, x	Longitudinal Axis, Cartesian Coordinates
{X}	Mass Distribution Matrix
Y, y	Pitch Axis, Cartesian Coordinates
Z, z	Yaw Axis, Cartesian Coordinates
Δ	Deflection, Displacement
Δr	Displacement in Radial Direction
Δx	Displacement in X Direction
Δy	Displacement in Y Direction
Δz	Displacement in Z Direction
δ	Virtual (Prefix used with various symbols)
ζ	Damping Factor
θ	Angular Measurement, Spherical Coordinates
ρ	Density
$\bar{\rho}$	Dimensionless Radial Coordinate
τ	Thickness
$[\phi]$	Matrix of Mode Shapes
ϕ	Mode Shape Function
$[\bar{\phi}]$	Matrix of Rigid Body Displacement Vectors
ω	Frequency

ABBREVIATIONS

AS-50N	Nth Apollo Saturn V space vehicle
CM	Command Module
dB	Decibel
DOF	Degree of Freedom
Hz	Hertz, cycles per second
IU	Instrument Unit
LES	Launch Escape System
LH ₂	Liquid hydrogen
LM ²	Lunar Module
LOX	Liquid oxygen
LRC	Langley Research Center
MSFC	Marshall Space Flight Center
NASA	National Aeronautics and Space Administration
Pogo	A divergent longitudinal oscillation produced by regenerative coupling between the vehicle structure and propulsion system
RP-1	A kerosene-like fuel used in the S-IC stage
S-IC	First Boost Stage of Saturn V Vehicle
S-II	Second Boost Stage of Saturn V Vehicle
S-IVB	Third Boost Stage of Saturn V Vehicle
SLA	Saturn LM Adapter
SM	Service Module

ADVANCEMENTS IN STRUCTURAL DYNAMIC TECHNOLOGY
RESULTING FROM SATURN V PROGRAMS

By P. J. Grimes, L. D. McTigue, G. F. Riley,
and D. I. Tilden
The Boeing Company

SECTION 2 INTRODUCTION

2.0 GENERAL

The Apollo Saturn V Program was created by NASA to accomplish the objective of a manned lunar landing by the end of the decade. On July 20, 1969, the program objective was realized. This report covers the structural dynamic technology that was developed to support the Apollo Saturn V Program.

Apollo Saturn V structural dynamics programs considered in this document include the 1/10 scale model analysis and test program, the full scale analysis and test program, and the flight data evaluation program. The results of these programs were reviewed to the extent necessary to establish and document the following:

1. Technical contributions of the 1/10 scale model to Apollo Saturn V structural dynamic characteristics prediction.
2. Illustrations of what scale modeling can contribute to future programs.
3. Procedures for performing stiffness, inertia and vibration analyses of large booster vehicles.
4. Improvements in test techniques and data reduction procedures evolved during the experimental studies.
5. Problems in mathematical modeling and dynamic testing that require further study.

Practical guidelines for accomplishing structural dynamic analysis, dynamic test, and data reduction that were established within the successful Saturn V Program are defined in this document. These guidelines and recommended practices are presented so that major pitfalls and problems encountered in this program can be avoided in future programs.

The following procedure was used to generate the Saturn V flight predictions:

1. Develop mathematical models and methods of solution.

2.0 (Continued)

2. Perform replica model analysis and test to establish guidelines for the full scale program.
3. Perform pretest analysis using baseline math models and publish dynamic characteristics of the test article prior to the test.
4. Perform full scale tests and compare results with analytical predictions.
5. Revise the mathematical models as required to make them correlate with test data.
6. Modify these test-verified math models to represent the exact flight configuration of each flight vehicle.

2.1 DESCRIPTION OF APOLLO SATURN V VEHICLE

The Apollo Saturn V vehicle consists of the three stage Saturn V launch vehicle, an instrument unit and the Apollo spacecraft. Schematics of the three boost configurations and the coordinate system used throughout this report are shown in Figure 2-1. There are three stages of launch vehicle powered flight. The first stage boost configuration consists of the total Apollo Saturn V vehicle. The second stage boost configuration consists of the S-II stage, S-IVB stage, IU, and the Apollo spacecraft. The third stage boost configuration consists of the S-IVB stage, IU, and the Apollo spacecraft.

S-IC Stage - The first stage (S-IC) of the Saturn V launch vehicle has a nominal diameter of 396 inches (10.06 m). It has a liquid oxygen (LOX)/kerosene (RP-1) propulsion system and is powered by five F-1 engines with a total thrust of 7.5 million pounds (33,360,000 N). The fuel and oxidizer are in separate pressurized tanks, the LOX tank being forward. The tanks are joined by an unpressurized intertank structure. Internal construction, material, and fabrication of the two tanks are similar. The cylindrical portion of each tank is made up of four quarter-sections joined by longitudinal welds. Integrally milled tee-section stringers, located on the interior surface, provide additional structural rigidity. All bulkheads are elliptical in shape and are constructed from gores welded together. The bulkheads are joined to the cylindrical tank and skirt sections through a Y-section ring welded to the equator of each bulkhead.

Ring-type slosh baffles are fusion welded to the internal stringers in each tank, and cruciform baffles are located in each lower bulkhead. Five insulated tunnels lead through the fuel tank to permit passage of suction ducts which supply LOX to the engines.

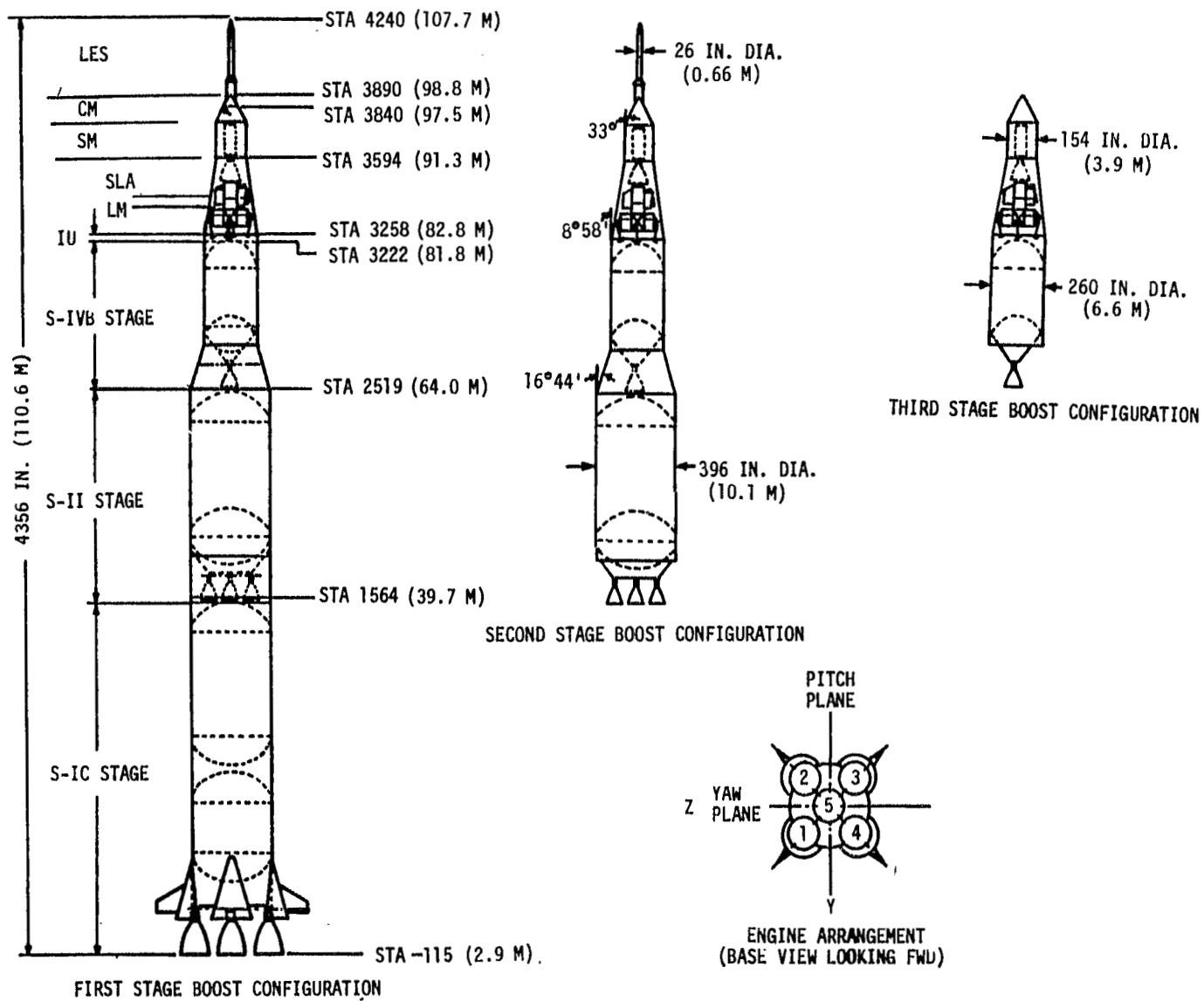


FIGURE 2-1 APOLLO SATURN V CONFIGURATIONS

2.1 (Continued)

The four outboard engines are attached to thrust posts located on the periphery of the aft skirt section. A cruciform beam supports the center engine. Four holddown posts provide anchor points for mounting the vehicle to the launcher. Aerodynamic fairings and stabilizing fins are provided at each outboard engine location. With the exception of the intertank structure, which is of corrugated skin-ring frame construction, all unpressurized skirts and fairings have extruded hat-section stringers riveted to the external surface.

S-II Stage - The second stage (S-II) of the Saturn V vehicle has the same diameter as the first stage. The two stages are joined by a series of skin-stringer type shells with hat-shaped stringers riveted to the external surface. The S-II propulsion system consists of five J-2 engines burning liquid hydrogen (LH₂) fuel with liquid oxygen (LOX) as the oxidizer and having a total thrust of about 1 million pounds (4,448,000 N). The fuel tank is forward and the oxidizer tank is aft. An insulated common bulkhead separates the two pressure vessels.

The cylindrical portion of the fuel tank has integral circumferential and longitudinal stiffeners which are machine milled on the inside surface to form a rectangular grid pattern. Five longitudinal and four circumferential fusion welds are utilized to assemble the cylinder. The upper fuel tank bulkhead and lower LOX tank bulkhead are fabricated from gores which are fusion welded together to form elliptical diaphragms. The common bulkhead is a sandwich structure consisting of gores, fusion welded to an elliptical shape and bonded to a fiberglass honeycomb core.

The thrust structure consists of a truncated cone with hat-shaped stringers riveted along the external structure. Thrust longerons, at the four outboard engine locations, transmit the engine force. The center engine is mounted at the center of a cruciform beam. All unpressurized shell structures are skin-stringer types with extruded hat-shaped stringers riveted to the skin.

S-IVB Stage - The third stage (S-IVB) of the Saturn V vehicle has a liquid hydrogen-liquid oxygen propulsion system utilizing a single J-2 engine, located on the stage center line, with 200,000-pound (889,600 N) thrust capability. This stage has a nominal diameter of 260 inches (6.60 m). The oxidizer tank is located aft of the fuel tank. An insulated common bulkhead separates the two tanks. A square waffle pattern having a 45 degree orientation to the vehicle longitudinal axis is machine milled on the inner surface of the fuel tank cylindrical section. Longitudinal fusion welds are used to join the six sheets forming this cylinder. Construction of the hemispherical bulkheads follows the pattern described for the S-II stage. The unpressurized structure fore and aft of the tankage, including the conical interstage, is of skin-stringer construction with extruded hat-shaped stringers riveted to the outside of the skin.

2.1 (Continued)

Instrument Unit - The instrument unit (IU) is a short cylindrical structure having a nominal diameter of 260 inches (6.60 m). Structurally the instrument unit is a sandwich shell consisting of aluminum face sheets bonded to an aluminum honeycomb core. Instrument packages are mounted to the inner walls of the structure.

Apollo Spacecraft - The Apollo spacecraft is composed of five sub-structures: Lunar Module (LM), Saturn Lunar Module Adapter (SLA), Service Module (SM), Command Module (CM), and Launch Escape System (LES).

1. Lunar Module - The LM is a two-stage, soft-landing spacecraft which carries two astronauts to the lunar surface from lunar orbit and subsequently returns these two men to a rendezvous with the orbiting CM. In the launch configuration the LM is attached at four points inside the LM adapter cone.
2. Saturn Lunar Module Adapter - The SLA structure is a conical frustum of aluminum face and honeycomb core sandwich material with diameters of 154 and 260 inches (3.91 and 6.60 m) at the fore and aft ends, respectively. The adapter also serves as an interstage structure between the Apollo Saturn V IU and the SM.
3. Service Module - The SM is an aluminum honeycomb shell with internal radial shear web partitions. The SM has a nominal diameter of 154 inches (3.91 m). Equipment on this part of the spacecraft supplies the power for midcourse corrections, retro-braking into lunar orbit, and return flight propulsion.
4. Command Module - The CM is a conical frustum fabricated of steel face-and-core honeycomb with interior accommodations and instrumentation for three astronauts. From this section of the spacecraft, the crew monitors and controls all functions throughout launch, translunar flight, lunar orbit, return flight and re-entry.
5. Launch Escape System - The LES consists of a titanium open truss tower supporting a launch escape motor. The motor is a solid propellant device with a steel case and having a nominal diameter of 26 inches (7.92 m). The tower attaches to the top of the CM cone and is jettisoned 32 seconds after second stage ignition.

2.2 HISTORY OF SATURN V STRUCTURAL DYNAMIC PROGRAMS

The Apollo Saturn V structural dynamics activity can be sub-divided into four major phases: the 1/10 scale analysis and test activity, full scale math modeling, full scale test activity, and actual Saturn V flight. These four phases are discussed in the paragraphs that follow.

2.2.1 1/10 Scale Model Program

With the commitment to design and fabricate a full scale test and to fly the largest space vehicle ever conceived, came the recognition that the replica model testing concept could pilot the program and resolve technical problems before they became insurmountable from both a cost and schedule standpoint. A 1/10 Scale Model Program was established to support the Apollo Saturn V Program and to accomplish several important research objectives. These research objectives were not directly concerned with the Apollo Saturn V Program and will not be discussed in this document.

A 1/10 scale replica model of the Saturn V vehicle was completed nearly 18 months in advance of full scale Saturn V hardware. A dynamic test program of the scale model was established to provide guidelines for performing the full scale dynamic test program. As a secondary objective, the program was expected to indicate possible loads, or dynamics problems that might be inherent in the full scale design so that these problems could be resolved before the first Saturn V vehicle was completed.

A more fundamental long-range objective of the scale model program was to supplement the full scale test program in verification of the Saturn V structural dynamic math models. A mathematical modeling program was outlined between Langley Research Center (LRC), Marshall Space Flight Center (MSFC), and The Boeing Company whereby the same basic analysis models and methods would be used for both the 1/10 scale and the full scale test articles. The results of both programs would be used to either verify the math models or to identify areas where the models were inadequate and structural idealization or analysis techniques required updating. Even though the schedule was tight, portions of the scale model test and analysis program preceded the full scale program enough to allow for the more important influences on the full scale pretest analysis and the test program.

The scale model test data showed that the liquid and structural coupling was not modeled adequately; that the truncated cones used to make vehicle diameter transitions produced a longitudinal and bending stiffness characteristic which was not being adequately modeled; that structural joint modeling is sensitive to axial loading (i.e., g-levels, mass, etc.); and that the ring mode activity, as suspected, was an important phenomenon for large shell structure. Data from the scale model tests were also useful in defining and assessing instrumentation and thruster requirements for the full scale program.

Math models were reviewed and improvements made in the stiffness representation. These improvements were developed in time to use them in the pretest analysis of the full scale dynamic test vehicle. The remodeling of the liquid and structural coupling and the cone area that resulted from correlation of the 1/10 scale test and analysis results prevented a schedule impact resulting from math modeling problems during the full scale test program.

2.2.1 (Continued)

The scale model and full scale test programs were well coordinated. For example, the same type ballast simulants and the same liquid fill conditions were being studied in both programs. The same general thruster locations and the same tank pressures were also used. The intent was to establish correlation between the scale model test results and the full scale tests. Conducting the scale model test program in advance of the full scale program answered many technical questions that might otherwise have impacted the much costlier full scale program.

2.2.2 Full Scale Math Modeling

The dynamics of the flight article differed from the dynamics of the ground test article in several significant ways. Hardware substitutions had to be made in the test article because of the cost of the actual hardware, availability of hardware from vendors, and because the schedule required results well in advance of flight. The test suspension system did not duplicate the free-free conditions of flight, and the cryogenic propellants of the flight vehicle had to be replaced with less hazardous simulants for ground test. As a result, ground test data could not be used directly for flight assessment.

The math model was used for projecting the ground test results to the flight vehicles. On the Saturn V Program, dynamic test results were used primarily to verify math models of the test article. After verification, differences between the test and flight articles were modeled, and the resulting models were used to predict flight characteristics with a high level of confidence. The frequencies of the bending modes that were detected in flight of the first stage boost configuration were predicted within five percent accuracy. The frequencies of the detectable longitudinal modes were predicted within three percent accuracy. The correlation of the first stage flight data and analytical predictions are presented in Reference 2-1.

Mathematical analyses of the Saturn V vehicle started with the development of basic beam-rod models to answer questions in support of dynamic test requirements. These early uniaxial models were used to obtain answers to such questions as: what is the effect of replacing LOX with water as a test simulant?, what are the effects of replacing a flight article component with a dynamic simulator?, what size of thruster is required to excite the vehicle to readable levels?, and where should the vehicle be instrumented in order to obtain accurate mode shape characteristics? These early math models were also used to help establish the regions where modeling of local shell characteristics was required so that more detailed idealizations of these sections could be made in subsequent mathematical models. A schematic of math model development history is shown in Figure 2-2.

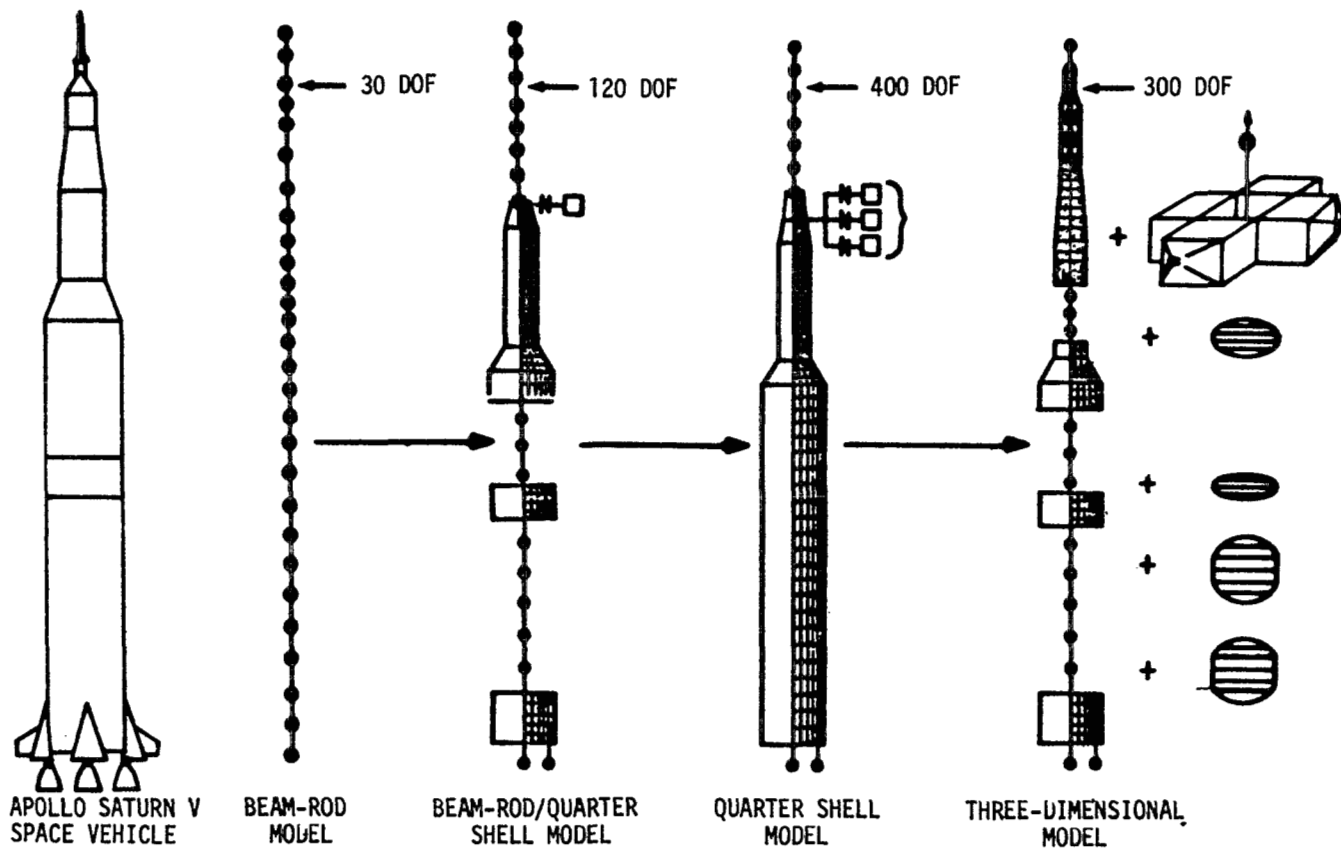


FIGURE 2-2 MATH MODEL EVOLUTION

2.2.2 (Continued)

The next step in the math model evolution was to add detailed quarter-shell sections to the basic uniaxial model in regions where local effects were considered important. The primary objective of these math models was to predict accurately flight control gain factors between a gimballed engine and a flight control sensor response. This required shell models of the thrust structure regions and the flight control sensor areas. When the dynamic test program was initiated, the forward skirt of the S-IC stage, and the aft skirt of the S-IVB stage were both potential locations for the flight control sensors, in addition to the primary location in the IU. All locations were designed to accommodate three axis sensors, with one axis always oriented normal to the skin. As a result, shell models were required to represent local out-of-plane bending in these regions. The combination beam-rod/quarter-shell models were used in the analysis of the 1/10 scale model.

Computer size limitations at that time (up to 130 degrees of freedom could be handled in the eigenvalue routine) required the development of separate math models to emphasize detail in the S-IC thrust structure area, the S-IC forward skirt, the S-IVB aft skirt and the IU. For example, if accurate transfer functions from the S-IC thrust structure to the S-IVB aft skirt were desired, then one particular model would be used. If transfer functions between the S-IC thrust structure and the IU were desired, another math model would be used. This approach resulted in slightly different modal parameters being predicted by each of the separate models, and required a decision as to which solution should be used.

To prevent this and still have the ability to predict the local anomalies that might become evident from test or from flight, a single shell model was developed. This model included a quarter-shell representation of the total launch vehicle and SLA with a uniaxial model of the service/command modules and the launch escape tower. Knowledge gained from correlation of 1/10 scale model analysis and test results was included in this math model. The size problem in analyzing this model was resolved by a process of modal stacking. In this approach, cantilevered modes of the S-IVB stage and spacecraft were obtained. These were then used in the analyses of the second flight stage, which consisted of the S-II stage, the S-IVB stage, and spacecraft. Then cantilevered modes from this combination, in turn, were used to analyze the total vehicle.

The modal stacking approach required additional flow time, but proved to be an accurate and economical means of analyzing the individual configurations and in predicting the characteristics of the dynamic test vehicle. Results from this approach were valuable in monitoring dynamic test results and in evaluating their validity.

The math model proved highly accurate in predicting overall modal properties of the dynamic test vehicle. There were, however, several areas where the math model proved inadequate. First, the model did not predict

2.2.2 (Continued)

local slopes of the flight control sensors with the desired degree of accuracy. Second, asymmetries in the spacecraft introduced coupling between pitch, yaw, longitudinal and torsional planes. Third, interplane coupling proved to be even more significant in the flight vehicles than in the test article. Fourth, the quarter shell model did not have the capability of predicting this coupling.

To eliminate these problems a three-dimensional model of the total vehicle was developed. In parallel with this, a computer program was developed that had the capability of analyzing systems starting with 12000 stiffness degrees of freedom and reducing to 300 dynamic degrees of freedom. Dynamic test program experience showed that the bending and longitudinal properties of the launch vehicle stages could be represented by beam and axisymmetric shell elements, respectively, for frequencies up to 25 Hz. This allowed the three-dimensional characteristics of the Apollo Saturn V vehicle to be represented with only 300 dynamic degrees of freedom. This simplified full shell math model was used in Pogo, loads, and flight control predictions on a vehicle-by-vehicle basis to support the Saturn V Program.

2.2.3 Full Scale Dynamic Test and Correlation

Results from the dynamic tests not only proved invaluable in establishing verified math models but the converse was also true. The pretest analysis results were the basic tool used for on-site evaluation and verification of dynamic test data.

The dynamic test program contributed several hardware changes to the Saturn V vehicle. First, the test results showed that a longitudinal and lateral coupling mechanism existed in the CM and SM interface. This mechanism, coupled with the stiffness asymmetry and weak torsional stiffness of the CM and SM interface produced large torsional responses of the CM. Acting upon test results, the spacecraft contractor modified this interface to eliminate the torsional weakness. Second, the dynamic tests proved that the location of the flight control sensors was not satisfactory. The flight control package, which was located at the top of a plate in the IU, was susceptible to strong local effects involving bending of the plate itself, as well as shell deformation introduced by spacecraft dynamics, particularly the dynamics of the LM. To correct this, the flight control package was relocated to the bottom of the plate where local effects were much less pronounced. The dynamic test of this new configuration was then run to provide data for establishing verified math models. The local characteristics of the plate and bracketry, including the stiffening effect of the components attached to the plate, had to be modeled in detail to predict flight control sensor rotations with required accuracy. In addition to the relocation of the flight control sensor, some minor revisions in the flight control filter network were necessary to ensure stability in the second and third vehicle bending modes during first stage boost.

2.2.4 Saturn V Flight

The baseline math model, which was verified by both replica model and full scale test, was the principal tool used to resolve Saturn V structural dynamic problems and to provide NASA management assurance that each flight vehicle was flight worthy. In March 1968, it was decided to expand the model to couple in the three dimensional dynamics of the spacecraft components to improve the accuracy of loads calculations. At the start of the program it was considered adequate to ignore cross axis coupling and verify the math models up to 10 Hz in frequency. These assumptions were proven incorrect by full scale test and events occurring on Saturn V flights. On the second flight in April 1968, the first stage exhibited a Pogo instability in a five Hz, first vehicle longitudinal mode. Because of stiffness asymmetry in the LM, this longitudinal mode was strongly coupled with a bending mode in the same frequency range. The combined longitudinal/pitch environment raised concern for the integrity of the structure and the comfort of the crew.

On the third and fourth flights, strong Pogo oscillations developed in the S-II stage in an 18 Hz crossbeam mode. During the fifth flight possible Pogo occurred on the S-IVB stage. The S-IVB oscillations were also in a high frequency mode (18 Hz). These flight experiences intensified the development of math models capable of predicting cross axis coupling to approximately 25 Hz in frequency.

In six years, the mathematical models of the Saturn V vehicle have grown from primitive uniaxial models used to support test requirement studies to detailed full shell models capable of investigating flight anomalies up to 25 Hz in frequency. The technology supporting this growth is contained in this document.

REFERENCE

- 2-1 Document D5-15575-1, SA-501 Postflight Structural Dynamic Flight Evaluation, The Boeing Company, Huntsville, Alabama, February 16, 1968.

SECTION 3 1/10 SCALE MODEL TECHNOLOGY

3.0 GENERAL

This section presents the contributions of the scale model to the full scale Saturn V Program and illustrates what scale modeling techniques can contribute to future programs.

The 1/10 Scale Apollo Saturn V model was conceived by Langley Research Center as an early, economical source of vibration response data. The model also supported the Saturn V Program by contributing to problem resolution, by providing test planning guidelines, and by early math model evaluation. The model was built in advance of the full scale vehicle so that data could be used to define potential vibration problems and suggest solutions to these problems without impacting scheduled launch. Dynamic test data from the model could also be used to validate the methods and procedures developed for both analytical and test investigation of the structural dynamic characteristics of the prototype. The scale model could also be used to investigate problems observed during flight test of the full scale vehicle.

The basic objectives of the scale model program were achieved. Data from the scale model verified that the shaker location selected for full scale test could excite all modes of interest. It also verified that the force capability of the shakers being developed for the full scale test would be adequate. It confirmed that the sensor locations selected for full scale tests were adequate, and that the acceleration levels selected for the full scale test were correct.

Data from the scale model tests also confirmed that the basic mode shapes predicted by early Saturn V math models were adequate to support preliminary design work. From the correlation of scale model analyses and scale model tests results, several shortcomings of the math modeling approaches were uncovered. Most significant of these was the manner in which the liquid was represented in the longitudinal analysis. As a result of this early warning, more accurate math modeling procedures were developed in advance of the start of the full scale program.

After the full scale program was well under way, the scale model still proved useful in supporting investigations of problem areas. The model was used to demonstrate the integrity of the structure around the LM attach points during the investigation of a local structural failure that occurred during flight of the second Saturn V (AS-502) vehicle. Detailed replica models of the SLA, SM, and LM were built. From the scale model tests and other related studies it was determined that the in-flight failure did not stem from local failure around LM attach points. The model was also used to check out a gravity simulation harness proposed for a full scale test to investigate the AS-502 anomaly.

3.0 (Continued)

While the scale model program did achieve its basic objectives, its potential value to the Saturn program was never realized because correlation was not achieved between the model and the prototype. Because of scaling effects, testing of the 1/10 Scale Model in a 1 g environment is equivalent to testing the prototype in a 1/10 g environment. Several joints along the model opened slightly in this equivalent low g environment resulting in local flexibility being introduced into the scale model. The joints would have required redesign to eliminate this flexibility. Had this been accomplished, the dynamic characteristics of the scale model would have provided an excellent simulation of the prototype for overall vehicle characteristics. Following comparison of scale model and full scale results, the scale model should have been revised to establish correlation.

Because the scale model was built before all secondary structure and major components were designed on the prototype, the replica model was not up to date. The model should have been updated as the program progressed to include definition of this hardware. Had these changes been made, the AS-502 anomaly study could have been performed without the delay required to redesign and fabricate the SLA, LM, and SM models.

In retrospect, it is clear that significant advantage would also have been obtained if the same data reduction methods had been applied to both the scale model data and the full scale data. Approximately six months were required to check out the data reduction methods and automate them sufficiently to handle the volume of data being obtained from the full scale tests. This six month training period could have been completed in advance of the full scale test by using scale model data.

The scale model program was cost effective and did provide much useful information to the full scale program. Because of the technological advances gained from the 1/10 Scale Program, a future scale model could take advantage of these advances and provide even greater benefits to similar space programs.

3.1 THE SCALE MODEL TEST PROGRAM

3.1.1 Scale Model Description

The 1/10 scale Apollo Saturn V dynamic model consisted of five basic units, representing the S-IC stage, the S-II stage, the S-IVB stage, the IU of the Saturn V launch vehicle, and the Apollo spacecraft. The spacecraft was composed of the LM, SM, CM and LES systems. Each of these modules is illustrated in Figure 3-1. The complete model is shown supported in the test facility by a four-cable suspension system (designed to provide the proper simulation for free-free longitudinal vibration response) in Figure 3-2. The interior of the 1/10 scale fuel tank is shown with that of the prototype in Figure 3-3. This figure illustrates the fidelity with which the Saturn V launch vehicle was modeled.

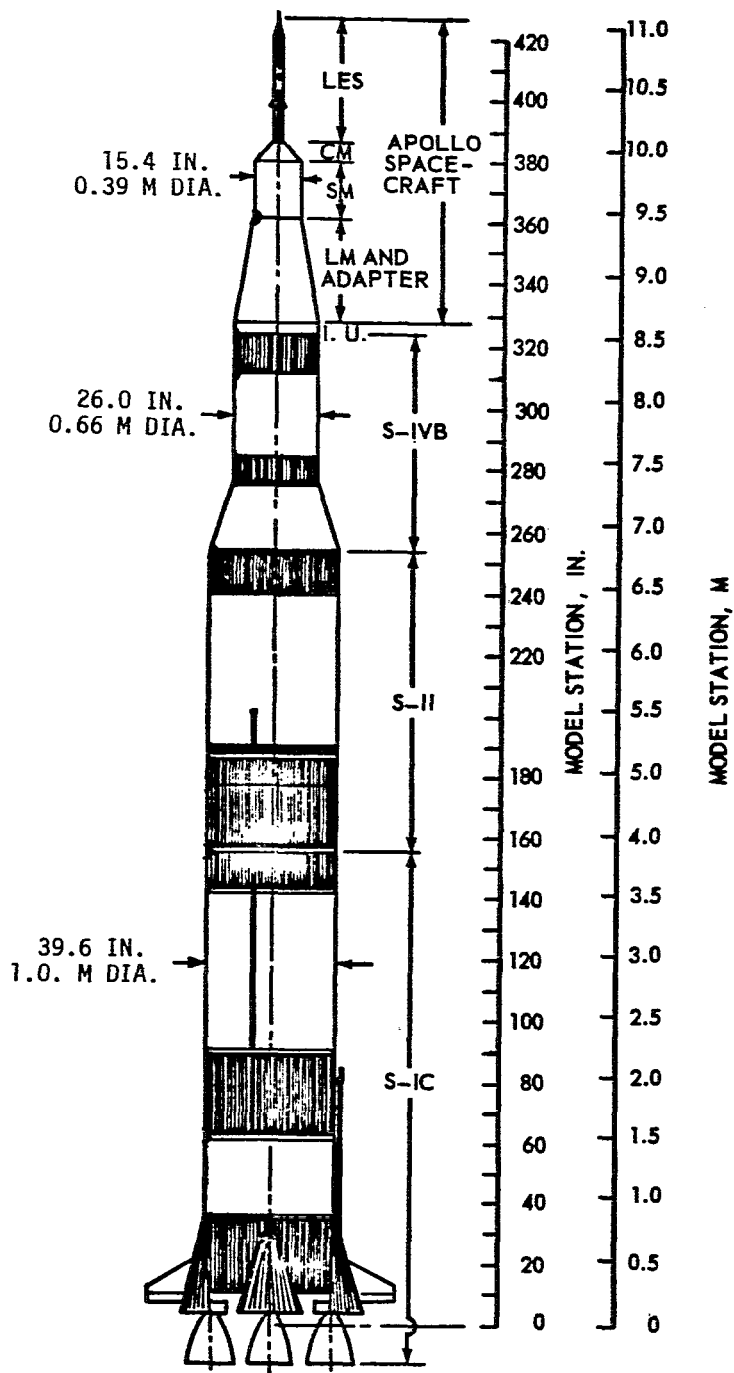


FIGURE 3-1 SCHEMATIC OF 1/10 SCALE APOLLO SATURN V MODEL

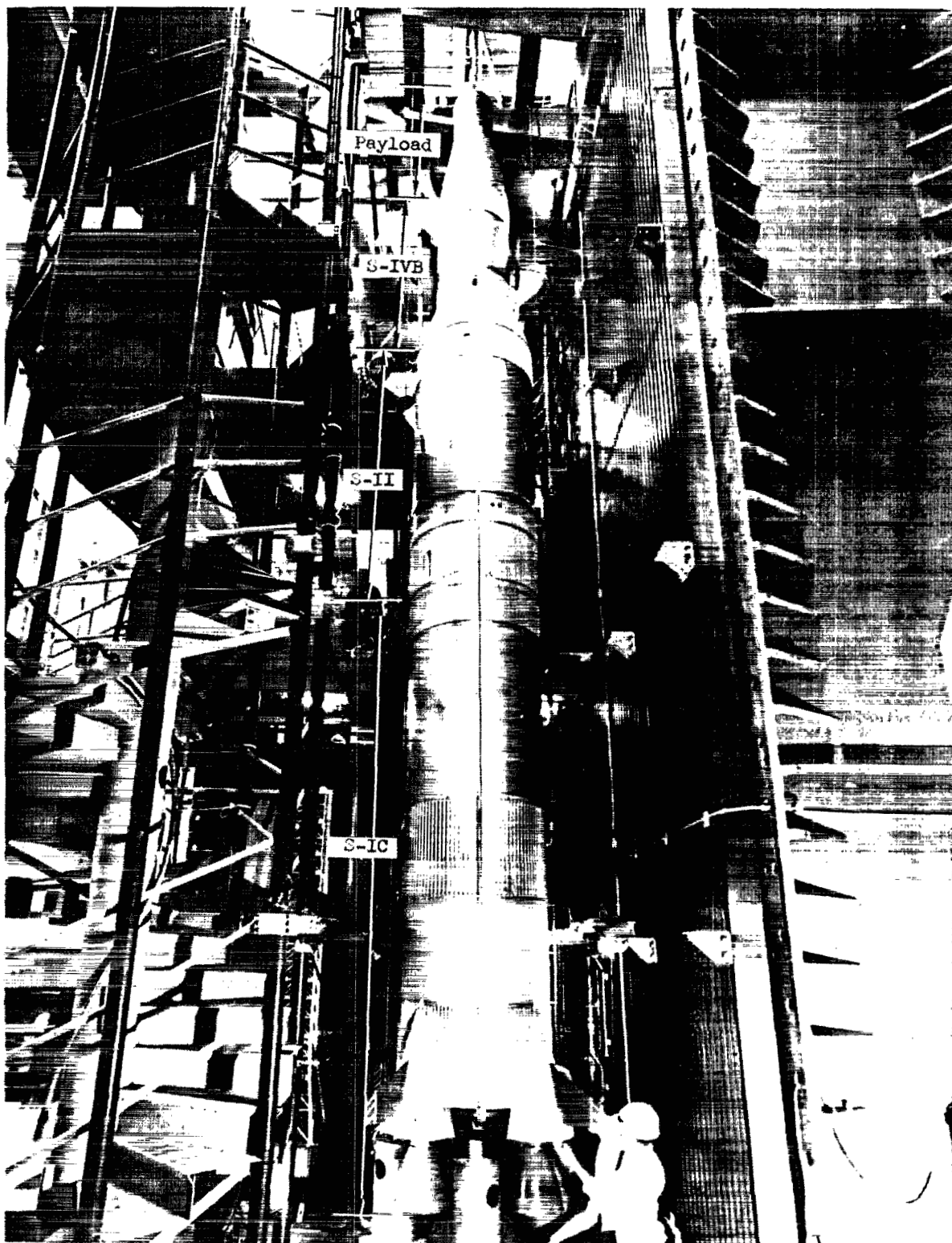
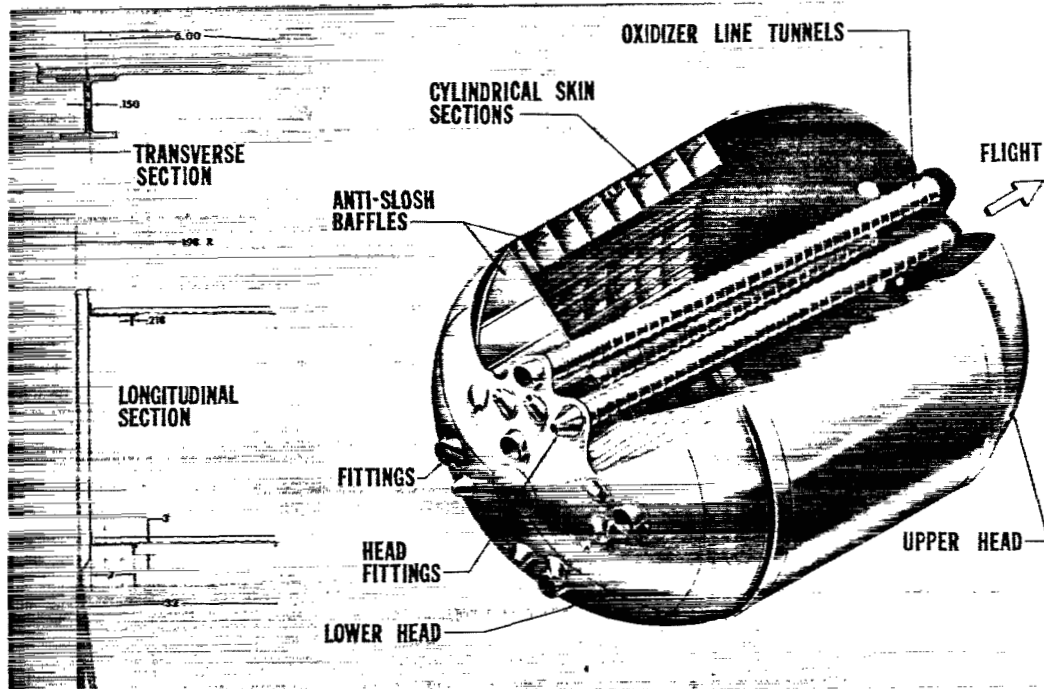
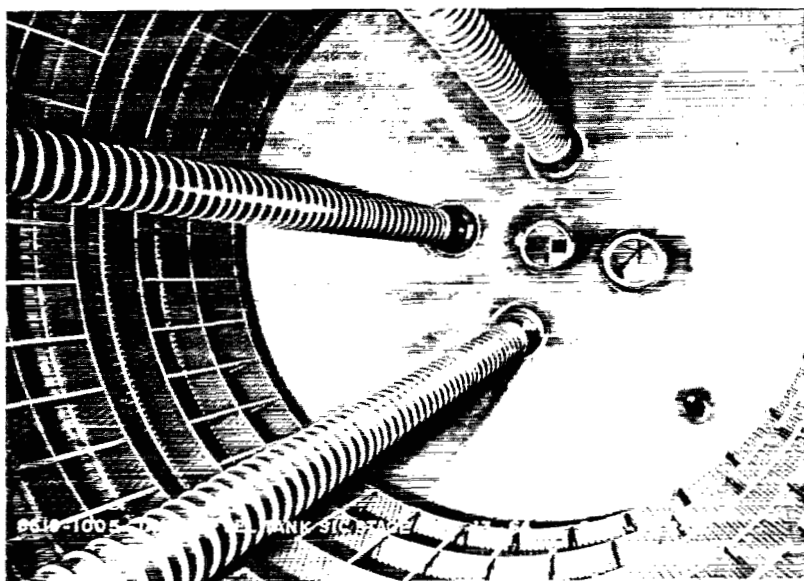


FIGURE 3-2 1/10 SCALE MODEL IN TEST STAND



SATURN V S-IC FUEL TANK ASSEMBLY



1/10 SCALE S-IC FUEL TANK MODEL

FIGURE 3-3 ILLUSTRATION OF DETAIL ACHIEVED IN MODELING

3.1.1 (Continued)

Where state-of-the-art permitted, the primary load-carrying structure of the launch vehicle and spacecraft were geometrically scaled in the model. Above the LM adapter, geometric scaling was not feasible due to the time and cost required. However, the external dimensions and gross stiffness properties were scaled. The major spacecraft component, the LM, was mass simulated.

A comparison of the 1/10 scale model and full scale vehicle bending stiffness properties is presented in Figure 3-4. This comparison shows the accuracy with which the overall stiffness properties were reproduced. A complete description of the scaling and manufacturing techniques is presented in Reference 3-1.

3.1.2 Scale Model Test

A special facility was established at Langley Research Center to test the 1/10 scale model. A cable support system, which simulated free-free boundary conditions, suspended the model in the pendulum-like manner shown in Figure 3-2.

The scope of the actual tests exceeded that of the full scale test program which followed. In addition to supporting the Saturn V program, the model was used to check out a new booster design concept, and to explore the limits of scale model technology in the areas of impedance and dynamic test.

The model was used to investigate pitch, yaw, and longitudinal properties for each of the three stages of launch vehicle boost. The longitudinal test data are presented in Reference 3-2. The pitch and yaw test data are being documented in NASA Technical Notes, that will be published later by Langley Research Center. The test conditions were selected to parallel those planned for the full scale test. For example, water was used to simulate the LOX and RP-1 propellants in both the scale model and prototype tests and the same tank pressures were used. This allowed scale model test results to carry forward and directly support the prototype test program.

3.2 CONTRIBUTIONS TO FULL SCALE TEST

One of the major objectives of the full scale test was to define the transfer function between the control engines and the flight sensor locations. To satisfy this objective, the vehicle had to be excited through the gimbal blocks of the control engines. Preliminary math model work indicated that the modes of interest probably could be excited to readable levels from the gimbal block. To add confidence to the analytical results, the 1/10 scale model was excited through the same basic thrust structure location. Results indicated that the proposed thruster location was satisfactory to accomplish basic full scale test objectives, and that the modes obtained from exciting at this location were essentially normal modes.

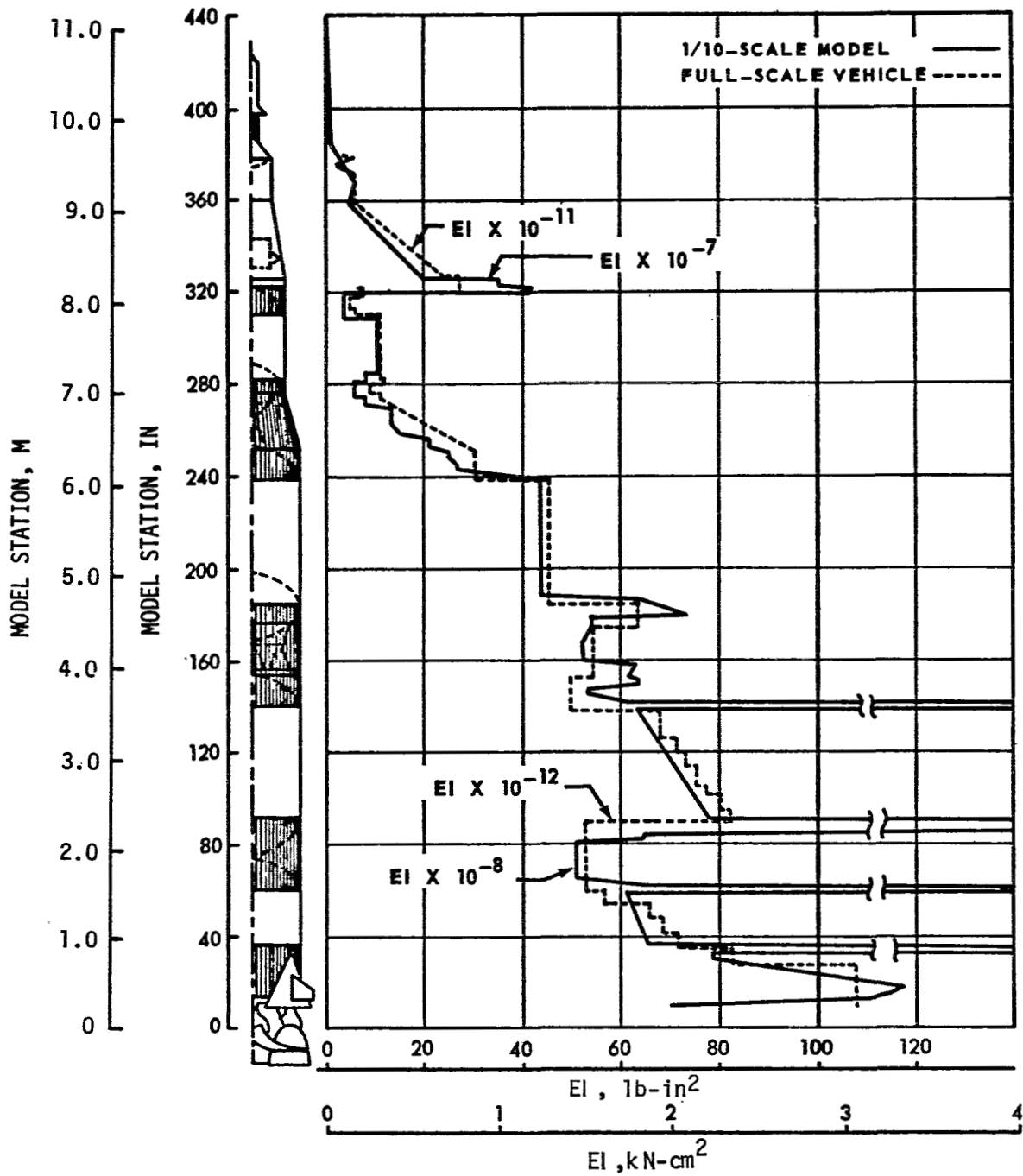


FIGURE 3-4 COMPARISON OF 1/10 SCALE MODEL AND FULL SCALE VEHICLE BENDING STIFFNESS

3.2 (Continued)

The ability to use the single shaker location throughout the test greatly simplified test conduct and enabled test objectives to be met on an optimum schedule. The evidence gained from the scale model tests was later confirmed by the full scale results, as all modes of interest were suitably excited from the gimbal location.

Data from the scale model were also used to increase confidence that the thrusters being developed for the full scale tests could force the vehicle to readable response levels in all modes of interest. The acceleration per pound of force measured on the 1/10 scale model test was scaled to the prototype. This required that the scale model accelerations per unit of force be reduced by a factor of 1000 to simulate the prototype condition. A correlation and discussion of the 1/10 scale and full scale acceleration/force ratios are presented in Section 3.5.

A parameter study was performed on the scale model to determine the effects of different propellant tank ullage pressure on the dynamic characteristics. Results of this study indicated that reducing the ullage pressure from 30 to 10 psi had very little effect on the dynamic characteristics. The lower pressure was used for both the full scale and scale model tests to reduce the hazard to test personnel.

The calibration levels required on the full scale test program were supported by data from the scale model. For example, in instrumenting the bending test, accelerometer ranges had to be determined. Information obtained from the scale model confirmed that accelerometers selected were adequate. Data from the scale model also confirmed that the sensor locations were adequate to obtain enough information from the test for accurate plotting of overall vehicle mode shapes. The scale model data showed that the most complex modal deflection patterns occurred in the spacecraft region of the vehicle and that it would be necessary to instrument this region in considerably more detail to obtain accurate modal information.

3.3 CONTRIBUTIONS TO SATURN V MATH MODELING

The early mathematical models of the full scale Saturn V vehicle used to support major program decisions were primitive, and had no test data to support their reliability or to indicate their weaknesses. Data from the scale model filled the gap between the time the early models were developed and when actual test data were available. Scale model results added confidence that the basic math models of the Saturn V vehicle were predicting overall vehicle modal frequencies and shapes with reasonable validity.

Scale model test data helped identify major shortcomings in the mathematical model. At the start of the analysis program, structural drawings of the spacecraft were very difficult to obtain. In the absence of detailed drawings, a crude LM mathematical model was developed from results of a vibration test that indicated the LM had a fundamental pitch and yaw frequency of 4.5 Hz (Reference 3-3).

3.3 (Continued)

Quick look data from full scale dynamic test of the S-IVB/IU/ spacecraft combination showed a strong mode around 4.5 Hz, which could have been a LM mode, plus two modes around 9 Hz for which the math model had no equivalent. Here the scale model test data helped isolate the math model problem area. The scale model -- which had an equivalent LM simulator frequency of 14 Hz -- showed that there was a strong vehicle mode around 4 Hz, but no vehicle modes around 9 Hz.

The absence of vehicle modes at 9 Hz led to the conclusion that the 9 Hz resonances of the prototype were probably LM modes. Drawings of the LM were obtained as required to develop a detailed model. This model showed that the fundamental mode of the LM was around 9 Hz. It also showed that the twin 9 Hz resonances were produced by pitch and longitudinal coupling caused by stiffness eccentricities in the LM.

3.3.1 Mathematical Analysis of the 1/10 Scale Model

A vibration analysis of the scale model was performed using the same basic models and methods being developed for the Saturn V vehicle. The beam-rod/quarter shell model shown in Figure 2-2 was used in this analysis. Results from the analysis were correlated with scale model test data to uncover major weaknesses in the models and/or analysis techniques. A discussion of the results obtained from this correlation follows.

3.3.2 Scale Model Test and Analysis Correlation

Figure 3-5 presents a 30.6 Hz mode obtained during the scale model testing. This mode is the fundamental bulging mode of the S-IC tanks caused by coupling between the propellant and structure. This phenomenon occurs in a large liquid propelled vehicle like the Saturn V, when the shell deformations produced by the liquid exert a dominant influence on the longitudinal modes of the vehicle.

A counterpart to the 30 Hz mode was not obtained from the math model, and subsequent investigation of this problem showed that the coupling between propellant and structure was modeled inadequately. Due to this lack of correlation, the matrix method presented in Section 4.4.3 was developed to simulate the interaction between the liquid and structure in time to support the full scale program.

The results of the second longitudinal mode obtained from the scale model test and analysis are presented in Figure 3-5. These results show that the scale model is more flexible in the S-IC intertank and IU areas than predicted by the math model. The test frequency was also six percent lower than the analysis frequency.

The 1/10 scale model test and analysis correlation of the first two pitch modes for the fully filled condition is presented in Figure 3-6. Although the overall correlation of these mode shapes is good, there is still evidence of local flexibility in the scale model data. The test frequencies

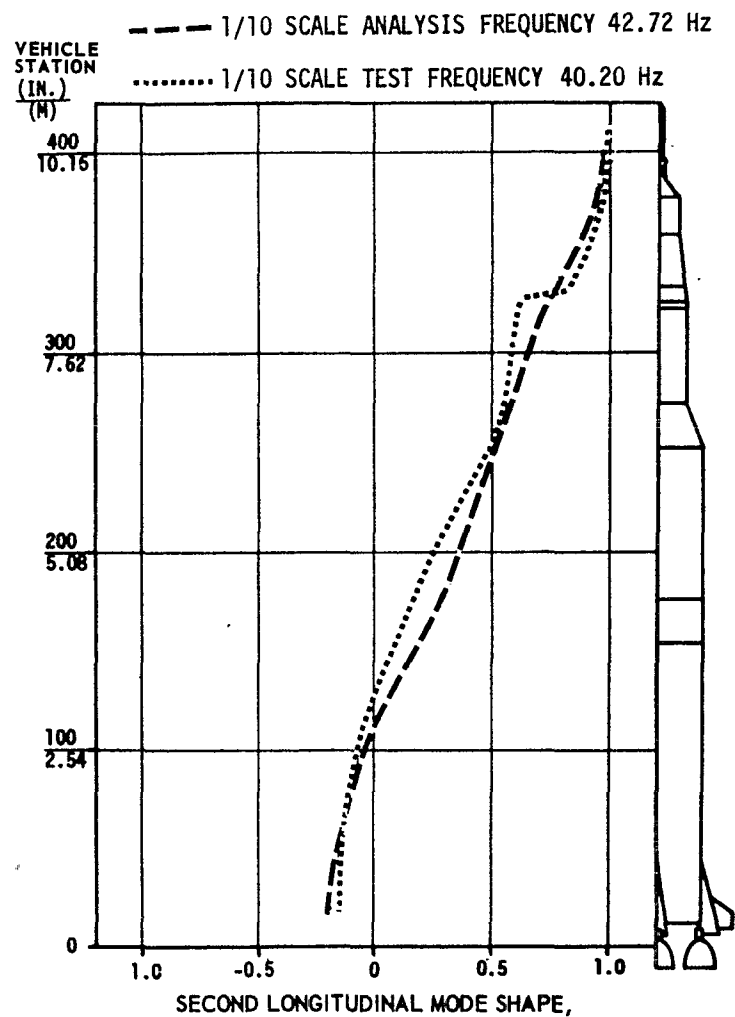
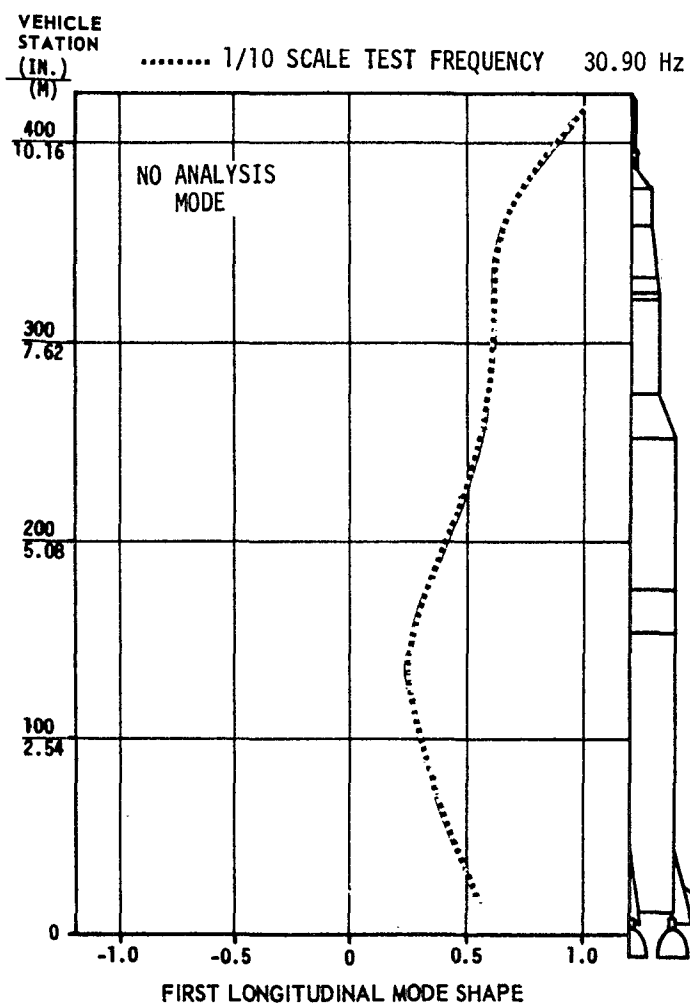
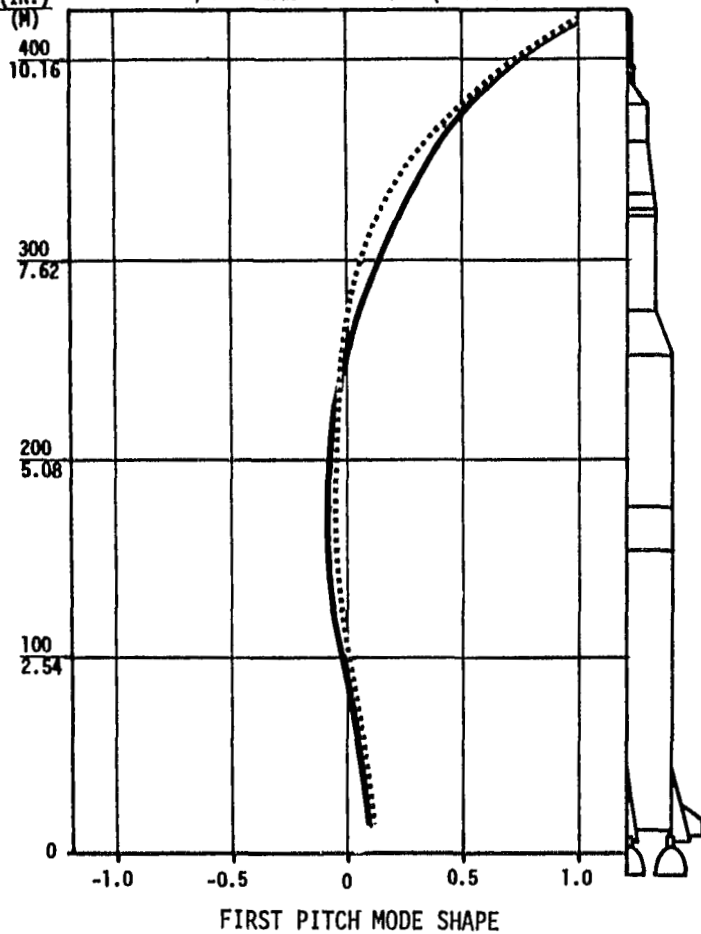


FIGURE 3-5 COMPARISON OF 1/10 SCALE LONGITUDINAL TEST AND ANALYSIS RESULTS -100 PERCENT PROPELLANT

VEHICLE STATION (IN.) ——— PRETEST ANALYSIS FREQUENCY 10.69 Hz
 1/10 SCALE TEST FREQUENCY 9.12 Hz



VEHICLE STATION (IN.) ——— PRETEST ANALYSIS FREQUENCY 20.18 Hz
 1/10 SCALE TEST FREQUENCY 15.99 Hz

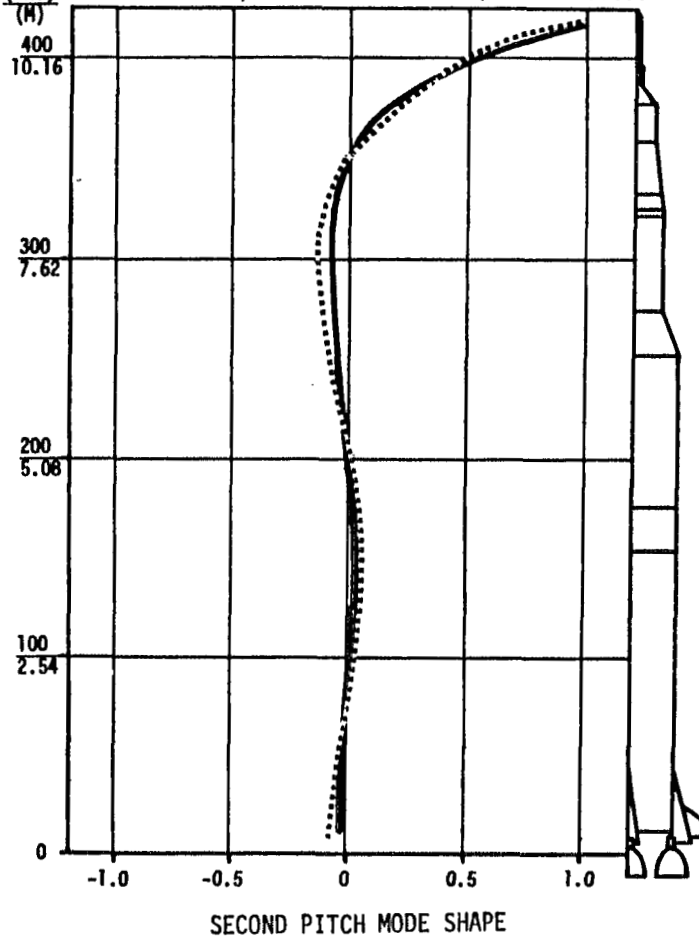


FIGURE 3-6 COMPARISON OF 1/10 SCALE PITCH TEST AND ANALYSIS RESULTS - 100 PERCENT PROPELLANT

3.3.2 (Continued)

are 17 and 26 percent lower, respectively, than the analysis frequencies.

3.4 CONTRIBUTIONS TO SATURN V ANOMALY RESOLUTION

During the second flight (AS-502), Pogo oscillations developed in the S-IC stage. During the Pogo oscillations, a local failure of one of the SLA panels occurred. The most popular failure hypothesis was that the panel failed around the LM attach points under combined static (4 g) and dynamic (+0.6 g) loads. To explore this hypothesis, a special scale model of the SLA, LM and SM was built. A special harness was also constructed to simulate the 4 g static load. This model was tested as part of the total first stage boost configuration.

Electrodynamic shakers were used to excite the suspended vehicle to scaled AS-502 oscillation levels. No sign of a local failure was observed. The static loads were increased to the flight condition, but no failure was produced. From this and related studies conducted throughout the aerospace industry, it was firmly established that a local failure around the LM attach points could not have occurred. It was later determined that moisture had penetrated one of the honeycomb SLA panels. It was hypothesized that aerodynamic heating had vaporized this moisture and explosively delaminated a section of the honeycomb.

3.5 COST AND ACCURACY

3.5.1 Cost

The 1/10 scale model was built at a cost of approximately 1/20 of the full scale test vehicle. The dynamic tests that were conducted on the model required a crew of four engineers and technicians. The cost of the scale model test program was roughly 1/10 the cost of an equivalent full scale test program.

3.5.2 Accuracy

A correlation between the 1/10 scale model test and full scale test results was made to assess the accuracy of scale modeling techniques. This comparison showed that the scale model provided a fair prediction of vehicle response characteristics. The response per unit force of the model and the prototype are compared in Table 3-I. The scale model responses have to be reduced by a scale factor of 1000 to compare with prototype values. The ratio of the 1/10 scale to full scale for the bending response ranged from 0.45 to 1.85, and the longitudinal response ranged from 0.17 to 1.50. Most of the differences are due to:

1. Joint flexibility (this is discussed in Section 3.5.3).
2. Configuration differences - The SM tank and the CM-SM interface was not modeled adequately for the 1/10 scale

TABLE 3-I CORRELATION OF 1/10 SCALE MODEL
AND FULL SCALE RESPONSE DATA

MODE	G'S/UNIT FORCE		RATIO
	1/10 SCALE MODEL	FULL SCALE	1/10 SCALE FULL SCALE
1ST PITCH	0.10	0.22×10^{-3}	0.45
2ND PITCH	0.23	0.23×10^{-3}	1.00
3RD PITCH	0.26	0.14×10^{-3}	1.85
4TH PITCH	0.14	0.26×10^{-3}	0.54
1ST LONG.	0.001	0.006×10^{-3}	0.17
2ND LONG.	0.007	0.019×10^{-3}	0.37
3RD LONG.	0.006	0.004×10^{-3}	1.50
4TH LONG.	0.002	0.004×10^{-3}	0.50

3.5.2 (Continued)

model. Also, excessive motion of the scale model LM simulator was produced by localized deformation of the simulator at the support strut locations.

3. Damping differences caused by innate differences in the two vehicles, and by exciting the vehicles to different amplitude levels (full scale testing showed that damping changed non-linearly with amplitude).

The response per unit force is a difficult parameter to predict. Before test data was available to define modal damping, the response per unit force predicted by the math model differed from the full scale results by factors of 0.2 to 1.4 (which is the same type of accuracy obtained from the scale model).

A correlation of the first four pitch modes of the 1/10 scale and full scale tests are presented in Figures 3-7 and 3-8. The correlation of the first mode shapes is excellent, but the full scale frequency is 22 percent higher than that of the 1/10 scale model. The second mode shapes show the 1/10 scale model is more flexible in the IU area than the full scale model. The correlation of the mode shapes is good, but the full scale frequency is 14 percent higher than the 1/10 scale. The third pitch mode frequency of the full scale model is approximately three percent higher than the 1/10 scale model. Both the third and fourth mode shapes show that the 1/10 scale model is much more flexible around the SM-CM interface than the full scale vehicle. The full scale frequency for the fourth mode is 12 percent higher than the 1/10 scale frequency.

A correlation of the first and second longitudinal modes of the 1/10 scale and full scale test is presented in Figure 3-9. The first mode is produced by coupling between the liquid propellant and structure. The 1/10 scale mode shape follows the general trend of the full scale mode shape, but the amplitude is smaller at most locations. The full scale frequency of this mode is 23 percent higher than the 1/10 scale. The correlation of the second mode shapes shows the same general trend with the 1/10 scale model being more flexible in the IU area. The full scale frequency for this mode is 11 percent higher than the 1/10 scale frequency.

The third and fourth longitudinal modes of the 1/10 scale and full scale test are correlated in Figure 3-10. The correlation of the third mode shows that the 1/10 scale model is more flexible in the IU area. The full scale frequency of this mode is 13 percent higher than the 1/10 scale model frequency. The correlation of the fourth mode shows the 1/10 scale model responding more in the S-II stage, S-IVB stage, IU, and payload than the full scale model. Also, the flexibility of the IU joints is clearly shown by the kink in the 1/10 scale model mode shape at Station 3250. The full scale frequency is 6 percent higher than the 1/10 scale model frequency.

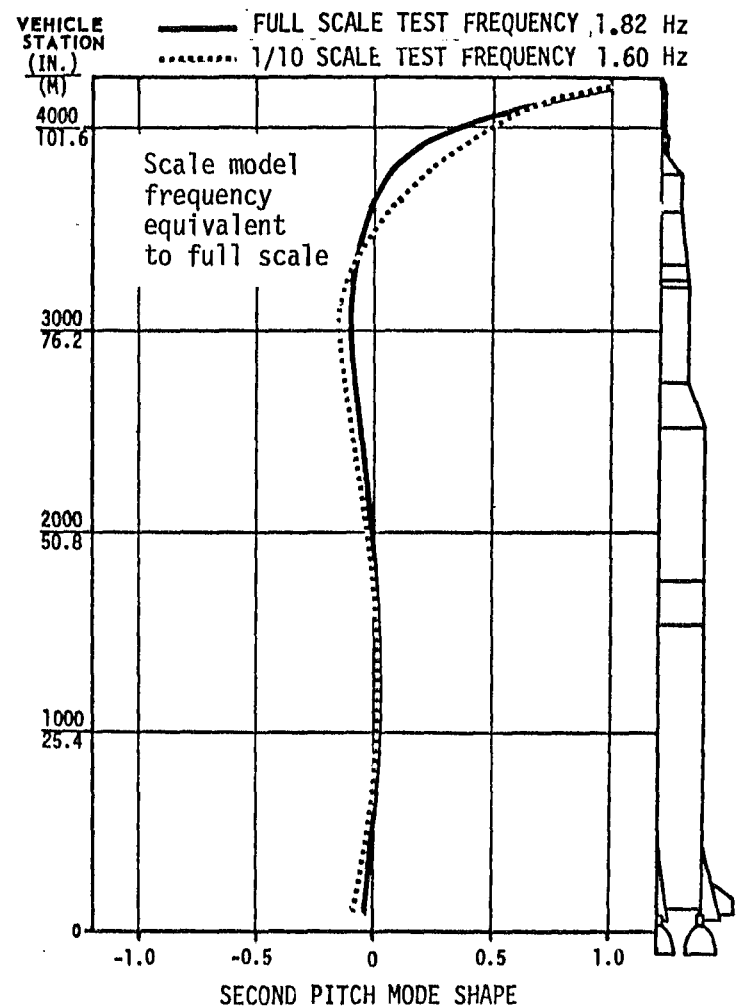
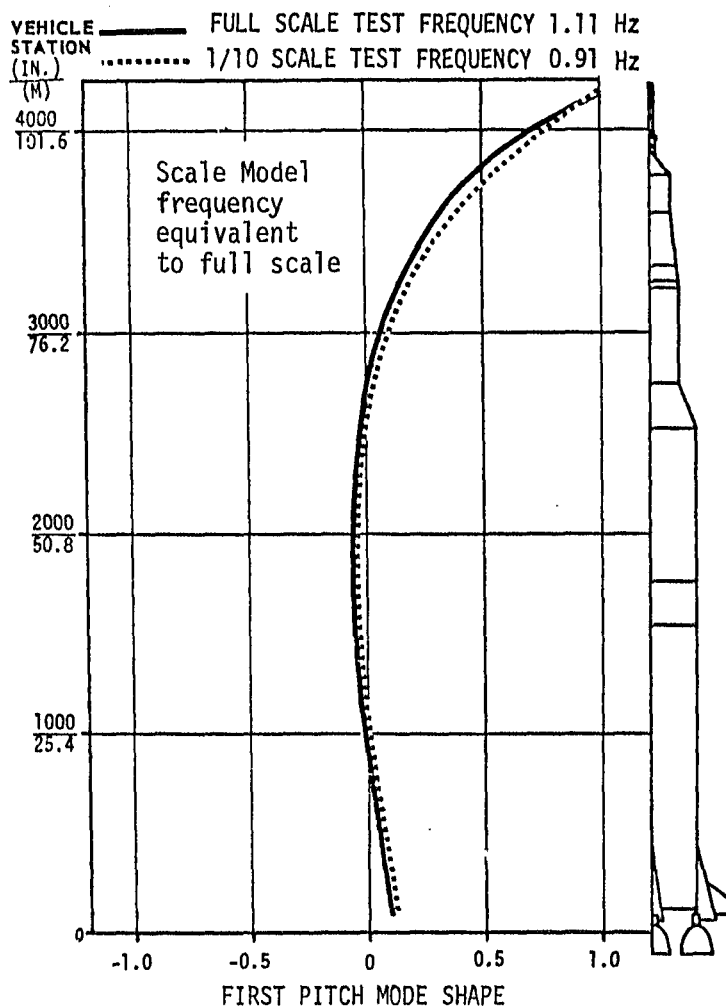
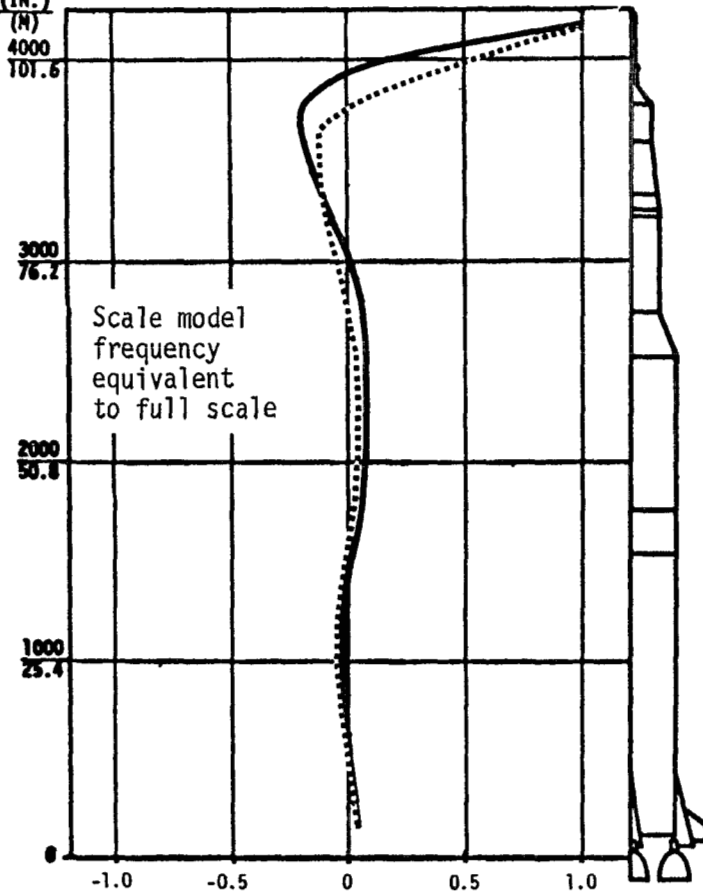


FIGURE 3-7 COMPARISON OF 1/10 SCALE AND FULL SCALE PITCH TEST RESULTS - MODES 1 AND 2 - 100 PERCENT PROPELLANT

VEHICLE STATION (IN.)
 (H)
 4000 101.6
 3000 76.2
 2000 50.8
 1000 25.4

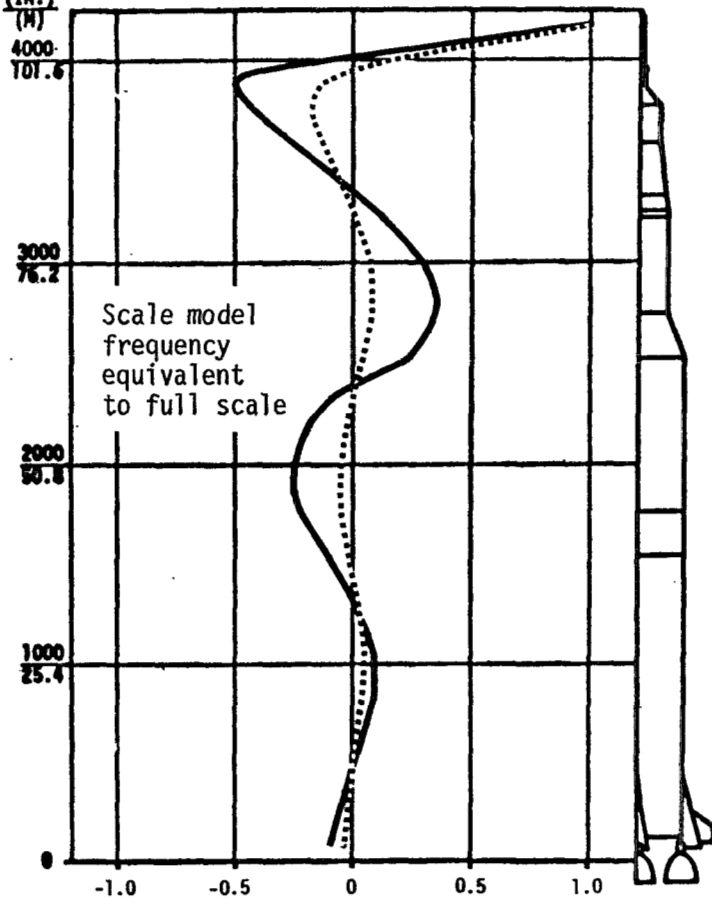
— FULL SCALE TEST FREQUENCY 2.55 Hz
 1/10 SCALE TEST FREQUENCY 2.48 Hz



THIRD PITCH MODE SHAPE

VEHICLE STATION (IN.)
 (H)
 4000 101.6
 3000 76.2
 2000 50.8
 1000 25.4

— FULL SCALE TEST FREQUENCY 3.44 Hz
 1/10 SCALE TEST FREQUENCY 3.04 Hz



FOURTH PITCH MODE SHAPE

FIGURE 3-8 COMPARISON OF 1/10 SCALE AND FULL SCALE PITCH TEST RESULTS - MODES 3 AND 4 - 100 PERCENT PROPELLANT

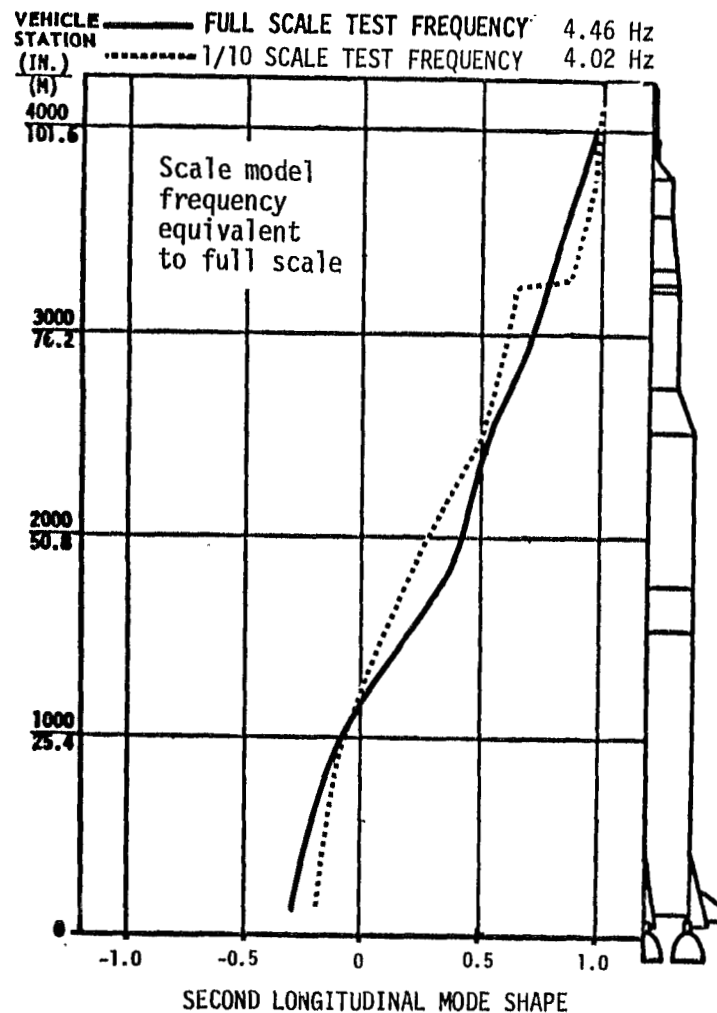
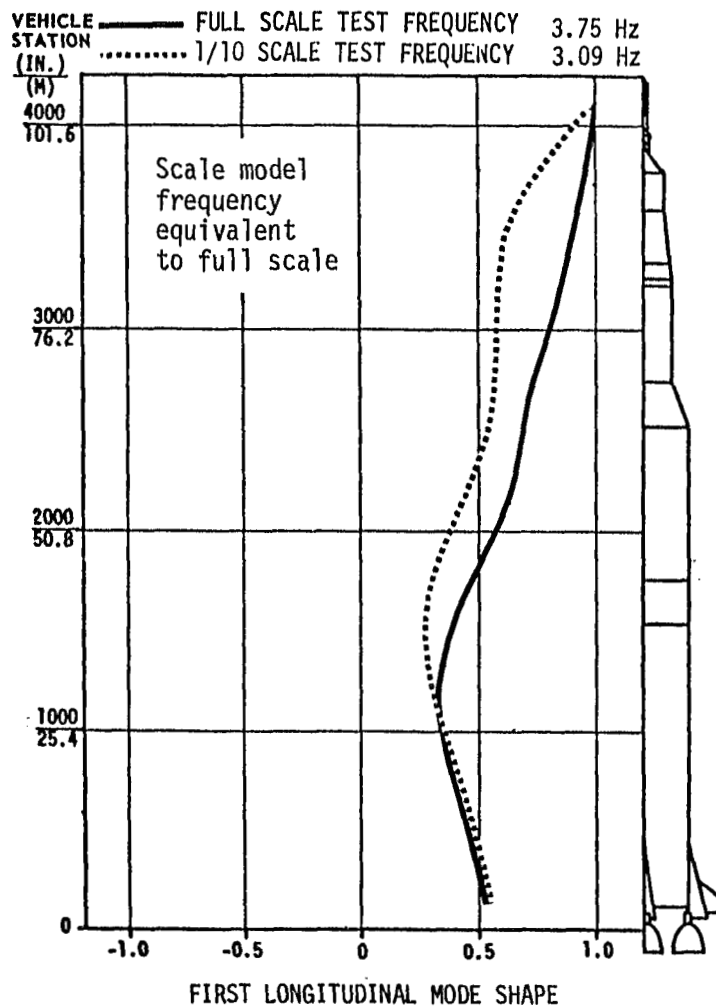
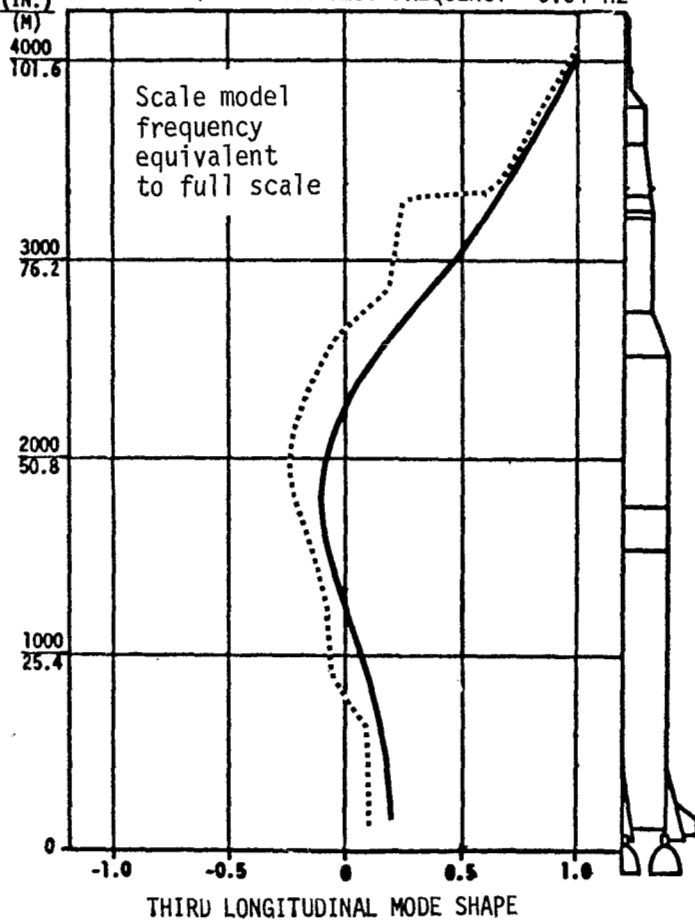


FIGURE 3-9 COMPARISON OF 1/10 SCALE AND FULL SCALE LONGITUDINAL TEST RESULTS - MODES 1 AND 2 - 100 PERCENT PROPELLANT

VEHICLE — FULL SCALE TEST FREQUENCY 6.51 Hz
 STATION (IN.) 1/10 SCALE TEST FREQUENCY 5.64 Hz



VEHICLE — FULL SCALE TEST FREQUENCY 7.57 Hz
 STATION (IN.) 1/10 SCALE TEST FREQUENCY 7.13 Hz

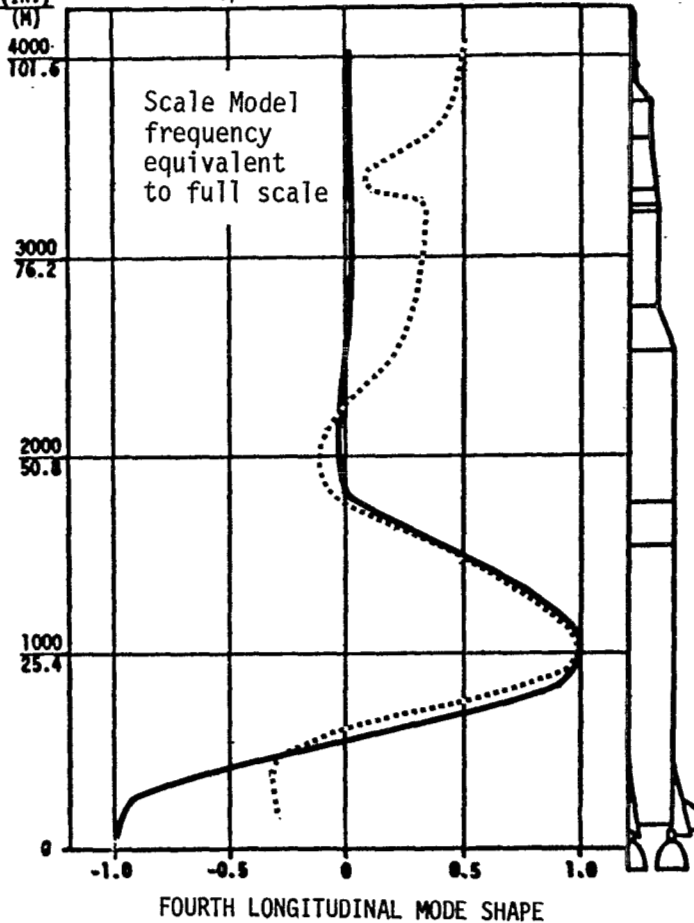


FIGURE 3-10 COMPARISON OF 1/10 SCALE AND FULL SCALE LONGITUDINAL TEST RESULTS - MODES 3 AND 4 - 100 PERCENT PROPELLANT

3.5.3 Scale Model Joint Flexibility

While analysis and test correlation uncovered major weaknesses in the math model, it also revealed a problem with the scale model joints. The model joints are scaled duplications of the prototype joints. Replica scaling of the joints was used since considerable engineering time would be required to properly design an easily manufactured connection with comparable dynamic properties.

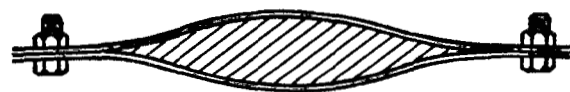
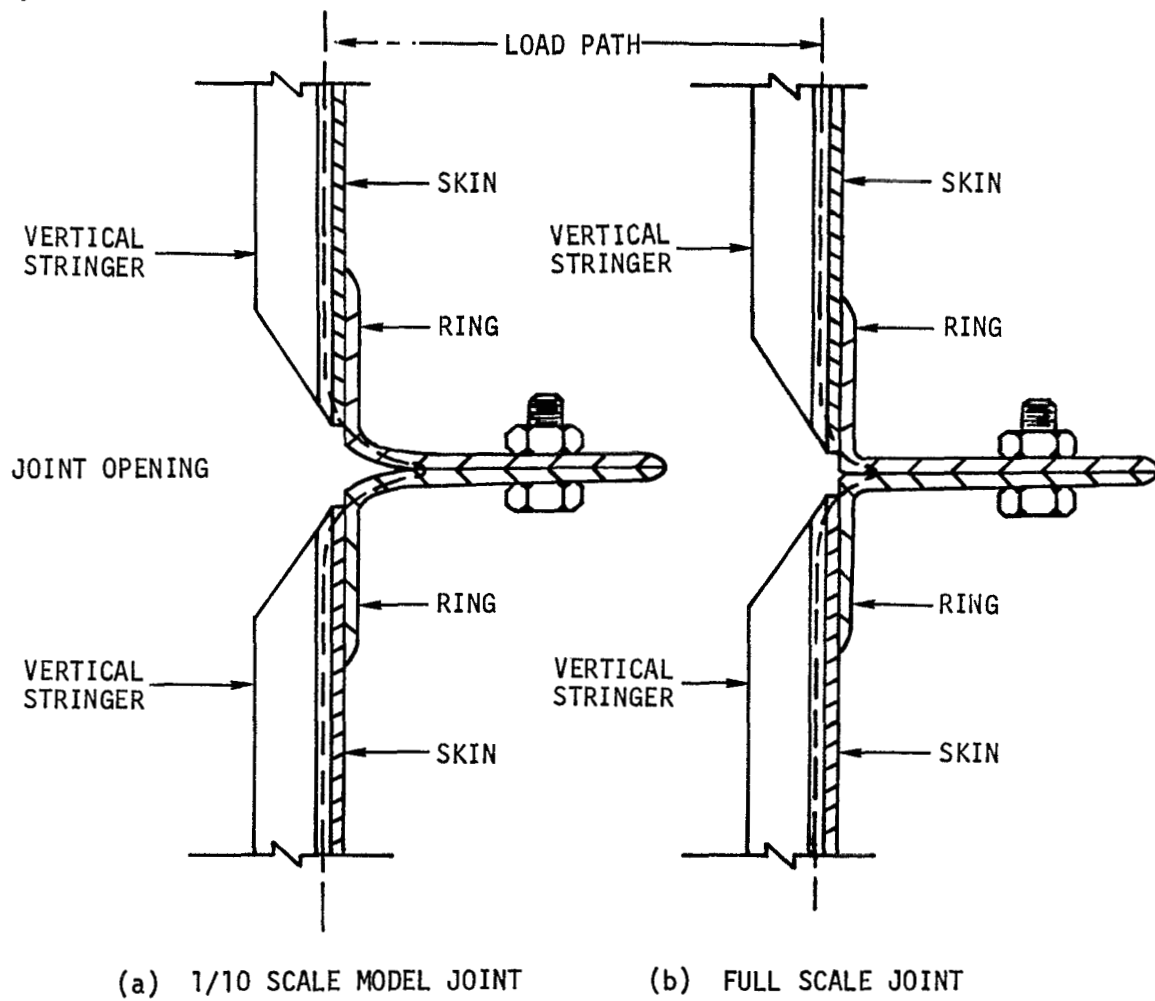
The joint flexibilities exhibited by the scale model can be explained if the joints are assumed to behave as illustrated in Figure 3-11. The physical rationale supporting these types of joint behavior is given below:

1. Due to the fabrication tolerances and the differences in ratios of stiffness and mass between the model and full scale vehicle, some model joints open slightly at the surface of the vehicle after the two flanges are bolted together. This phenomena is illustrated in Figure 3-11 (a) and is discussed in Reference 3-4. A fully effective joint, that is, where the stiffness of the joint approaches the stiffness of the skin, is presented in Figure 3-11 (b).

2. The model joints could gap between fasteners as shown in Figure 3-11 (c). This type of phenomenon could occur because the thin-flange ring frames used in the scale model would not hold their planar shape. Also, the number of fasteners used on the model was less than the number used on the full scale vehicle. Gapping between fasteners was observed along the joint between the S-IVB forward skirt and IU.

The stiffness of the joints presented in Figure 3-11 (a) and (c) is nonlinear and tends to increase under load.

The major cause of differences between scale model and full scale test results is the joint flexibility of the model. An additional cause was configuration differences between the scale model and test article spacecrafts. Had the model been redesigned to eliminate these differences, overall correlation would have been excellent for primary vehicle characteristics.

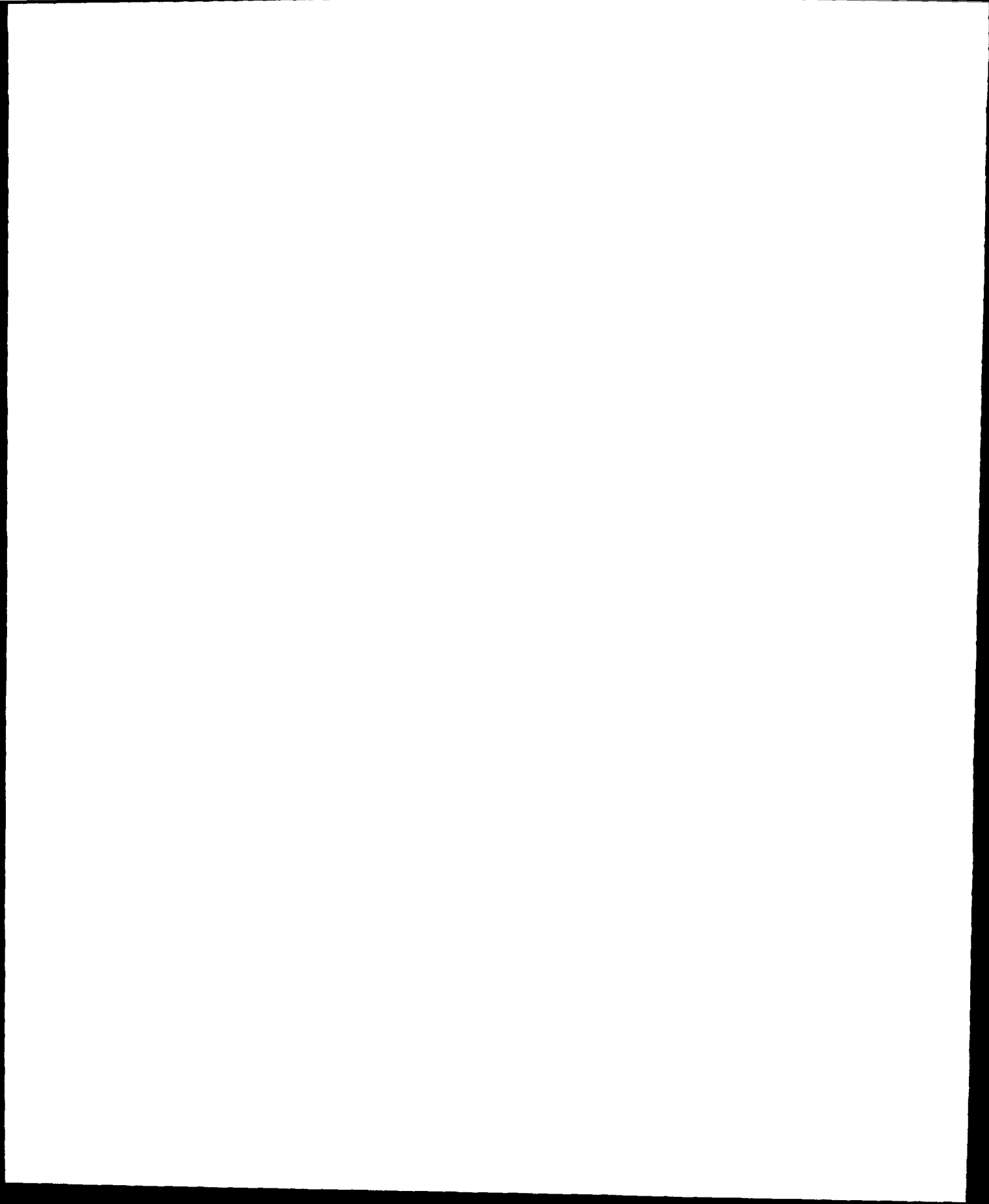


(c) SCALE MODEL GAPPING BETWEEN FASTENERS

FIGURE 3-11 LOAD PATH THROUGH 1/10 SCALE MODEL AND FULL SCALE JOINTS

REFERENCES

- 3-1 Leadbetter, Sumner A., Leonard, H. Wayne, and Brock, John E. Jr., Design and Fabrication Considerations for a 1/10 Scale Replica Model of the Apollo/Saturn V, NASA TN D-4138, October, 1967.
- 3-2 Pinson, Larry D. and Leonard, H. Wayne, Longitudinal Vibration Characteristics of 1/10 Scale Apollo/Saturn V Replica Model, NASA TN D-5159, April 1969.
- 3-3 Report LED-520-8, LTA-2 Vibration Survey at G.A.E.C., Grumman Aircraft Engineering Corporation, Bethpage, Long Island, New York, March 2, 1965.
- 3-4 Document D5-15631-A, 1/10 Scale Saturn V Model Structural Dynamic Analysis, The Boeing Company, Huntsville, Alabama, May 1, 1967.



SECTION 4.0 MATHEMATICAL MODEL TECHNOLOGY

4.0 GENERAL

This section presents procedures and guidelines for forming mathematical models of large space vehicles such as the Saturn V. The section includes discussions of math model philosophy, stiffness and inertia matrix development, and vibration analysis techniques. Problems that have been encountered are discussed along with the rationale for the solution; also guidelines for mathematical model development are presented.

The math modeling techniques used in the Saturn V structural dynamics program were adequate for predicting the overall vehicle dynamic characteristics. Most of the problems encountered in the program were associated with local deformation or component dynamics. These problems occurred because:

1. Proper emphasis was not given to math modeling of local and component dynamic effects.
2. Structural dynamic techniques require test results to guide the modeling of these effects.

Some of the problems associated with modeling local effects are presented in Section 4.3.

4.1 TECHNICAL APPROACH

Matrix formulation of structural dynamics problems was used extensively in the Saturn V program. The methods used in the pretest analysis are documented in Reference 4-1. These methods have since been revised and documented in internal Boeing documents. Each Saturn V structure was idealized as a lumped parameter system that satisfied the following matrix equation:

$$[M_{ij}] \{\ddot{q}_j\} + [C_{ij}] \{\dot{q}_j\} + [K_{ij}] \{q_j\} = F_i \quad (4.1)$$

Inertia	Damping	Elastic	Applied
Forces	Forces	Forces	Forces

The generalized coordinates, the q_j 's, used in a lumped parameter analysis are frequently chosen to be the Cartesian components of displacement and/or rotation at discrete points on the system. These points are known as nodes. A typical nodal breakdown is shown in Figure 4-1. In the lumped parameter approach the elastic properties of an actual structure are represented by a network of linear springs coupling the node points together. These spring constants, in matrix array, form the structural stiffness matrix. A typical element, K_{ij} , in this matrix represents the stiffness of the effective structural spring coupling q_i and q_j motions. All forces are applied to a lumped parameter model at the nodes and are distributed into the model by the springs which simulate the load paths in the actual structure. For example, when a force is applied in the q_i

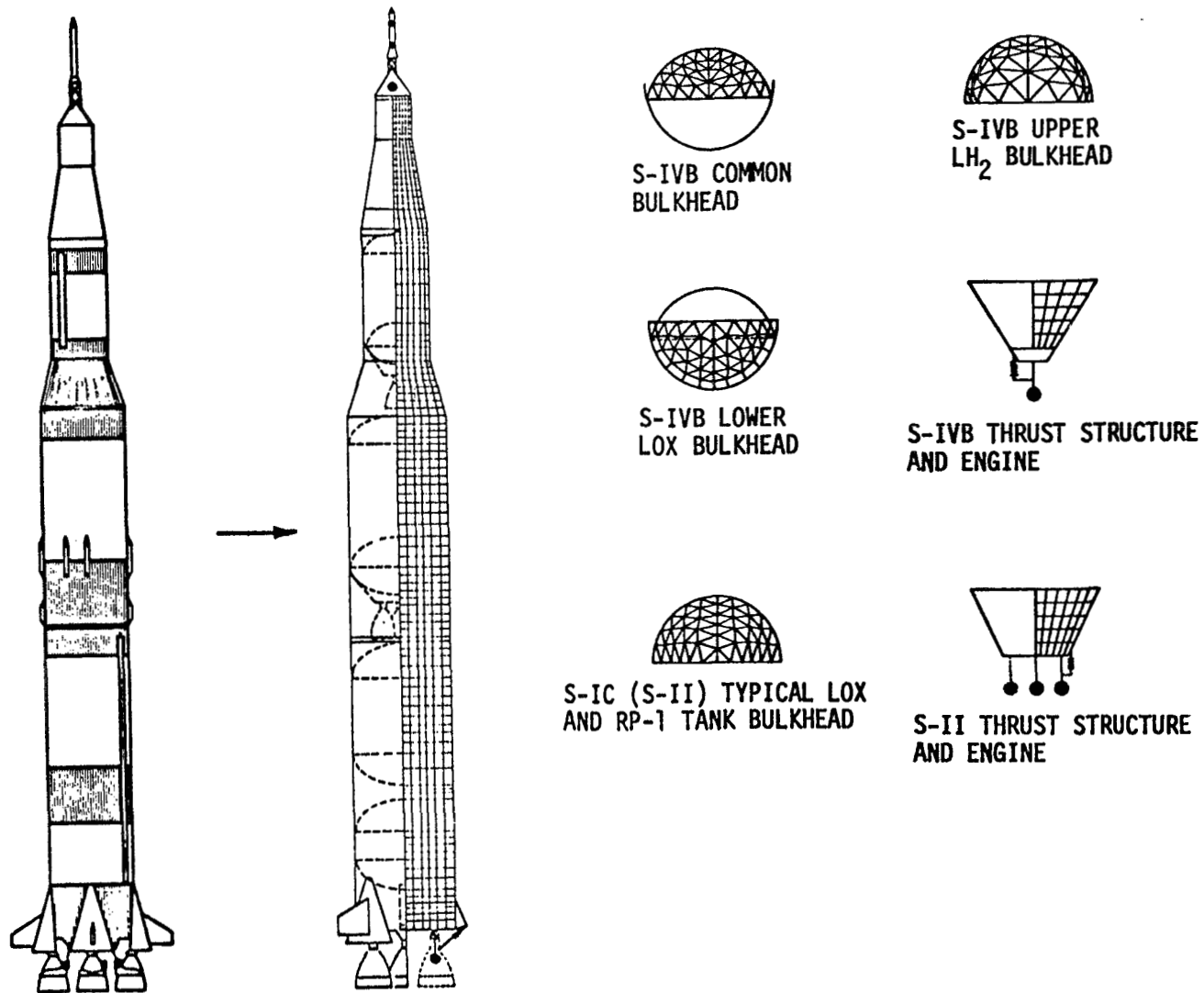


FIGURE 4-1 TYPICAL SATURN V NODAL BREAKDOWN

4.1 (Continued)

direction, a portion of the force will be transmitted through the spring K_{ij} to induce motion in the q_j direction.

In a dynamic model, mass matrices are developed to represent the distributed inertia characteristics of the actual system. These generalized inertia matrices range in complexity from a simple diagonal array of lumped masses to the strongly coupled generalized inertia arrays developed in Section 4.4.

Energy dissipative elements may be introduced into the model to simulate the effects of damping forces on the actual structure. Normally, the damping elements used in the model are linear. The characteristics of these damping elements are chosen so that the average rate of energy dissipation in the model over a cycle of oscillation is the same as that of the actual structure. Damping values used in the Saturn V analyses were obtained from the full scale dynamic test. These damping values are proportional, that is, all sections of the structure are assumed to have the same damping.

The lumped parameter model is completed by a set of concentrated time dependent loads applied at the node points. These loads represent the distributed forces, temperatures, or prestresses acting on the real system.

The most difficult part of the process of creating a lumped parameter model is obtaining a spring network that adequately describes the elastic properties of the system being analyzed. The structural spring networks may be obtained from a finite element displacement method, known as the direct stiffness method (Reference 4-2 and 4-3).

The direct stiffness method is derived from energy considerations. If the deformed shape of a system can be adequately described in terms of a limited number of independent quantities, for example, the deformations of a limited number of points on the structure, the actual system can be represented by a mathematical model having a finite number of degrees of freedom. The strain energy of the system can be expressed in terms of these generalized coordinates. The stiffness coefficients are derived from the strain energy quadratic.

4.1.1 Stiffness Analysis

Prior to establishing a stiffness model, detailed drawings of the structure are studied in order to determine mechanisms by which loads are transmitted through the system. Next, nodes are located on structural drawings at points along the primary load paths or in regions of critical motion. The actual structure connecting these nodes is then described in terms of combinations of the following basic elements:

1. beam - stringer - torque tube
2. plate (membrane)

4.1.1 (Continued)

3. plate (bending)

4. Axisymmetric shell

The plate and shell elements may be either isotropic or orthotropic.

Once the structural model has been established, the stiffness analysis computer program input data are compiled. These data include a list of node numbers, the geometric coordinates and boundary conditions of each node, along with the physical properties of each structural element; i.e., cross-sectional area, moment of inertia, thickness, type of material and temperature. Load information also may be contained in the input data. This includes prestresses, external forces, and nodal temperatures.

The stiffness program generates stiffness matrices for each structural element defined in the input data. Each matrix is generated in its own local coordinate system. Transformation matrices are computed and applied to obtain the stiffness coefficient components of each element in a central coordinate system. This system may be Cartesian, cylindrical, or spherical at the user's discretion. The stiffness matrix transforms from one coordinate system to another as follows:

$$\begin{array}{c} \text{NEW} \\ [K_{ij}] \end{array} = \begin{array}{c} \text{ORIGINAL} \\ [T_{pi}]^T [K_{pq}] [T_{qj}] \end{array} \quad (4.2)$$

where $[T_{pi}]$ is the transformation relating displacements in the original system to the generalized coordinates in the new system, and $i, j, p,$ and q are row and column indices.

Once the stiffness matrices for all elements have been generated and transformed to the central coordinate system, the stiffness coefficients are merged. The merging operation is basically a process of matrix addition in which corresponding stiffness coefficients from each structural element connecting at a given node are combined to obtain the stiffness properties of the structural model at that node.

After merging, the boundary conditions for the nodes can be imposed and matrix reductions performed. Boundary conditions for a stiffness analysis are determined by structural symmetry or antisymmetry as well as by physical constraints. For example, a typical launch vehicle, which has at least two orthogonal planes of symmetry, can be represented by a quarter shell model. The effects of the missing three quadrants of the structure can be represented by appropriate boundary conditions. Fixed boundary conditions are imposed on a stiffness matrix by deleting the rows and columns associated with the degrees of freedom at undeformable points on the structure. A pin joint is introduced by reducing the appropriate rotational freedom prior to merging.

4.1.1 (Continued)

Imposing boundary conditions is not the only way the size of the stiffness matrix is decreased. Frequently, the degrees of freedom subjected to small inertia loads are assumed to be unloaded. These degree of freedom can then be eliminated from the force-deformation relationships by a process of matrix reduction. Assume that the stiffness matrix is ordered so that direct stiffness of the unloaded degrees of freedom appear in the upper left corner of the matrix. The force-deformation matrix equation can then be partitioned as follows:

$$\begin{bmatrix} K_{uu} & K_{u\ell} \\ K_{\ell u} & K_{\ell\ell} \end{bmatrix} \begin{Bmatrix} q_u \\ q_\ell \end{Bmatrix} = \begin{Bmatrix} 0 \\ F_\ell \end{Bmatrix} \quad (4.3)$$

where the q_u are the displacements of the unloaded nodes, and the q_ℓ and F_ℓ are the displacements and forces, respectively, at the loaded nodes. The equation above can be solved for the q_u in terms of the q_ℓ :

$$\begin{Bmatrix} q_u \\ q_\ell \end{Bmatrix} = \begin{bmatrix} -K_{uu}^{-1} K_{u\ell} \\ I \end{bmatrix} \begin{Bmatrix} q_\ell \end{Bmatrix} = [T] \begin{Bmatrix} q_\ell \end{Bmatrix} \quad (4.4)$$

Applying the reduction transformation to Eq. 4-3 gives

$$[K_{REDUCED}] = [T]^T [K] [T] = [K_{\ell\ell} - K_{\ell u} K_{uu}^{-1} K_{u\ell}] \quad (4.5)$$

This same transformation will be used to develop consistent inertia matrices in Paragraph 4.4.3.

The dimensions of the reduced stiffness matrix are R rows and R columns smaller than the original matrix, where R is equal to the number of unloaded degrees of freedom.

The size of a stiffness matrix can also be decreased by the constraints transformation procedure. In the Saturn V models, the motion of many of the nodes was expressed in terms of polynomial shape functions satisfying the appropriate geometric boundary conditions. The shape functions were used to represent ring modes, simplify bulkhead models, and idealize near rigid substructure. These constraint transformations were applied to both stiffness and mass matrices so that consistency would be maintained.

4.1.2 Inertia Analysis

In the past, it was standard practice to construct mass matrices by simple lumping techniques. However, the improved accuracy obtained by developing inertia matrices and stiffness matrices in an identical manner is now widely recognized (Reference 4-4 and 4-5). Inertia coefficients are generated for the same fine nodal breakdown used in the stiffness analysis. The inertia matrices are reduced or constrained using the same transformations applied to the stiffness matrix.

The inertia characteristics of liquid filled tanks are handled by special techniques that represent the dynamics of the liquid as well as interaction with the elastic tank structure. On large booster systems, the liquid is usually treated as being incompressible, and the liquid free surface is assumed to remain plane. Under these conditions, the motion of the liquid can be defined by the elastic degrees of freedom of the tank. A technique for relating liquid motions to tank deformations is developed in Section 4.4.3.

4.1.3 Eigenvalue Analysis

After generating consistent inertia and stiffness matrices, the normal modes and frequencies of the system are obtained by solving the equation of undamped free vibration for the eigenvalues and eigenvectors.

$$[M_{ij}] \{q_j\} + [K_{ij}] \{q_j\} = \{0\} \quad (4.6)$$

If the system is free-free, the equation above will have up to six zero frequency solutions which are the rigid body modes of the system. These zero frequency solutions can be developed directly from the geometry of the system. The eigenvalue solution of large order systems can be costly, however. Modern computer techniques still take up to 75 minutes of computer time to obtain all of the mode shapes of a 300th order system, calculate the generalized mass matrix and plot the results.

4.2 MODELING PHILOSOPHY

The first step in developing a math model is to understand how results from the model will be used. The three prime uses for the Saturn V math models were for flight loads analyses, flight control analyses and Pogo stability analyses. Each of these analyses required special refinement in certain areas. Unfortunately, time and cost does not permit the use of sophisticated general purpose models. Consequently, it must be determined in advance where detail is needed and where gross representation will be adequate. In shell structures, such required foresight is often beyond realism. Ground and flight test data will point out deficiencies in the engineer's judgement. For this reason, there should be room in the model for growth. Growth potential is also required to allow for changing objectives of the program. For example, on the Saturn V, an accurate prediction of dynamic activity above 10 Hz was not required early in the program. After 18 Hz oscillations were observed in the flight data, it was necessary to develop mathematical models that could produce accurate results up to 25 Hz.

4.2 (Continued)

Once the use of the analytical results is established, the next step is to define a model that can satisfy user requirements. This requires that a number of technical decisions be made, such as:

1. Should the model be three-dimensional, two-dimensional, uniaxial, or some combination of these?
2. Where is shell activity important?
3. How fine should the nodal network be?
4. What are the limitations of the computer software and hardware used in the model analysis?

The first decision is to determine whether the dynamic characteristics must be described in the coupled (three dimensional) sense or whether a coplanar (two dimensional) or even a uniaxial model will suffice. Many space vehicles, including the Saturn V, have at least two orthogonal planes of symmetry for the primary structure. However, the internal structure and major components are often not symmetrical. These secondary asymmetries are a mechanism for coupling the coplanar modes of the primary structure together. If two of these modes should coalesce, even a small asymmetry can produce significant coupling that requires a three dimensional model. Another consideration is whether follow-on analyses can use three dimensional modeling and also whether the extra refinement is warranted. For example, if the dynamic loads are only 10 percent of the total load, the refinement in using a coupled model may not be warranted. A third consideration is whether restraining the structure to act in one plane will result in accurate characteristics in that plane. Using the Saturn V as an example, the proper in-plane characteristics of the LM cannot be predicted without allowing the LM to have out of plane motion.

The second decision is to determine where shell action must be included. Initial Saturn V models allowed for shell deformation throughout the complete launch vehicle. However, full scale tests confirmed that a beam model would represent launch vehicle bending action adequately up to a frequency of twenty times the fundamental bending mode. They also showed that the shell characteristics required a much finer nodal network than was originally provided, both in the instrument unit where flight sensors were located and in the bulkheads that carried the longitudinal propellant load. The present solution for Saturn V models is a combination of beam and shell modules that includes a detailed nodal network only in areas of significant local deformation.

The third decision is to determine how fine the nodal network should be. The first consideration here is the numerical accuracy that can be maintained during the solution procedure. The final stiffness matrix must be homogeneous, that is, the order of magnitude of like stiffness terms along the diagonal should be similar. If term-to-term fluctuations of two or more orders of magnitude occur, the analyst should anticipate

4.2 (Continued)

a large round-off error in his solution. The stiffness of each element is dependent on its size. Thus the nodes must be located so that stiffness magnitude changes occur gradually rather than abruptly.

In many cases, the structure itself dictates the degree of fineness. The engineer must allow sufficient nodes to simulate the physical load path and to allow efficient use of the elements available in the software program. When a stiffness mathematical model is developed on this basis, the engineer looks for sensitive areas in the structure from a dynamic standpoint. For example, the payload on the Saturn V is a highly active area compared with the launch vehicle. Consequently, the density of nodes is much higher in the payload than in the launch vehicle. Also, where high load gradients occur, such as in the thrust structure, additional model detail is required.

The final decision point in establishing a model involves the available computer software and hardware capability. This capability includes the size of the individual stiffness matrix modules that can be generated, the complexity of merging and reducing these modules, the order of the dynamic matrix that can be handled and the flow time and cost associated with each of the above computations. The natural tendency is to have a model as large as the computer capability will allow. This occurs either because of lack of confidence in the idealization of the structure or because the mathematical model may be required to do many different things. Both of these situations occurred in the Saturn V analyses. Initial model development did not include sufficient engineering judgement. The models presently in use, while greatly simplified in certain areas, are still complex because they handle problems in all dynamic disciplines.

Unless the resources are available to permit production analyses using large mathematical models, size limitations should be established early in the program. Of course, restricting the size of the model will increase engineering tolerances that must be placed on the math model data. Section 4.6 of this document describes the evolution of the Saturn V models. Resources required for math modeling were controlled to some extent by correlating a basic sophisticated model with test results and then carefully eliminating detail until a degradation of results became noticeable.

In large programs, such as Saturn V, the requirements of the mathematical models continually change as the program matures. Because of the constant state of change, the following two ground rules cannot be over-emphasized.

1. Establish a baseline model that where possible, is test verified.
2. Develop new models in parallel with the baseline model; do not change the baseline until the new models are completely verified.

4.2 (Continued)

Two baseline models were used in Saturn V analyses. The first baseline was a beam model that was useful in full scale pre-test work as well as in providing a gross check on the three-dimensional models. The second baseline model was the test-verified coplanar model. All subsequent models developed were validated by comparison of results with the baseline model. Only when these models had proven their superiority to the baseline model were they accepted as the new baseline.

Dynamicists were trapped in several instances by not adhering to the first ground rule listed previously. The "man on the moon in this decade" goal required strict adherence to schedules. Pioneering with new models and new software programs should not be attempted when the matrix order is large and the outputs of the analyses are program critical, both from a schedule and quality standpoint. New models should be developed in parallel with production analyses and phased into the analysis system only when they are fully checked out. Engineers and programmers habitually underestimate the cost and flow time for these changes.

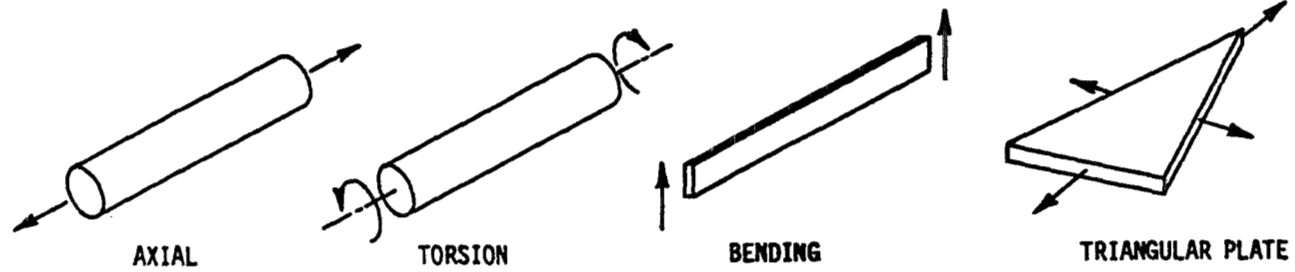
The dynamic characteristics generated from the Saturn V mathematical models were used by many government and contractor agencies. Structural dynamic characteristics were developed for each space vehicle and rigorously documented in source data documents. The configuration of each vehicle was tracked and when major changes were made, new structural dynamic characteristics were generated and the source data document updated. Despite this rigor, the dynamic characteristics were used improperly on a number of occasions. Experience has shown that written communication, although necessary, is not sufficient. Continuing face-to-face communication between the model developers and the users of the data is essential.

4.3 STIFFNESS MATRIX DEVELOPMENT

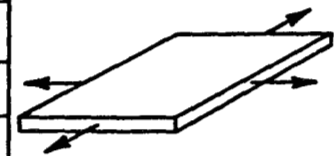
4.3.1 General Guidelines

Meeting the accuracy requirements of the Saturn V program made necessary a complex finite-element analysis. The linear direct stiffness method was used. The stiffness method is based on representing the actual structure by an assemblage of finite elements such as axial load members, bending members and plates. From basic structural theory the essential characteristics of each type of element are known. The science is well documented in References 4-2, 4-6, 4-7, and 4-8. But idealization of a structure to obtain a satisfactory, well behaved, mathematical model is an art as well as a science. The art as it applies to Saturn V math modeling will be covered herein and will involve the documentation of guidelines for using the finite element methods to solve practical structural problems.

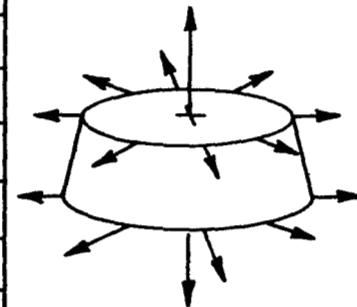
The elements used in the Saturn V analyses are shown in Figure 4-2 and are as follows:



INPUT PARAMETER	ELEMENT					
	AXIAL	TORSION	BEAM	△ PLATE	□ PLATE	SHELL
ELEMENT IDENTIFICATION	x	x	x	x	x	x
NODE IDENTIFICATION	x	x	x	x	x	x
MATERIAL CODE	x	x	x	x	x	x
NODE TEMPERATURE	x	x	x	x	x	x
TEMPERATURE GRADIENT				x	x	x
CROSS-SECTION AREA	x					
POLAR MOMENT OF INERTIA		x				
BENDING MOMENT OF INERTIA			x			
SHEAR WEB AREA			x			
MEMBRANE THICKNESS				x	x	x
BENDING THICKNESS				x	x	x



QUADRILATERAL PLATE



AXISYMMETRIC SHELL

FIGURE 4-2 MATH MODEL STRUCTURAL ELEMENTS

4.3.1 (Continued)

Axial members
Torsion members
Beam members
Isotropic triangular plates
Isotropic quadrilateral plates
Orthotropic triangular plates
Orthotropic quadrilateral plates
Axisymmetric shell element

The following paragraphs present some guidelines for the use of these elements. While the guidelines in some instances are a function of The Boeing Company software programs, they are typical of the types of limits imposed by software.

One of the prime considerations in defining a nodal network is to follow prescribed rules for plate geometry. To avoid numerical difficulties the length-to-width ratio of each plate element should not be greater than two and no angle within a triangular plate should be greater than 90 degrees. Triangular plates are generally used in making the transition from large plates to small plates. An example is shown in Figure 4-3. When making a transition from a stiff structure to a relatively soft structure, care must be taken in the transition zone. The soft structure idealization would normally imply a finer nodal network. The plate geometry rules previously cited must be kept in mind in creating the transition nodal pattern.

One of the common problems that occurs in the idealization of a structure is the generation of redundant degrees of freedom. Redundant degrees of freedom can be introduced into the math model unintentionally during the process of coordinate transformation. Such mechanisms are not present in the actual structure but arise through reorientation of the structural elements. This may be illustrated by means of a simple example. Consider a horizontal bar pinned at one end and supported by a vertical bar at the other end as shown in Figure 4-4 (a). Since only the axial behavior of the bars is of interest, the bending behavior is ignored. Assuming both bars have the same cross-sectional area, the stiffness matrix is:

$$[K] = \frac{AE}{L} \begin{bmatrix} \Delta x_1 & & \\ 2 & -1 & 0 \\ -1 & 1 & 0 \\ 0 & 0 & \Delta y_2 \\ & & 1 \end{bmatrix} \quad (4.7)$$

4.3.1 (Continued)

No lateral stiffness terms appear in the matrix for node 1 because the bending stiffness of the bar has been neglected. The matrix is non-singular and may be inverted to solve for the displacements of the nodes in a straight-forward manner.

Now consider the same physical problem but with the bars oriented at an angle of 45 degrees to their former positions as shown in Figure 4-4 (b). The stiffness matrix and load column for the rotated structure are obtained by coordinate transformation of the form.

$$\begin{aligned} [\bar{K}] &= [T]^T [K] [T] \\ \{\bar{F}\} &= [T]^T \{F\} \end{aligned} \quad (4.8)$$

where $[T]$ is the matrix of direction cosines relating the (x,y) system to the (\bar{x},\bar{y}) system. In this case, the transformed stiffness matrix and load column are,

$$[\bar{K}] = \frac{AE}{L} \begin{matrix} & \begin{matrix} \Delta\bar{x}_1 & \Delta\bar{y}_1 & \Delta\bar{x}_2 & \Delta\bar{y}_2 \end{matrix} \\ \begin{matrix} 1 \\ 1 \\ -1/2 \\ -1/2 \end{matrix} & \begin{bmatrix} 1 & 1 & -1/2 & -1/2 \\ 1 & 1 & -1/2 & -1/2 \\ -1/2 & -1/2 & 1 & 0 \\ -1/2 & -1/2 & 0 & 1 \end{bmatrix} \end{matrix} \quad (4.9)$$

$$\begin{Bmatrix} F_{1\bar{x}} \\ F_{1\bar{y}} \\ F_{2\bar{x}} \\ F_{2\bar{y}} \end{Bmatrix} = \frac{\sqrt{2}}{2} \begin{Bmatrix} F_{1x} \\ F_{1x} \\ F_{2x} - F_{2y} \\ F_{2x} + F_{2y} \end{Bmatrix} \quad (4.10)$$

The stiffness matrix in Equation (4.9) is obviously singular since the first two rows are identical. The process of transformation has introduced a redundant equation in the variable $\Delta\bar{y}_1$. The singularity arises from introducing two degrees of freedom at node 1 for the transformed structure where only one independent degree of freedom is defined. In this example either $\Delta\bar{x}_1$ or $\Delta\bar{y}_1$ may be considered as a redundant degree of freedom and may be constrained out. Choosing $\Delta\bar{y}_1$ as the redundant degree of freedom and imposing the constraint $\Delta\bar{y}_1 = \Delta\bar{x}_1$ gives:

4.3.1 (Continued)

$$[\bar{K}] = \frac{AE}{L} \begin{matrix} & \Delta\bar{x}_1 & \Delta\bar{x}_2 & \Delta\bar{y}_2 \\ \begin{bmatrix} 4 & -1 & -1 \\ -1 & 1 & 0 \\ -1 & 0 & 1 \end{bmatrix} \end{matrix} \quad (4.11)$$

and

$$\begin{Bmatrix} F_{1\bar{x}} \\ F_{2\bar{x}} \\ F_{2\bar{y}} \end{Bmatrix} = \frac{\sqrt{2}}{2} \begin{Bmatrix} 2F_{1x} \\ F_{2x} - F_{2y} \\ F_{2x} + F_{2y} \end{Bmatrix} \quad (4.12)$$

The stiffness matrix of Equation (4.11) represents the structure with a supporting roller on a 45 degree plane at node 1 as shown in Figure 4-4 (c). This renders the stiffness matrix non-singular and it may be inverted to solve for the displacements. An alternate solution is to include bending stiffness in the horizontal bar. This introduces an independent $\Delta\bar{y}_1$ equation which eliminates the redundancy.

If reductions are inadvertently performed at a node having a redundant degree of freedom, in theory a row and column of zeroes will be generated. These zero rows and columns are often automatically deleted within stiffness analysis programs so that the solution can proceed normally. However, because of numerical accuracy, true zero rows and columns are seldom generated in the reduction process. The result then is the retention of highly ill-conditioned nonphysical terms in the matrix.

In this simple example, the freedom to be constrained is quite obvious. But in more complicated structures using beams, axial members, torque tubes, and plates, redundant freedoms are easy to miss, especially if the engineer is not intimately familiar with the mathematics of the analysis program he is using. If he is aware of the program limitations, he can idealize the structure to eliminate redundant degrees of freedom. There are three ways of avoiding redundant degrees of freedom:

1. Include stiffness elements that resist forces and moments in all directions.
2. Constrain out redundant degrees of freedom, and
3. Choose a coordinate system consistent with the geometry of the problem.

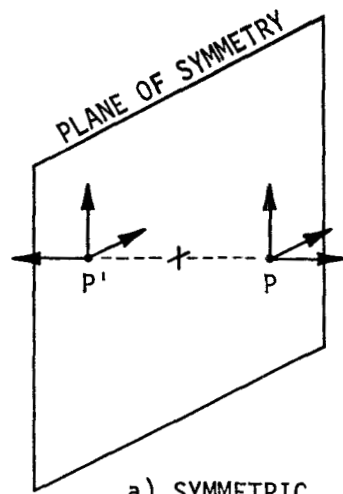
4.3.1 (Continued)

The first solution is not always acceptable. Adding additional elements introduces new force/deformation equations that may not be well conditioned. For example, a longeron may be stiff axially but weak in bending. If its bending properties are included, the resulting ill conditioned equations added to the problem may prevent an accurate solution from being obtained. The optimum solution is a combination of the last two solutions: choose the coordinate system to minimize transformation reorientation, then constrain all redundant degrees of freedom that appear.

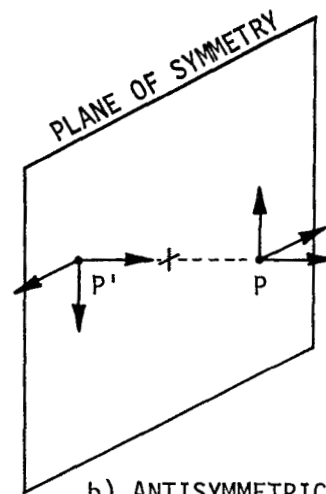
Taking advantage of a plane of structural symmetry to reduce the number of variables in a linear deflection analysis is a technique often used by structural engineers. The procedure derives from the fact that any part of a linear structure may be considered cut away and analyzed as a separate entity while retaining the effect of the whole structure by applying the proper boundary conditions at the cut. When the cut is made at a plane of structural symmetry, the boundary conditions are simply and uniquely defined by two distinct types of displacement modes, symmetric and antisymmetric. These boundary conditions may be deduced by considering the relative displacement of a point on the structure and its conjugate point, or "mirror image", on the opposite side of the plane of symmetry. For a symmetric displacement mode, any movement of the point will be accompanied by a corresponding mirror image behavior of its conjugate point as in Figure 4-5(a). For an antisymmetric mode the movement of the conjugate point will be exactly opposite to that produced in the mirror image. This is illustrated in Figure 4-5(b).

As the location of point P is chosen closer to the plane of symmetry, it is seen that points P and P' become coincident in the limit. Symmetric behavior of the coincident points is contradictory unless the motion is restricted by imposing constraints against translation out of the plane of symmetry and against rotation about any axis lying in the plane of symmetry. These constraints are the appropriate boundary conditions for symmetric behavior at a plane of structural symmetry. For antisymmetric behavior the appropriate boundary conditions are determined by similar reasoning to be just the opposite; i.e., constraints are imposed against translation in any direction lying in the plane of symmetry and against rotation about an axis normal to the plane of symmetry.

Apollo Saturn V stiffness and mass asymmetries were identified and assessed. The launch vehicle, below the payload, was found to be essentially symmetrical about the pitch/longitudinal and yaw/longitudinal planes. This symmetry allowed the launch vehicle to be represented by quarter-shell (coplanar) models. Four coplanar models were formed by applying either symmetric or antisymmetric boundary conditions at the quarter-shell cuts. These models were for pitch, yaw, longitudinal, and torsional analyses. Figure 4-6 shows the coordinate system and the quadrant used in the Saturn V analysis.



a) SYMMETRIC



b) ANTISYMMETRIC

FIGURE 4-5 STRUCTURAL SYMMETRY EXAMPLE

4.3.1 (Continued)

For pitch analysis (motion in the Z-direction), antisymmetric boundary conditions were applied at Boundary A, while symmetric boundary conditions were applied at Boundary B. For yaw analysis (motion in the Y-direction), symmetric boundary conditions were applied at Boundary A, while antisymmetric boundary conditions were applied at Boundary B. For longitudinal analysis (motion in X-direction), symmetric boundary conditions were applied at both Boundaries A and B. For torsional analysis (rotation about X axis), antisymmetric boundary conditions were applied at Boundaries A and B. The imposed boundary conditions used above constrain the vehicle centerline to move in a single plane. Cross axis coupling cannot be studied with such a model.

The Saturn V vehicle undergoes two temperature extremes. One extreme is due to the cryogenic propellants whereas the other is due to inflight aerodynamic heating. There are two methods of accounting for thermal effects in the finite element software program. The program has the capability of accepting discrete temperature values for each node plus a temperature gradient across plate sections. Through table look-up features, the program automatically accounts for temperature changes in the modulus of elasticity. The alternate method is to scalar multiply the free-free stiffness matrix of a module of the structure that is affected before merging with the other modules. The first method has the advantage of accuracy but the disadvantage that a new stiffness matrix must be developed for every flight time point analyzed. The latter method, which assumes a uniform temperature across the entire module, was used in Saturn V analyses to represent the average effect of temperature on the modulus of elasticity.

With large analysis programs that have critical schedules attached to the outputs, there is a tendency to forego normal engineering discipline in checking procedures and documentation of engineering calculations. In other words, the program tends to move faster than the documentation. Engineering management must take a firm stand on controlling checking procedures and insuring the preparation of good engineering notes. It is better to have a simple analysis rigorously checked and documented than to have an elegant analysis that is incompletely substantiated. The following guidelines for avoiding a schedule squeeze resulted from Saturn V experience.

1. Scope the model effort allowing a realistic "pad" for contingencies.
2. Never make model changes or improvements on a tight schedule if an existing model can produce acceptable results.
3. Place the most experienced engineers in the checking loop. A check on arithmetic is only a partial check.

4.3.1 (Continued)

Lapses in these disciplines result in severe penalties in doing the same work twice. Even more important, relaxing the checking discipline increases the risk that erroneous data will be released for use. Stiffness calculations must be prepared in a formal manner with adequate sketches and reference to the structural drawing number and the different vehicles for which the drawing is effective. All calculations require an independent check and should be initiated by both the originator and the checker. This is the prime engineering task in that it certifies as accurate the structural idealization and the elastic properties of the finite elements.

The structural geometry input to the computer program should be plotted to scale. The nodal points and finite elements should be positioned on this sketch. Using this technique, nodes out of position, elements missing, and elements duplicated will show up clearly. The above procedure should be automated.

The accuracy with which the nodal coordinates are described is highly important. For example, if a cylinder is being described in Cartesian coordinates, six significant figures should be used to define the nodal coordinates. The accuracy of the transformations from local to central coordinates depends on the accuracy with which the nodes are located.

The idealization will be determined more by the limitations of the computer programs (both in size and in numerical accuracy) than by physical properties of the structure itself. The analyst should investigate these limitations and be thoroughly familiar with them before ever starting an analysis. For example, if a stiff structure connects to a flexible structure, the difference in stiffness introduces numerical problems that may invalidate the analysis. The stiff structure will require wider spacing of the nodes, or will have to be represented as a rigid body. On flexible structure, too fine a breakdown can introduce numerical problems that destroy accuracy. Consider a ring represented by flat beam elements as shown in Figure 4-7. As the elements become smaller the angle θ between the elements becomes small. One of the three independent stiffness terms (Δx , Δy , Rz) approaches dependency. Eventually, reduction of one of these terms will introduce significant round-off error into the solution.

The computer generated stiffness matrix should be checked both mechanically and automatically. The mechanical check involves checking the stiffness matrix to insure all diagonal terms are positive and to check the diagonal terms against the physical situation. Ill-conditioned degrees of freedom or improper idealization often produce terms of unusually large or small magnitude. The automatic check consists of programming the computer to perform the following computations:

$$[K]^T - [K] = [0] \quad (4.13)$$

$$[K] \{\bar{\phi}\} = 0 \quad (4.14)$$

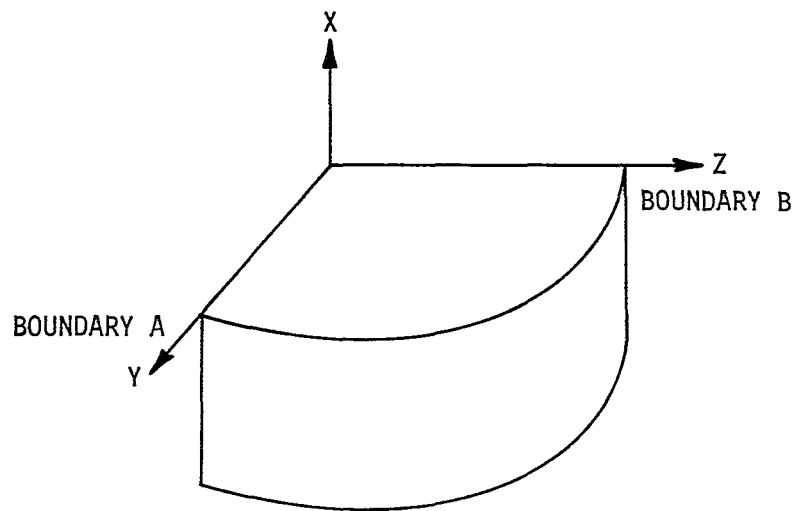


FIGURE 4-6 QUARTER SHELL ANALYSIS COORDINATE SYSTEM

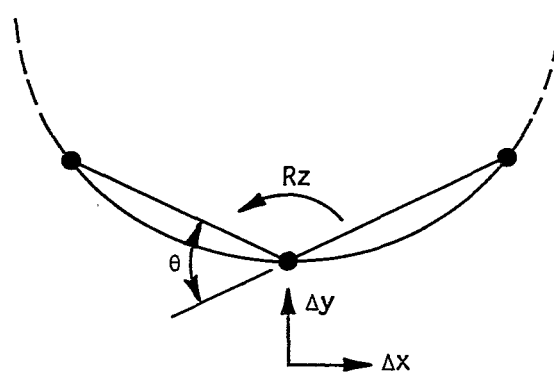


FIGURE 4-7 BEAM ELEMENTS FOR RING MODELING

4.3.1 (Continued)

where $[K]$ is the stiffness matrix and $\bar{\phi}$ is a rigid body vector.

The first computation checks symmetry and should result in a matrix of zeros. This check can be avoided if through all stages of stiffness manipulation (generation, merge, reduction, constraints), only a symmetrical half of the matrix is used. The second computation, used in a free-free system only, involves multiplication of the stiffness matrix by as many rigid body displacement vectors as the system has kinematic singularities. The resulting column matrices should show residual forces that approach zero. Due to numerical round off errors in forming and reducing the stiffness matrix, these residual force terms will not be exactly zero. Checking the output by this method will uncover improper restraints on the structural system introduced either in the idealization or the constraints operations. It is also a powerful check on round-off errors. For each row of the stiffness matrix, the permissible residual force resulting from a unit rigid body displacement should be at least five orders of magnitudes smaller than the diagonal stiffness term in that row. If the round-off errors are larger than this, the math model should be reviewed and the idealization changed to improve numerical accuracy.

In conducting a computer analysis of a complex system, it is easy to lose sight of the physical realities of the problem being solved. Computer programs are an aid to experience and engineering judgement, not a substitute for them. A computer solution requires all of the skills displayed in a hand solution, plus an intimate knowledge of how the computer program works, what its limitations are, and what numerical problems are apt to occur.

At all points in the computer analysis, checkpoints with physical reality need to be planned in. Always precede a complex analysis with a good simplified analysis. This will provide a gross check on the answers a complex analysis is giving. In checking out a complex analysis, cantilever the system and invert the stiffness matrix. Multiply the stiffness matrix by its inverse. This product should yield an identity matrix. Check the product matrix. If the diagonal terms are different than unity by more than +0.001, or the off-diagonal terms are different than zero by more than +0.001, the idealization should be reviewed to eliminate the source of the numerical difficulty. Plot the force/deflection coefficients. Examine them carefully. Does point B deflect to the left when engineering judgement says it should go to the right? If so, stop and investigate until either an understanding of the physical mechanism that makes point B deflect to the left is gained or a modeling error has been identified.

Take advantage of all available test data. The major structural assemblies such as thrust structures, interstages, and tanks, are usually subjected to static loading. Become familiar with these tests. Try to influence the tests to obtain data that can be used to check the model. Never pass up an opportunity to put the model to the test. Has someone else modeled the same structure? Meet and compare notes; where differences exist, resolve them on the basis of physical arguments rather than size

4.3.1 (Continued)

and complexity. A 10th order model may reveal a major flaw in a 1000th order model.

Over the period of time covered by a major program, continuing computer hardware development will dictate software changes. On the Saturn V program, early work was done with computer routines developed in the 1950's. The advent of new generation hardware forced the conversion of virtually all structural dynamics routines. In a limited number of cases, the conversion was accomplished directly from one computer language to another; however, for the majority of programs the opportunity to open up operational routines for updates, improvements and general cleanup was irresistible. Consequently, the conversion process becomes time consuming and costly, since some amount of new programming and error elimination activities are required.

Even direct conversion requires some amount of programming, such as revising machine language level routines to FORTRAN compiler levels. Due allowance for these types of perturbations and their associated schedule impacts must be made. In the case of the Saturn V dynamic analysis work, the change from IBM 7094 to the IBM 360/67 system required the revision of the direct stiffness finite element program, slosh dynamics program, eigenvalue solution programs, various dynamic response programs, and associated programs such as matrix algebra and mass characteristics. These revisions took place over a period of 18 months and required the full time participation of 12 engineers and programmers. This was three times the original estimate. The impact was caused by such subtle items as lack of proper assessment of the effect of word length differences between the two machines. The IBM 360 has a shorter single precision word length than the IBM 7094. The same math models being analyzed successfully on the IBM 7094 would not provide satisfactory accuracy on the IBM 360. All stiffness analysis algorithms had to be reprogrammed in double precision arithmetic to give acceptable results.

The problem of computer system accuracy is of immediate concern to the practicing dynamicist. The finite element approach to stiffness analysis of a complex structure necessarily involves thousands (quite possibly millions) of multiplication-addition operations on the computer. Round-off and truncation errors, small differences of large numbers, division by near zero and other similar numerical problems cannot be assumed as automatically self-cancelling. Indeed, the computation process can become unstable as problem size increases. It is difficult to design the math model complexity to be optimal from the computation standpoint; however, there is a distinct trade between model size and numerical accuracy.

An investigation was conducted to compare the numerical accuracy of the IBM 7094 and 360 computers. The model used in this investigation was a uniform straight bar of cross section A and length L . The baseline model represented this bar as a single finite element with an end-to-end stiffness of AE/L . Then the bar was divided into equal length elements, in steps of 50, up to 300 elements as illustrated in Figure 4-8. For each

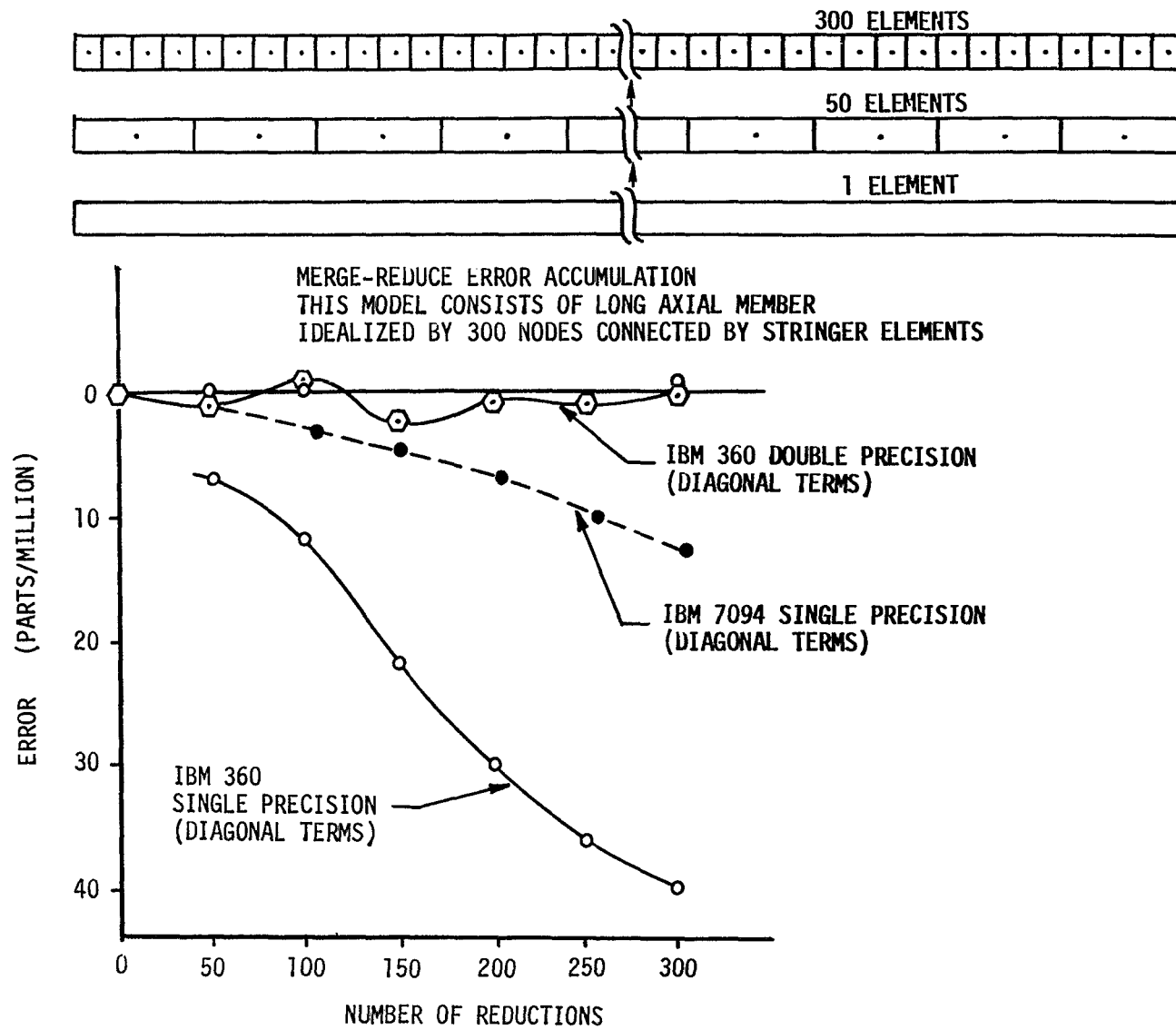


FIGURE 4-8 MERGE-REDUCE ERROR ACCUMULATION

4.3.1 (Continued)

step the element stiffness was calculated, merged, and reduced to obtain a single end-to-end stiffness term for the bar. For each model, stiffness error terms were calculated and plotted as a percent of the baseline stiffness as shown in Figure 4-8. The error was the difference between the calculated stiffness and the theoretical stiffness AE/L .

For the 300 element model, the IBM 7094 error was 10 parts per million, while the IBM 360 error was 40 parts per million. Both machines were using single precision arithmetic. The maximum error of 40 parts per million may seem small. However, this is near the threshold where results obtained from the stiffness matrix start showing accuracy problems. For example, moment coefficient diagrams may fail to close satisfactorily. The roundoff error also occurred after only 300 reductions. In an actual system, tens of thousands of reductions are often required.

The accuracy obtained using single precision arithmetic on the the IBM 360 computer was not adequate for the Saturn V analysis. Conversion of key algorithms to double precision arithmetic solved the IBM 360 accuracy problem. As shown in Figure 4-8, the maximum round-off error in the uniform bar problem was reduced from 40 parts per million to four parts per million by using double precision arithmetic.

Another case considered was that of inverting a 100th order stiffness matrix, with the check performed on the KK^{-1} product. Single precision arithmetic on the IBM 360 produced off-diagonal terms (which should be zero), in excess of unity. Double precision operations improved the results such that no off-diagonal terms exceeded 0.1, but still the results could not be used. The model had to be re-idealized to improve the numerical accuracy. These examples indicate the necessity for the dynamicist to understand the limitations of computer analyses, and to be alert for the symptoms of numerical round-off error.

4.3.2 Idealization Examples

The Saturn V vehicle can be represented by several classes of structures. Specific examples of these classes are presented in the following sections, providing practical applications of the techniques discussed in the preceding section. Even though the vehicle can be physically represented by the following classes of structures, the final model may be simplified in certain areas. For example, the initial idealization of the Saturn V launch vehicle included shell modeling for all tanks, inter-stages, and thrust structures. Subsequent correlation with dynamic test results showed that this level of detail was not required to represent bending in the launch vehicle, although axisymmetric shell modeling was required to represent longitudinal liquid and structural coupling in the tanks. Test results also showed the necessity for a shell representation in the payload, including a very fine grid in the instrument unit area to allow correlation at flight control sensors. See Figure 4-9 for decomposition of Saturn V into classes of modules.

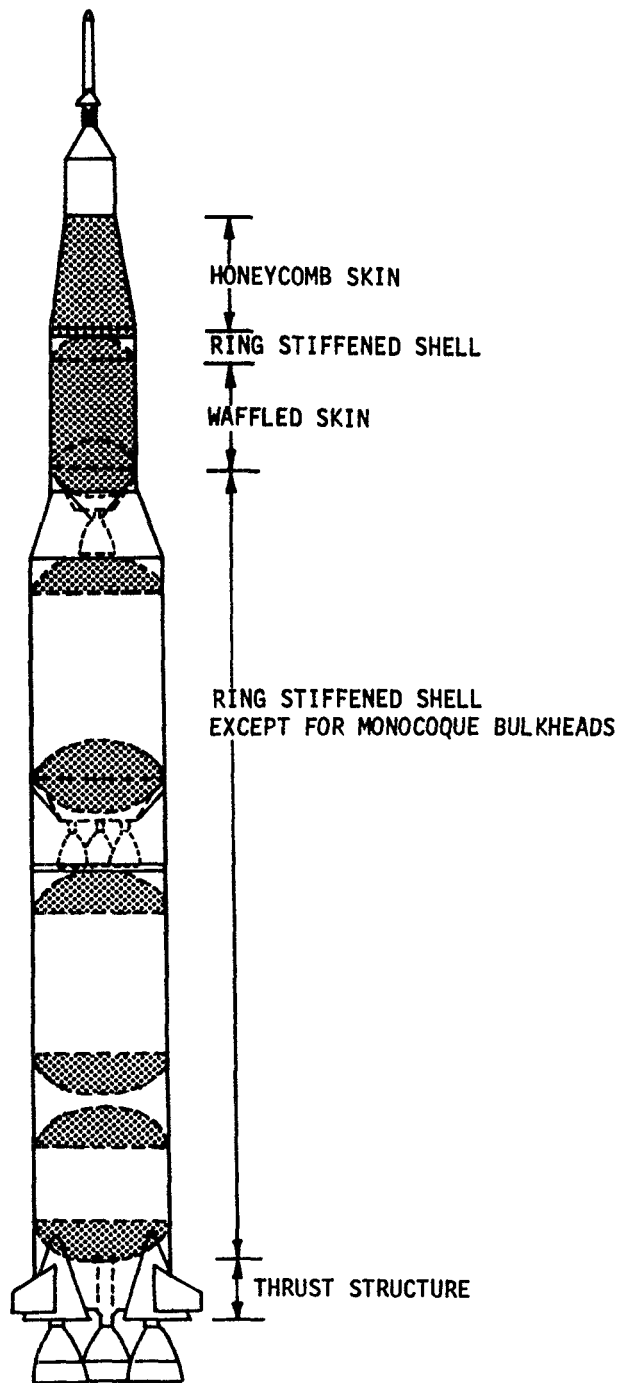


FIGURE 4-9 CLASSES OF MODULES FOR THE SATURN V MODELS

4.3.3 Shell Idealizations

Shell structure employed in the Apollo Saturn V vehicle can be classified into four groups: (1) ring and stringer stiffened shells, (2) honeycomb shells, (3) monocoque bulkheads, and (4) thrust structures.

A. Ring and stringer stiffened shell idealization

Most of the mainline structure of the Saturn V launch vehicle consists of ring and stringer stiffened shells. An example of a ring stiffened shell is the S-IVB forward skirt shown in Figure 4-10. Note that the 108 hat stiffeners have been idealized as only eight stringers having the same total cross sectional area. The stringers on the Y and Z boundaries in the model have half of the cross sectional area of the others.

The Apollo Saturn V shell structure consists of horizontal ring stiffeners, vertical "hat" stiffeners, and thin plates. In idealizing the basic ring stiffened shell it is advantageous to locate node lines on the rings. On Saturn V, it was found that a ring of nodes could be located at each ring stiffener without violating the plate geometry limits given in Section 4.3.1 if the nodes were placed at 15 degree intervals around the perimeter. If there had been too many rings to use this technique, then the rings would be "smeared" over the distance between the nodes. For the case with nodes at each ring, only the membrane properties of the plates are required to define well conditioned load paths. If more nodes are required than there are physical rings, node lines are positioned between rings. The bending properties of the plates must then be included so that the math model represents a kinematically stable system or the actual rings must be subdivided into a greater number of idealized rings.

When a shell is stiffened with vertical stringers, the axial characteristics of the stringer are included. The local bending characteristics are usually ignored because they contribute little to the overall bending stiffness of the cross-section. An exception to this is when accurate local deformations are required. Local discontinuities in the structure (such as cutouts, doors, local stiffeners or protuberances) may or may not be a concern. If local deformations are not required, the effects of local discontinuities can be ignored. For example, the hatch openings in the boosters are not considered in the idealization.

B. Honeycomb shell idealization

Much of the payload of the Saturn V is made of honeycomb shells. This includes the spacecraft lunar module adapter/instrument unit area (SLA/IU) in which the flight control sensors are located. Results from the dynamic tests showed that a very fine grid was required in this area to allow correlation of dynamic characteristics at flight control sensors. The SLA consists of a honeycomb skin with four ring stiffeners as shown in Figure 4-11. This Figure shows the required nodal breakdown for the SLA/IU

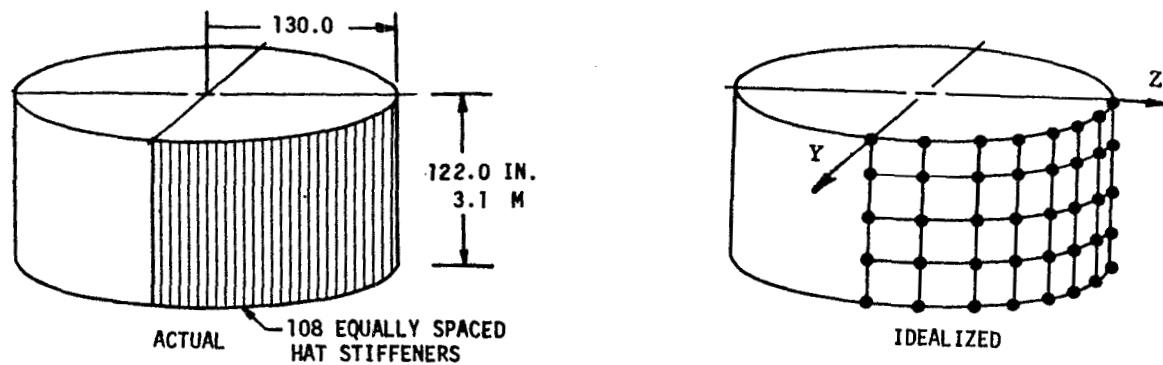


FIGURE 4-10 S-IVB FORWARD SKIRT NODAL BREAKDOWN

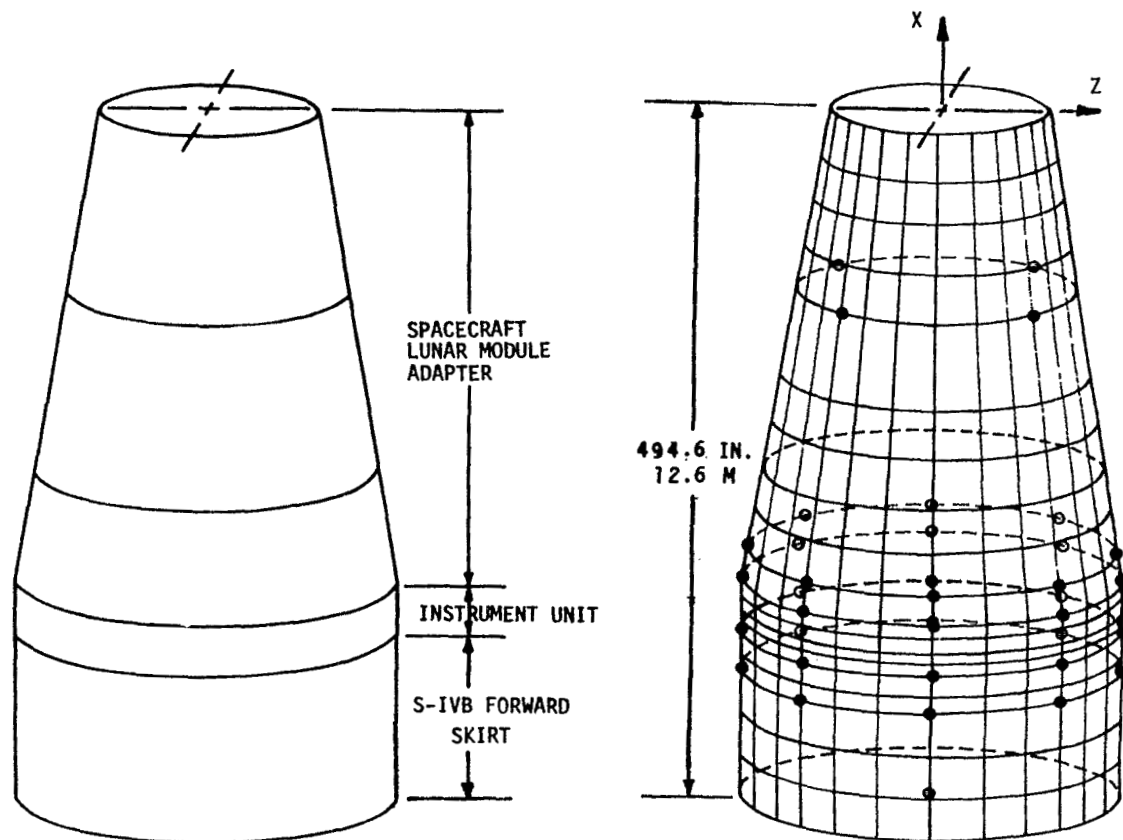


FIGURE 4-11 SHORT STACK NODAL BREAKDOWN

4.3.3 (Continued)

region. Ring stiffeners are located at only five levels of nodes. Consequently, the idealized plates in the honeycomb area are required to include the bending properties as well as the membrane properties.

The IU is a 36 inch (91.5 cm) high honeycomb section with small ring stiffeners at top and bottom. Within the instrument unit, "Black Boxes" are mounted on 16 thermal conditioning plates around the interior circumference. These plates are 30 inches (76.2 cm) square and approximately 1.25 inches (3.18 cm) thick (see Figure 4-12). In some modes, local deformations cause a change in sign of the slope between the top and bottom of the plate. These local deformations are produced by the way dynamic loads from the spacecraft are carried through the instrument unit. Up to 20 Hz, local IU dynamics had little influence on these deformations. In turn, these local effects have little influence on overall vehicle response. Therefore, the local deformations can be obtained by applying dynamic loads from the top of the SLA, bottom of the IU, and the LM and solving an equivalent static problem.

The honeycomb plate is idealized as an equivalent monocoque plate. Equivalent membrane and bending thicknesses are calculated as follows:

$$\tau_{em} = \tau_u + \tau_l \quad (4.15)$$

$$\tau_{eb} = \{12[\tau_u d_u^2 + \tau_l d_l^2]\}^{1/3} \quad (4.16)$$

where τ_{em} = equivalent membrane thickness, τ_{eb} = equivalent bending thickness, τ_u and τ_l are the thicknesses of the two honeycomb face sheets, and d_u and d_l are the distances from the honeycomb neutral axis to the centers of the two face sheets. The honeycomb geometry is shown in Figure 4-13. The engineer must be careful to include enough structural members to prevent any redundant freedoms, especially normal to the plate. (See Section 4.3.1).

C. Bulkhead idealization

When the propellant tanks are full, the lower and common bulkheads in the Saturn V structure support 90 percent of the total vehicle mass in the longitudinal direction. Consequently, the stiffness idealization of this structure is of prime importance in modeling for longitudinal dynamics. The interaction between breathing motion of the shell and longitudinal motion of the liquid must be understood and modeled. The first longitudinal mode of the S-IC boost configuration at liftoff is a tank and bulkhead mode characterized by large bulging motion of the S-IC LOX and fuel tanks. Consequently, the bulkhead and tank mathematical model must be compatible with the technique that will be used to represent liquid and tank interaction. The technique used in the Saturn V analyses is presented in Section 4.4.3.

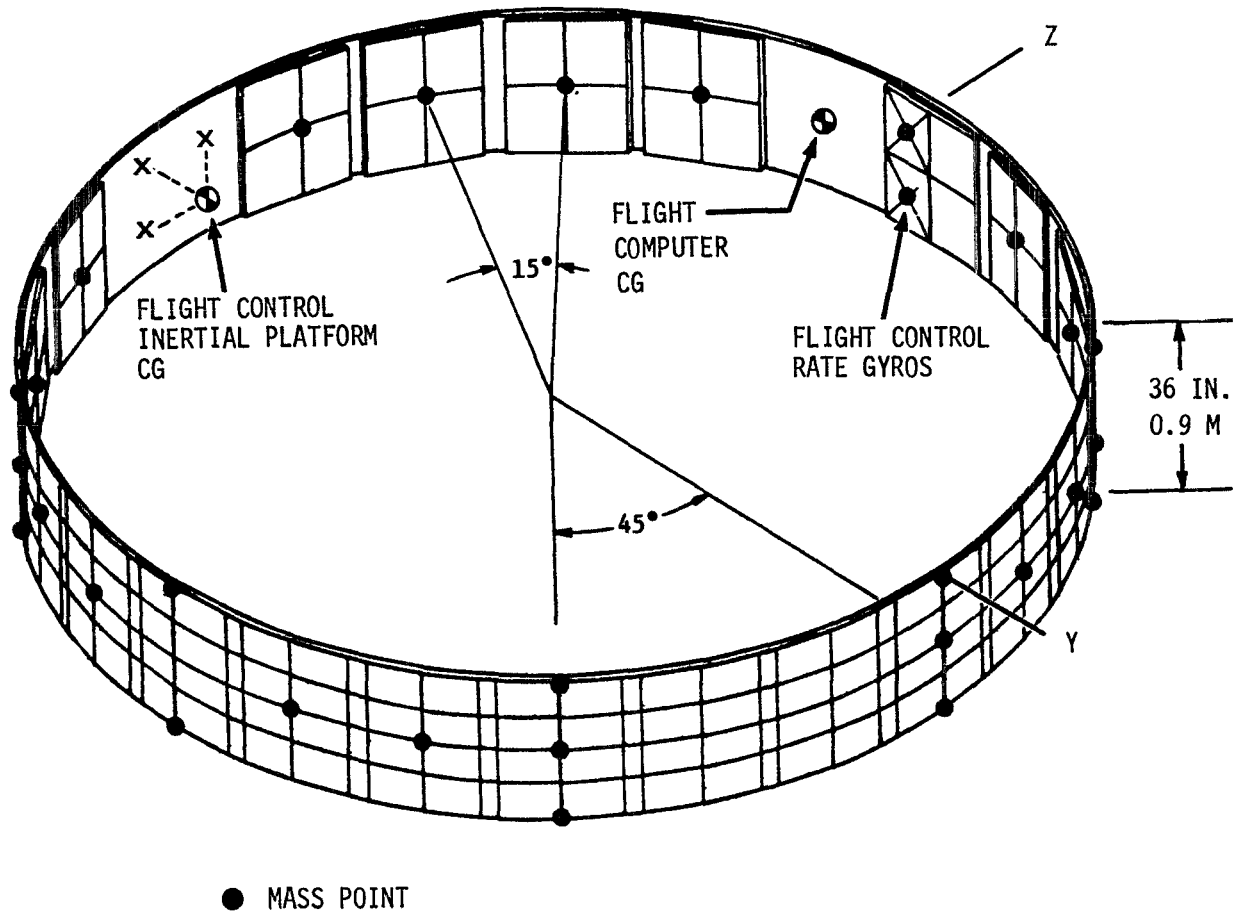


FIGURE 4-12 INSTRUMENT UNIT MODEL

4.3.3 (Continued)

The Saturn V bulkheads were modeled in quarter-shell detail with appropriate constraints at the boundaries. The bulkheads were idealized by a network of triangular plates. The limitations on the plate geometry discussed in Section 4.3.1 were observed in defining the nodal breakdown. Quite often "waffle" skins with milled stiffeners exist in bulkheads. These plates are represented by uniform plates with the same average thickness and bending moment of inertia.

In lower bulkheads, the stiffening effect of the membrane prestress from the static load is important. In ellipsoidal shells, a major section in the bottom of the tank is quite flat. Using flat plates or truncated cones to represent the curved surface exaggerates this flatness. Under static load, the shell stretches until the bulk of the load is carried via membrane action. The load carrying mechanism is analogous to a stretched cable. (See Figure 4-14.) The higher the prestress S , the more effective the cable is in carrying the normal load F . If small perturbations, $\delta\Delta$ about the loaded equilibrium position are being investigated, the cable action can be approximated by a linear stiffness relationship

$$\delta F = \frac{2S}{L} \delta\Delta \quad (4.17)$$

A similar linear approximation applies for prestressed plates. If this prestress mechanism is not modeled, the load carrying capability of the idealization is limited to bending action alone in the bottom of a bulkhead. The idealization will be much more flexible than the actual bulkhead.

The prestress stiffening effect can be developed as an incremental stiffness matrix to add to the linear solution.

$$[K_{TOTAL}] = [K_{LINEAR} + K_{PRESTRESS}] \quad (4.18)$$

The linear stiffness matrix is independent of tank pressure and propellant level. Only the stretch stiffness terms change for each propellant and pressure condition analyzed.

To avoid having to change the stiffness matrix with flight time, the prestress effect was not included in the Saturn V analyses. Instead, polynomial shape functions were used to simulate the correct inertia load and to distribute this reaction higher in the bulkhead where the problem just discussed does not occur. This approach represented the dynamics of the primary structure accurately; however, it did not predict tank bottom fluid dynamics adequately. The latter characteristics proved to be important in resolving high frequency Pogo problems. A discussion of the Saturn V tank models, their accuracy and limitations, is presented in Section 4.4.3.

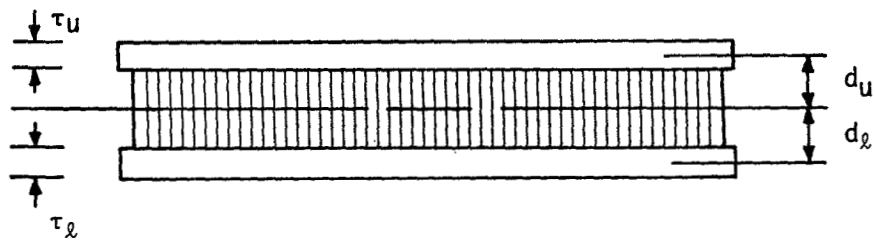


FIGURE 4-13 HONEYCOMB GEOMETRY

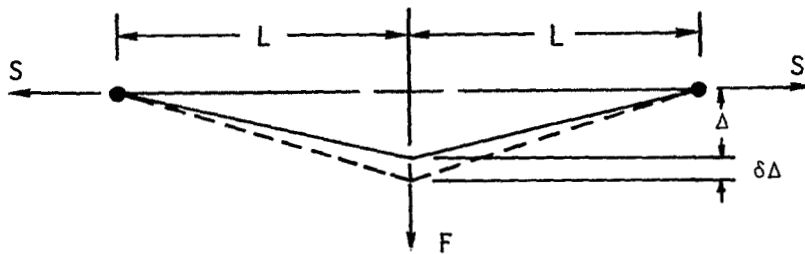


FIGURE 4-14 BULKHEAD/CABLE ANALOGY

4.3.3 (Continued)

D. Thrust structure idealization

The thrust structures for each stage of the Saturn V are different. The S-IC structure requires massive rings, crossbeams, and longerons to allow the loads from holddown and thrust to be equally distributed around the circumference in the tank area. The thrust structure is a ring stiffened shell with four vertical thrust posts and four vertical holddown posts as shown in Figure 4-15. The thrust and holddown loads are distributed into the ring stiffened shell through shear in the plates.

Early in the Saturn V program, the S-IC thrust ring was found to be so rigid that it was introducing numerical problems into the model. These problems were eliminated by constraining the ring to be rigid. This assumption was adequate for predicting overall dynamic characteristics, but prevented the model from representing the local shear flow loads around the thrust and holddown posts. The crossbeam, a deep I-beam attached to the holddown posts, was idealized by three levels of nodes.

The S-II thrust structure is a ring stiffened, truncated cone shell with four stiff longerons to shear out the thrust loads. The center engine is supported by a tapered, pin-ended beam attached at the base of the shell as shown in Figure 4-16. Until the flight of the third Saturn V (AS-503), modeling this area was not considered to be a problem.

Longitudinal oscillations observed in AS-503 flight data and reported by the astronauts dictated a detailed review of the model. The oscillations were produced when the frequencies of the crossbeam mode and first LOX tank mode coalesced at 18 Hz, producing Pogo in the inboard engine. The crossbeam and thrust structure models were revised, but correlation with flight data indicated that analyses frequencies were still too low and the coupling between crossbeam and tank was not being adequately predicted. The modeling problems were due to:

1. Uncertain end conditions of the pinned crossbeam under thrust,
2. Tank stiffness not representing membrane pre-stress,
3. Lack of enough flexibility in shell-liquid coupling assumptions,
4. Nonlinear crossbeam damping.

Models developed throughout the industry have proved inadequate for investigating Pogo stability. The analyses have had to fall back on test data to identify model inadequacies.

The S-IVB thrust structure (Figure 4-17) is a ring stiffened cone attached to the lower bulkhead and consequently it has considerable influence on the bulkhead dynamics. The first coupled mode of the tank and thrust cone occurs around 18 Hz.

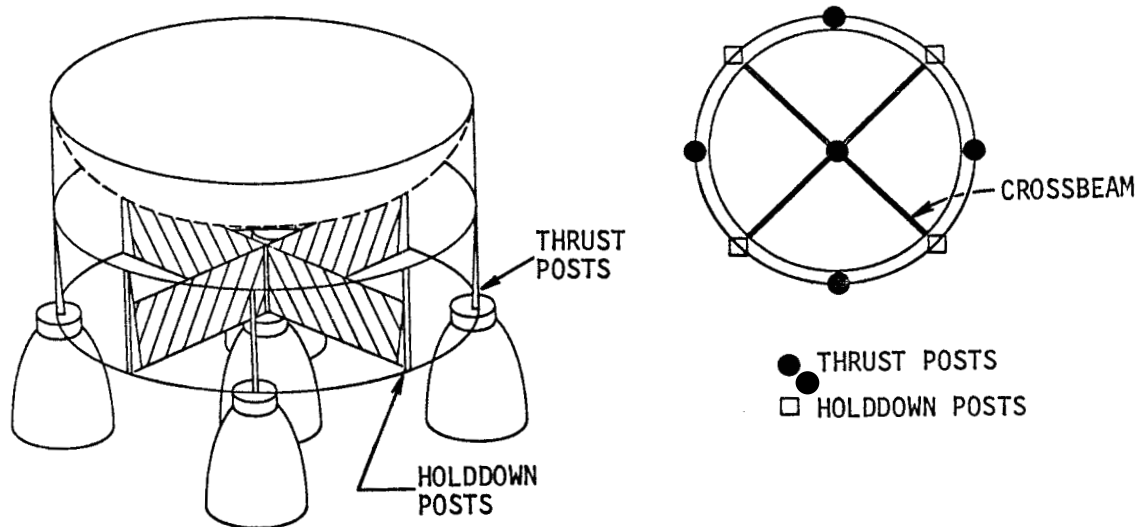


FIGURE 4-15 S-IC THRUST STRUCTURE

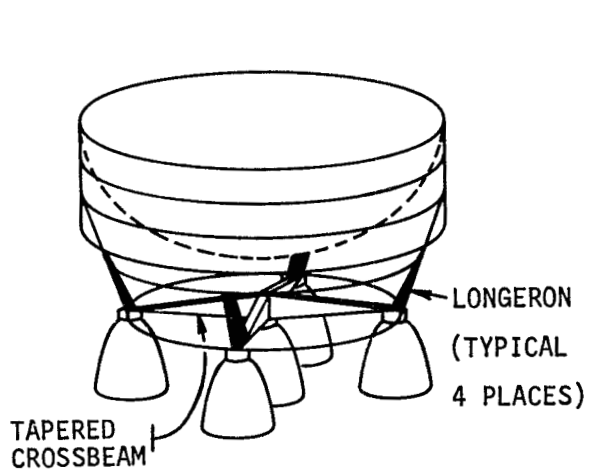


FIGURE 4-16 S-II THRUST STRUCTURE

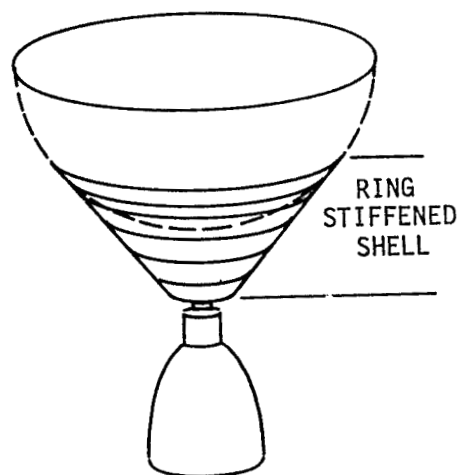


FIGURE 4-17 S-IVB THRUST STRUCTURE

4.3.4 Major Component Idealization

The lunar module is a good example of the importance of modeling major components adequately. The LM is the two stage vehicle illustrated in Figure 4-18. Both the ascent and descent stages are nearly symmetrical in mass. However, the connection between the two stages is asymmetrical in stiffness. Because of this asymmetry, longitudinal oscillation of the lunar module will induce both longitudinal and pitch response, as shown in Figure 4-19.

The efficiency with which the LM couples pitch and longitudinal responses in the vehicle was demonstrated during the second Apollo Saturn V flight. The frequency of the vehicle first longitudinal mode coalesced with the 5 Hz first pitch mode of the LM and spacecraft after 130 seconds of first stage boost. As coalescence was approached, the coupling became so strong that longitudinal oscillation of the LM produced more pitch than longitudinal response in the spacecraft (see Figure 4-19).

Usually cross-plane coupling causes a decrease in the in-plane response. But, this was not the case in this particular mode. The strong pitch and longitudinal coupling increased the gain of the first longitudinal mode. As used here, structural gain is the dynamic response produced by a unit longitudinal sinusoidal force applied at the engine thrust pad.

The math models used prior to the second Apollo Saturn V flight neglected the LM coupling mechanism. These models predicted the vehicle would not experience a Pogo instability as shown by the lower (coplanar) curve in Figure 4-19. During the flight, a Pogo instability did occur between 100 seconds and 135 seconds of flight time. After the math model was revised to include the pitch and longitudinal coupling mechanism, a 30 percent increase in first longitudinal mode gain was obtained. This coupled model closely reproduced the Pogo characteristics as shown by the upper curve in Figure 4-19.

There are four basic questions that require an answer before the level of detail in math modeling of components can be assessed:

1. Are the dynamics of the component as a separate entity of interest from a loads standpoint?
2. Will the dynamics of the component affect the primary modes of the vehicle?
3. Does the component have inherent mass and stiffness asymmetries that will provide a coupling mechanism between primary vehicle modes?
4. Will the component generate important local reactions on the vehicle, or affect the local deformation in the controls area?

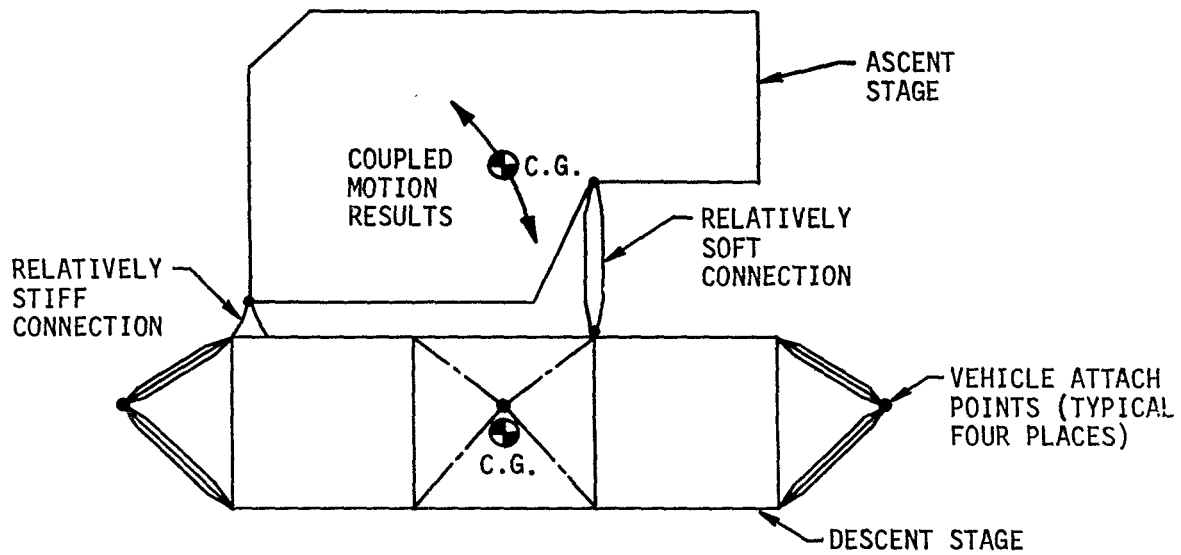


FIGURE 4-18 LM ASYMMETRY EXAMPLE

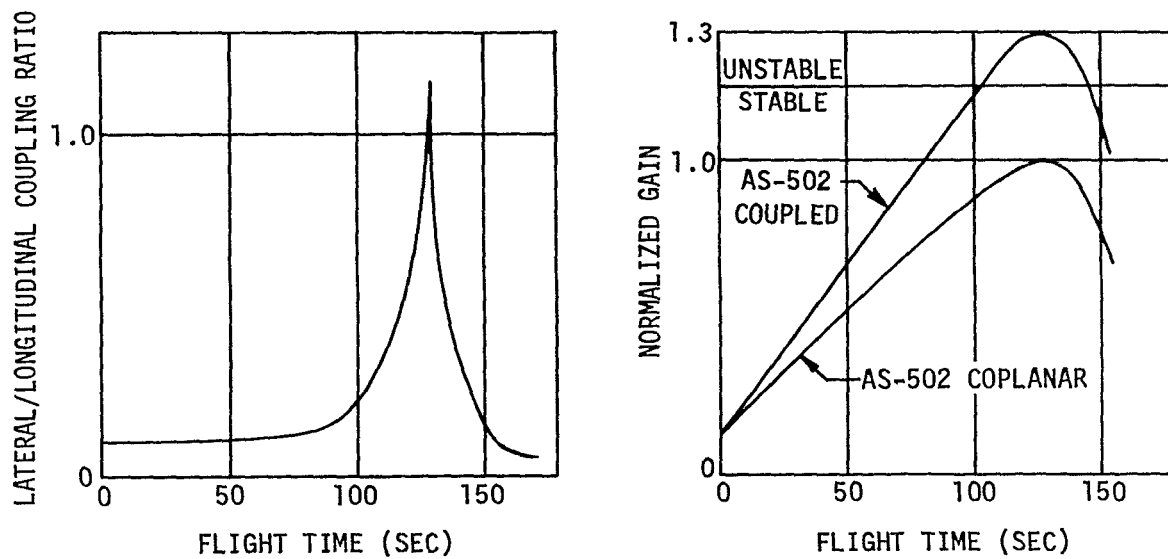


FIGURE 4-19 INFLUENCE OF MAJOR COMPONENTS ON VEHICLE DYNAMICS

4.3.4 (Continued)

The LM, mainstage engines, and service module tanks are typical examples of major components. Actually the lunar module contains propellant tanks that themselves qualify as major components. The criteria above must be applied to the sub-components. The LM is attached to flexible structure (SLA shell) which also requires detailed modeling.

The LM presents a real challenge in structural idealization. Correlation with ground test data is essential for this type of structure. There are no basic ground rules that can be established for this type of structure other than to spend as much preparation time as necessary to thoroughly understand the load paths under all loading conditions.

The engines are often quite rigid and have primitive frequencies above the range of interest. However, they should be analyzed to determine this. Control engines and their actuator assemblies have a low rotational frequency that is of interest and is accounted for by two methods. When only the effects on the primary resonances are of concern, the engine is treated as an undamped elastic model. When the engine and its servo-actuator system are considered as a closed loop system, the engine lateral characteristics are deleted from the dynamic characteristics analysis and included in the dynamic stability and response analyses. If the engines are removed in the dynamic characteristic analysis, some means must be employed to include the local elastic deformation the engines produce on the thrust structure. When the engines are removed, this deformation comes from high frequency modes that are usually not included in the analysis (see Paragraph 4.5.3 for an explanation of this effect). On Saturn V analyses, when the engine elastic degrees of freedom were deleted, the engine mass was lumped on the appropriate thrust structure node to represent local thrust structure deformation produced by the engines.

The service module tanks (Figure 4-20) were considered rigid because their bending frequencies are about 20 Hz. However, they are mounted on a soft, flat bulkhead that results in basic cantilever resonances around 6 Hz. Consequently, the bulkhead where the tanks attach was modeled in considerable detail to allow the proper inertia loads to be transmitted into the vehicle shell at the proper frequency. The service module is unsymmetrical in both mass and stiffness, and is a significant coupling mechanism between pitch and yaw vehicle modes.

Small components also may require special attention. For example, each thermal conditioning plate that supports flight control sensors in the IU can be considered a component. Although this component does not fit the criteria heretofore established, the sensitivity of the local structure deformation warrants special modeling consideration.

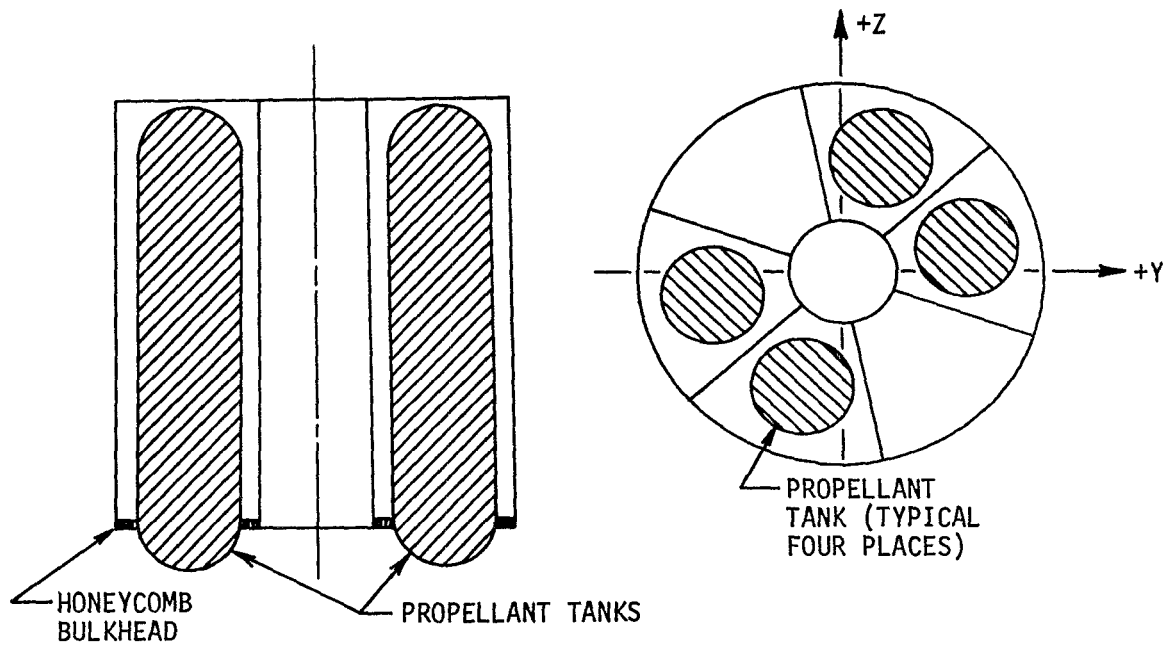


FIGURE 4-20 SERVICE MODULE TANKS

4.4 INERTIA MATRIX DEVELOPMENT

4.4.1 General Guidelines

In general, much more attention has been given to the development of stiffness model technology than has been directed toward mass modeling. This is partially justified in that the lower frequency system characteristics can generally be represented adequately by fairly crude means. However, ordinary mass lumping techniques may not suffice for higher frequency modes when these higher frequencies are near a local resonance of the structure. As an example, four masses lumped at the quadrant points around a cylindrical shell structure may be very adequate for predicting the lower frequency body bending modes but very inadequate for predicting local ring mode characteristics. Consequently, it is most important to keep the detail of the mathematical model consistent with the goals of the analysis.

The Saturn V dynamic analysis program has provided many examples which support the necessity for recognizing problem goals prior to model formulation. Deciding what is required to attain these goals without excessive detail calls for sound engineering judgement backed by adequate preliminary analysis. Preliminary analysis includes estimating unrealistic local resonances which arise due to mass lumping techniques, simplified analyses to establish basic system properties, and estimating probable static effects in critical areas of the structure. Static effects which can perturb the basic linearity assumptions include the effects of compressive loads on local panels and beam-column effects on lateral frequencies. These phenomena should be assessed prior to forming the dynamic model, to ensure that a realistic representation of the system characteristics is maintained.

Establishment of the goals of the analysis will require close coordination with the users of the dynamic characteristics such as the flight control system designers, the vehicle loads analysts, and the Pogo stability analysts, to insure that their requirements will be met by the proposed model. Once the model has been established, it is essential that clear communication be established with the engineers responsible for determining the structural mass distribution. In many cases they will not be familiar with the dynamic requirements of the problem and will not be able to employ sound judgement in interpreting incomplete requests for mass data. In addition to the clear communication required, it is essential that the mass data be carefully checked by the dynamic analyst prior to the performance of the dynamic analysis. Most of the engineering errors made in the Saturn V dynamic analyses involved mass data.

In its most basic form the mass matrix $[M]$ is a diagonal matrix with the system masses concentrated at discrete points $\{X\}$ of the structure. This procedure does not account for the distributed mass effects of the structure. Care must be taken to avoid the introduction of artificial resonances in the frequency range of interest due solely to mass lumping procedures.

4.4.2 Inertia Examples

For purposes of developing inertia matrices, a large space vehicle can be represented as some combination of the following modules:

1. Lightweight Shell Structure
2. Propellant Tanks and Contained Liquids
3. Rigid Subsections
4. Major Components

Methods of treating each module, such as Guyan's method, (Reference 4-4) constraints procedures, assumed shape functions, and modal synthesis are presented and illustrated with examples from the Saturn Program. The necessity of treating the stiffness and inertia matrices consistently is also covered.

4.4.3 Shell Inertia Matrices

The primary problem in formulating the shell mathematical model is to allow proper description of inertia loads without generating a model that is too large from a standpoint of both software and hardware capability and cost. The engineer must use judgment as to how the shell will act and then manipulate the model to permit this activity without degradation of results. The following considerations are involved in determining the detail of the model required:

1. Representation of ring dynamics with minimum number of degrees of freedom.
2. Representation of liquid and structural interaction.
3. Transition between shell and beam modules.
4. Prevention of artificial local resonances due to mass lumping.
5. Control of local distortion at nodes due to gross mass lumping.

Consistent inertia matrix techniques (Reference 4-5) were used to allow representation of ring dynamics and eliminate unrealistic distortion at nodes where local deformation are important (i.e. flight gyro locations). Although this technique is fully covered in the literature, examples will be given here to show the accuracy of the technique.

The consistent mass reduction technique uses the same coordinate transformation used to reduce the stiffness matrix in Section 4.1.1.

4.4.3 (Continued)

The reduced stiffness in equation 4.5 is:

$$[K_{\text{REDUCED}}] = [T]^T [K] [T]$$

Using the same transformation the reduced inertia matrix may be expressed as:

$$[M_{\text{REDUCED}}] = [T]^T [M] [T] \quad (4.19)$$

This consistent reduction of both the mass and stiffness matrices is known as Guyan's method (Reference 4-4). The transformation matrix $[T]$ which is given by equation 4.4 is derived directly from the stiffness matrix. The assumption is that the real inertia loads at the reduced degrees of freedom can be replaced by their effects at the loaded degrees of freedom in the form of inertial coupling terms. Application of this technique for the Saturn V has significant advantages for the IU and SLA model, the lunar module model and the command-service module models.

A study was conducted on the short stack section (S-IVB forward skirt, IU and SLA panels) of the Apollo Saturn V vehicle. The structural idealization of the short stack section is shown in Figure 4-11. The purpose of the study was to compare the accuracy of the consistent mass reduction method with that of the lumped mass method. To accomplish this, a baseline model of the short stack section was developed. This model contained 181 degrees of freedom. The normal modes and frequencies of this model were obtained and used to determine the accuracy of two different 78th order models.

The first 78th order model was obtained from the 181st order baseline model by a process of Guyan reduction. This model will be referred to as the "Guyan Consistent Mass Model". The second 78th order model was obtained from the 181st order baseline model by reducing the stiffness matrix and then independently relumping the mass matrix. The relumping maintained the same total mass and center of gravity. This model will be referred to as the "Relumped Mass Model".

Characteristics of the first free-free mode obtained from the 181st order baseline model, the Guyan consistent mass model, and the relumped mass model are shown in Figures 4-21, 4-22, and 4-23, respectively. Each figure indicates the predicted frequency and ring mode shapes at the bottom and top of the instrument unit.

The frequency of the first free-free mode of the Guyan consistent mass model is 6.5 percent higher than that of the baseline model. The ring mode shapes and node points are similar to those of the baseline model. The frequency of the first free-free mode of the relumped mass model is 20 percent lower than the baseline model. The two lobe ring mode shapes show little resemblance to the three lobe ring modes predicted by the baseline model.

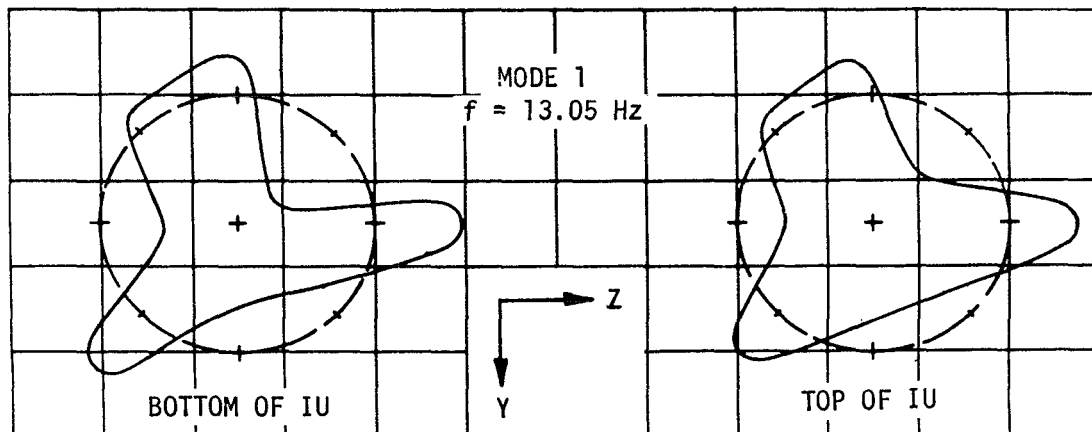


FIGURE 4-21 RING SHAPE OF THE 181ST ORDER (BASELINE MODEL)

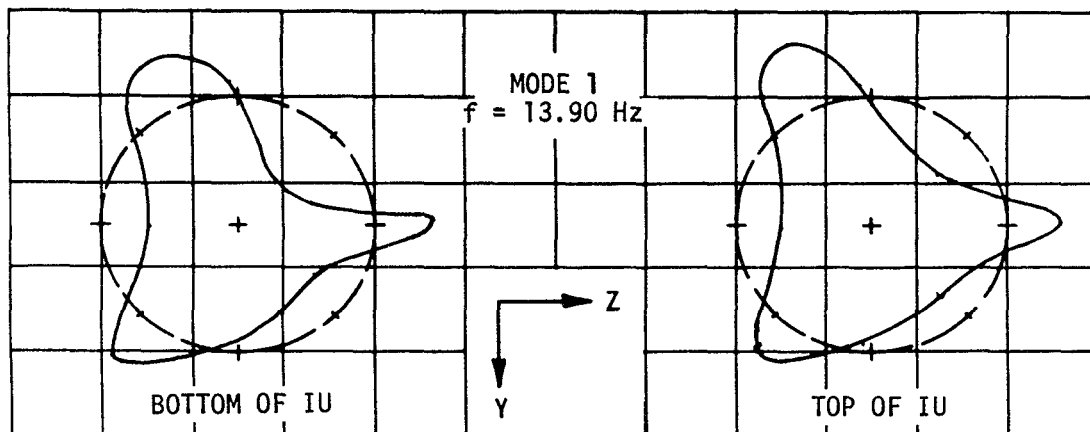


FIGURE 4-22 RING SHAPE OF THE 78TH ORDER (GUYAN CONSISTENT MASS MODEL)

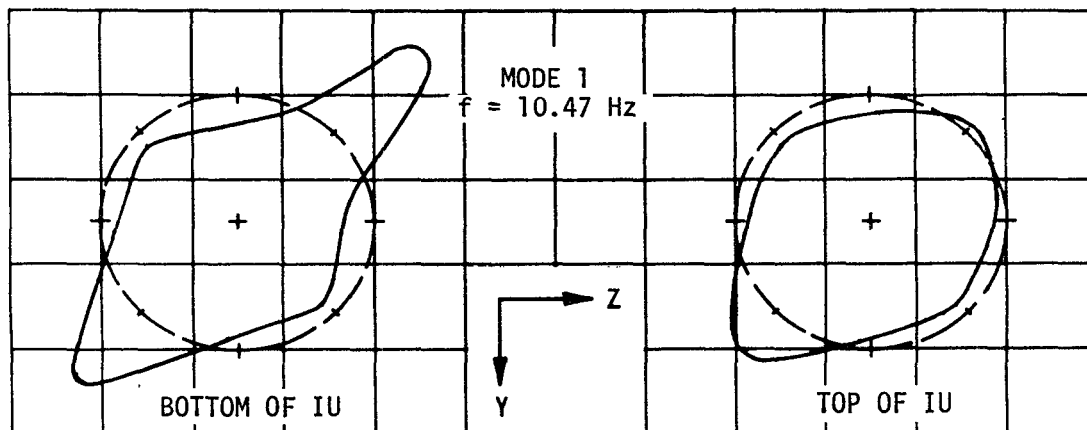


FIGURE 4-23 RING SHAPE OF THE 78TH ORDER (RELUMPED MASS MODEL)

4.4.3 (Continued)

The frequency variation in the two 78th order models is caused by the difference in the mass matrices. The relumped mass causes a concentration of mass that lowers frequencies, while the consistent mass reduction introduces a small constraint on the system that produces slightly higher frequencies.

4.4.4 Propellant Tank Inertia Matrices

Initial longitudinal math models of the Saturn V structure did not adequately represent interaction between the liquid and the structure in the propellant tanks. Correlation with 1/10 scale model dynamic test results showed a serious deficiency in mathematical modeling for the longitudinal case. A method was developed to correct this deficiency. This involved relating radial and vertical motion of the contained liquid to breathing motion of the tank.

When the tank walls deform, motion is produced in the contained liquid. For most practical problems, the change in tank volume due to elastic deformation is large compared with volume changes within the liquid due to liquid compressibility. As a result, the liquid can be assumed to be incompressible. In the Saturn tanks, which have a diameter of 33 feet (10.06 m), the frequencies of the fundamental surface waves are well below the frequencies of the tank modes themselves. Hence, the effects of surface wave motion can also be neglected. The liquid surface can be assumed to remain flat.

Under the above conditions, a simple relationship between vertical liquid motions and shell motions can be derived. Referring to Figure 4-24, the vertical motion of all liquid particles in a given cross section will be equal, i.e.:

$$\Delta x(r, \theta, X) = \Delta x(X) \quad (4.20)$$

The vertical motion in any plane $X = h$ will be equal to the volume of deformation $V(h)$ below $X = h$ divided by the cross sectional area $A(h)$.

$$\Delta x(h) = \frac{\int_0^h dV}{A(h)} = \frac{V(h)}{A(h)} \quad (4.21)$$

To simplify the finite element solution, the liquid can be divided into n laminae centering about the n elastic nodal circles. The radial velocity distribution can be derived from the conditions of incompressibility and uniform vertical velocity (Equation 4.20). Referring to Figure 4-25, if the liquid is incompressible, the volume of liquid contained in a cylinder originally of radius r and height X must be constant, i.e.

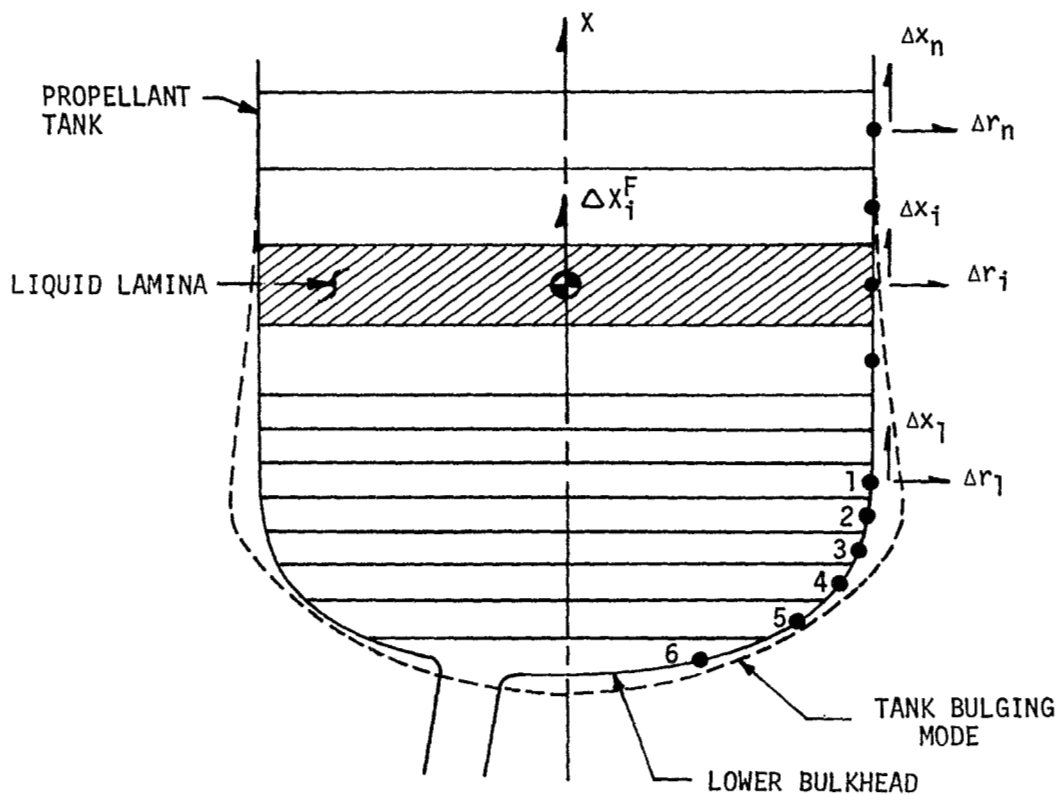


FIGURE 4-24 PROPELLANT TANK LIQUID IDEALIZATION

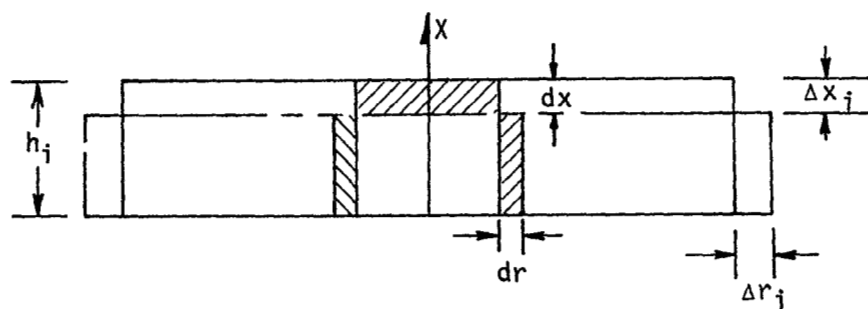


FIGURE 4-25 LIQUID MOTION DUE TO TANK EXPANSION

4.4.4 (Continued)

$$dV = 0 = 2\pi r X dr + \pi r^2 dX \quad (4.22a)$$

$$dr = -\frac{r}{2X} dX \quad (4.22b)$$

$$dX = -\frac{2X}{r} dr \quad (4.22c)$$

As dX is independent of r (Equation 4.20), it can be evaluated without loss of generality on the shell boundary where

$$r = r_i, X = h_i, dr = \Delta r_i, dX = \Delta X_i$$

$$\Delta X_i = -\frac{2h_i}{r_i} \Delta r_i \quad (4.23)$$

Using Equation (4.23) to evaluate Equation (4.22b) gives

$$\Delta r(r, h_i) = \frac{r}{r_i} \Delta r_i \quad (4.24)$$

In deriving Equation (4.24), it was assumed that the radial velocity distribution in each liquid lamina could be satisfactorily approximated by the radial velocity at the vertical midpoint of the lamina. A sufficient number of laminae were used in the Saturn V analysis to make this a good assumption. An effective radial mass m_{ie} will now be defined by equating kinetic energies.

$$\begin{aligned} \frac{1}{2} m_{ie} \Delta \dot{r}_i^2 &= \frac{1}{2} \int_V \rho (\Delta \dot{r})^2 dv \\ &= \frac{1}{4} M_i \Delta \dot{r}_i^2 \end{aligned} \quad (4.25)$$

where the intergral is taken over the volume of the i th liquid lamina, ρ is the mass density, and M_i is the total mass of that lamina. From Equation (4.25), it can be deduced that the effective mass is equal one-half the total mass

$$m_{ie} = \frac{1}{2} M_i \quad (4.26)$$

4.4.4 (Continued)

In order to obtain a continuous expression for liquid and shell motions in the bulkheads, the elastic deformations of the shell were represented by power series. The radial and vertical deformations were each represented by a power series in the dimensionless radial coordinate $\bar{\rho} = r/r_T$ (See Figure 4-26).

$$\Delta r(\bar{\rho}) = \sum_{n=0}^N a_n \bar{\rho}^n \quad (4.27)$$

$$\Delta x(\bar{\rho}) = \sum_{n=0}^N b_n \bar{\rho}^n \quad (4.28)$$

The coefficients a_n and b_n were chosen to satisfy the conditions of axisymmetry

$$\Delta r(0) = 0 \quad (4.29)$$

$$\frac{\partial x}{\partial \bar{\rho}}(0) = 0 \quad (4.30)$$

plus the displacement matching conditions

$$\Delta r(\bar{\rho}_i) = \Delta r_i \quad i = 1, 3, 5 \quad (4.31)$$

$$\Delta x(\bar{\rho}_i) = \Delta x_i \quad i = 1, 3, 5 \quad (4.32)$$

The equations above are satisfied by third order polynomials ($N = 3$ in Equations (4.27) and (4.28)).

The solution for the bulkhead shell displacement components will have the form

$$\Delta r^S(\bar{\rho}) = \langle 1 \ \bar{\rho} \ \bar{\rho}^2 \ \bar{\rho}^3 \rangle \begin{bmatrix} a_{ij} \end{bmatrix} \begin{Bmatrix} \Delta r_1^S \\ \Delta r_3^S \\ \Delta r_5^S \end{Bmatrix} \quad (4.33)$$

$$\Delta x^S(\bar{\rho}) = \langle 1 \ \bar{\rho} \ \bar{\rho}^2 \ \bar{\rho}^3 \rangle \begin{bmatrix} b_{ij} \end{bmatrix} \begin{Bmatrix} \Delta x_1^S \\ \Delta x_3^S \\ \Delta x_5^S \end{Bmatrix} \quad (4.34)$$

4.4.4 (Continued)

where the a_{ij} and b_{ij} coefficients are determined by making the third order polynomials satisfy Equations (4.27) through (4.32).

The volume of deformation up to the midplane of each of the bulkhead liquid laminae can be obtained by integration of Equations (4.33) and (4.34). The vertical displacements of these laminae can then be evaluated from Equation (4.21). These displacements will have the form:

$$\begin{Bmatrix} \Delta x_1^F \\ \Delta x_2^F \\ \vdots \\ \Delta x_6^F \end{Bmatrix} = \begin{bmatrix} & & & & & \\ & & & & & \\ & & & & & \\ & & & & & \\ & & & & & \\ & & & & & \end{bmatrix} \alpha_{ij} \begin{Bmatrix} \Delta x_1^S \\ \Delta x_3^S \\ \Delta x_5^S \\ \Delta r_1^S \\ \Delta r_3^S \\ \Delta r_5^S \end{Bmatrix} \quad (4-35)$$

LIQUID DISPLACEMENTS SHELL DISPLACEMENTS

The radial displacements in the midplane of each bulkhead lamina are obtained by combining Equations (4.24) and (4.33):

$$\begin{Bmatrix} \Delta r_1^F \\ \Delta r_2^F \\ \vdots \\ \Delta r_6^F \end{Bmatrix} = \begin{bmatrix} 1 \bar{p}_1 & \bar{p}_1^2 & \bar{p}_1^3 \\ 1 \bar{p}_2 & \bar{p}_2^2 & \bar{p}_2^3 \\ \vdots & \vdots & \vdots \\ 1 \bar{p}_6 & \bar{p}_6^2 & \bar{p}_6^3 \end{bmatrix} \begin{bmatrix} & & \\ & & \\ & & \\ & & \end{bmatrix} a_{ij} \begin{Bmatrix} \Delta r_1^S \\ \Delta r_3^S \\ \Delta r_5^S \end{Bmatrix} \quad (4.36)$$

SHELL DISPLACEMENTS

The liquid displacements in the cylindrical section of tank above the bulkhead will be the sum of the vertical displacement at the top of the bulkhead, Δx_1^F , plus the displacement due to radial expansion of the cylindrical sections. From Equation (4.23):

4.4.4 (Continued)

$$\begin{bmatrix} M_{pq}^S \end{bmatrix} = \begin{bmatrix} \lambda_{ip} \end{bmatrix}^T \begin{bmatrix} M_{ij}^F \end{bmatrix} \begin{bmatrix} \lambda_{jq} \end{bmatrix} \quad (4.40)$$

The tank math model is completed by using Equations (4.33) and (4.34) to perform an equivalent transformation on the shell stiffness matrix.

This method proved highly accurate in predicting the first two tank modes of the S-IC stage. The frequency of the first tank mode - 3.75 Hz - was predicted exactly by this method. Excellent mode shape correlation was also obtained. The method requires no special computer program, other than a standard matrix manipulation package. The coefficient matrices for all six Saturn V tanks were computed in two man-weeks. Different propellant level conditions can be analyzed rapidly by this method. The method just derived was selected because of its simplicity and ease of application.

This method is not applicable where higher tank modes, or local liquid effects such as tank bottom pressures, must be predicted accurately. However, the method could be extended to these cases by retaining more terms in the power series approximations to the shell displacements. A more accurate technique has been derived (Reference 4-9) and applied to the analysis of S-IC tank modes. Frequencies from this solution have been correlated with measured flight data through the first six modes.

4.4.5 Rigid Subsection Inertia Matrices

Rigid cross-section transformations are based on the assumption that the plane cross-section remains plane and rigid during deformation. These transformations can be used where shells are locally stiffened to maintain rigidity. They are very useful in coupling beam and shell models together.

Figure 4-27 is a sketch of a beam-shell model interface. The shell model interface has 24 degrees of freedom which consists of X, Y, and Z displacements at each of the eight nodes. These 24 degrees of freedom can be expressed in terms of the 6 degrees of freedom on the beam by employing the following rigid body relationships between coordinates:

Let $\Delta x_c, \Delta y_c, \Delta z_c, R_x, R_y, R_z$ represent the motion of the plane section assumed positive as shown in Figure 4-27 and $\Delta x_n, \Delta y_n, \Delta z_n$ represent the motion of mass M_n .

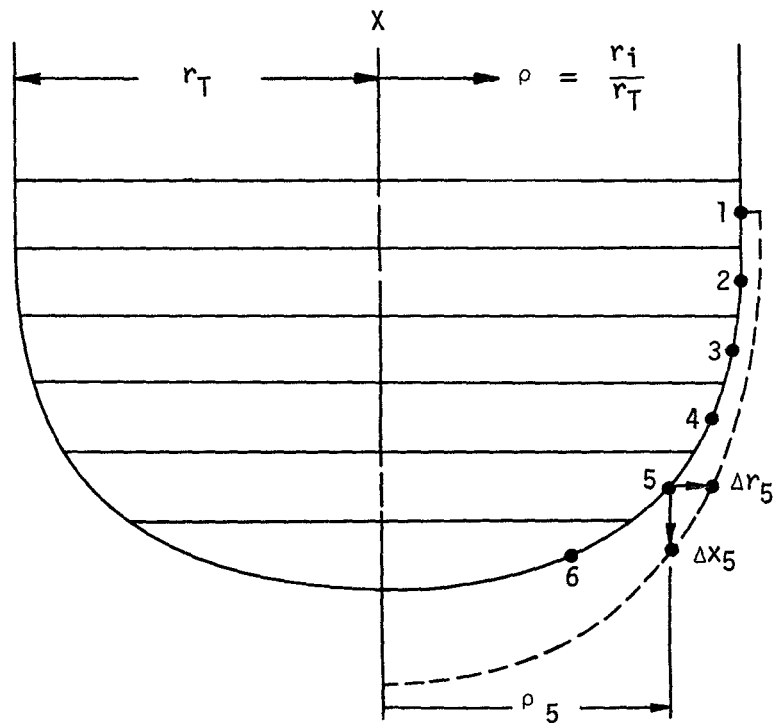


FIGURE 4-26 GEOMETRY OF DEFORMED BULKHEAD

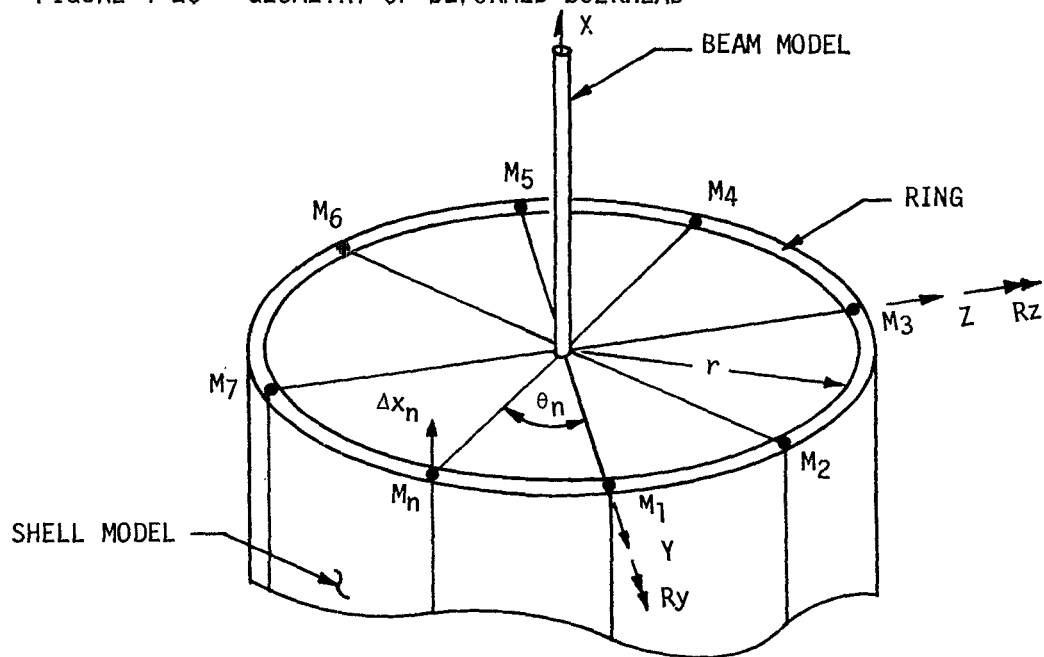


FIGURE 4-27 BEAM-SHELL MODEL INTERFACE

4.4.5 (Continued)

$$\Delta x_n = \Delta x_c + (r \sin \theta_n) R y_c - (r \cos \theta_n) R z_c \quad (4.41a)$$

$$\Delta y_n = \Delta y_c - (r \sin \theta_n) R x_c \quad (4.41b)$$

$$\Delta z_n = \Delta z_c + (r \cos \theta_n) R x_c \quad (4.41c)$$

Or expressed as

$$\begin{Bmatrix} \Delta x_1 \\ \Delta y_1 \\ \Delta z_1 \\ \vdots \\ \vdots \\ \Delta x_8 \\ \Delta y_8 \\ \Delta z_8 \end{Bmatrix} = \begin{bmatrix} 1 & 0 & 0 & 0 & r \sin \theta_1 & r \cos \theta_1 \\ 0 & 1 & 0 & r \sin \theta_1 & 0 & 0 \\ 0 & 0 & 1 & r \cos \theta_1 & 0 & 0 \\ & & & \vdots & & \\ & & & \vdots & & \\ 1 & 0 & 0 & 0 & r \sin \theta_8 & -r \cos \theta_8 \\ 0 & 1 & 0 & r \sin \theta_8 & 0 & 0 \\ 0 & 0 & 1 & r \cos \theta_8 & 0 & 0 \end{bmatrix} \begin{Bmatrix} \Delta x_c \\ \Delta y_c \\ \Delta z_c \\ R x_c \\ R y_c \\ R z_c \end{Bmatrix} \quad (4.42)$$

$$\{X\} = [T] \{\dot{q}\} \quad (4.43)$$

Transforming the mass matrix using Equation (4.43)

1. Sums the eight masses, $m_1 \dots m_8$, as the effective mass on each of the Δx_c , Δy_c and Δz_c coordinates,
2. Sums the mr^2 terms as the effective rotational inertia about the X axis.
3. Sums the $m(r \sin \theta)^2$ terms as the effective rotational inertia about the Y axis.
4. Sums the $m(r \cos \theta)^2$ terms as the effective rotational inertia about the Z axis.
5. Calculates the appropriate inertial coupling terms in the event the masses are not equal.

4.4.5 (Continued)

In areas where the plane section assumption is not realistic, linear constraint relationships can still be established through the use of polynomial shape functions. This technique requires that all coordinates involved in the transformation be on a curve or surface which is described by polynomial functions that satisfy appropriate boundary conditions.

The following calculations illustrate the steps which lead to the "warped cross section" transformation. This approach permits the cross section to warp either anti-symmetrically across the neutral axis or act as a plane section, whichever most closely approximates the natural structural action. This example is concerned with vertical displacements (Δx) due to rotation about the pitch axis only; however, the method is equally adaptable to other displacements. Application of the following transformation to the mass matrix will yield inertial coupling terms which represent the effective rotational inertia of the cross section. These calculations were made to develop vertical cross sectional constraints used in the original S-IVB/IU/spacecraft full shell model.

The model cross section was given freedom to rotate in both pitch and yaw. The constraint equations were written in terms of two freedoms for each motion so all " Δx " motions at a particular level were written as functions of four generalized coordinates. The constraint equations were flexible enough to allow a plane section or a warped plane symmetrical across one axis and anti-symmetric across the other. If it appears desirable, a fifth freedom which allows the entire cross section to translate vertically can easily be incorporated.

The following example is for vertical displacement Δx_n due to rotation about the pitch axis only. The general expression for the cross section deformation using the notation in Figure 4-28 is:

$$\Delta x(a_n) = A_0 + A_1 a_n + A_3 a_n^3 \quad (4.44)$$

where $a_n = r_n \cos \theta_n$

The following condition must be satisfied in Equation (4.44)

$$\Delta x(a_n) = \Delta_1 \quad (4.45a)$$

$$a_n = a_1$$

$$\Delta x(a_n) = \Delta_2 \quad (4.45b)$$

$$a_n = a_2$$

4.4.5 (Continued)

$$\begin{aligned} \Delta x(a_n) &= 0 \\ a_n &= 0 \end{aligned} \quad (4.45c)$$

The constants A_0 , A_1 , and A_3 are functions of the two independent variables Δ_1 and Δ_2 . Once they are solved from the given boundary conditions, the displacement Δx can be written as:

$$\Delta x = \langle 1 \ a \ a^3 \rangle [C_{ij}] \begin{Bmatrix} \Delta_1 \\ \Delta_2 \end{Bmatrix} \quad (4.46)$$

The relationship between the variables Δ_1, Δ_2 and a typical dependent variable Δx_n at coordinate a_n can be solved by substituting the a_n value into the polynomial. This process leads to a linear coordinate transformation of the form:

$$\begin{Bmatrix} \Delta x_1 \\ \vdots \\ \Delta x_p \end{Bmatrix} = \begin{bmatrix} T \end{bmatrix} \begin{Bmatrix} \Delta_1 \\ \Delta_2 \end{Bmatrix} \quad (4.47)$$

4.4.6 Major Component Inertia Matrices

Inertia matrices are formed for components such as the lunar module just as they are for primary structure. When the component is rigid compared with the structure it attaches to, a simple transformation is used to express the motion of the component center of gravity motion in terms of the motion of its attach points. An example of how the S-IVB engine was represented in the final math model follows. The thrust structure and engine structure were assumed rigid. The actuator was flexible and the engine could pivot about the gimbal. Figure 4-29 shows the essential elements involved. The redundant freedom Ry_2 was expressed in terms of the retained freedoms z_1 , Ry_1 and Δz_2 in matrix form in Equation (4.48).

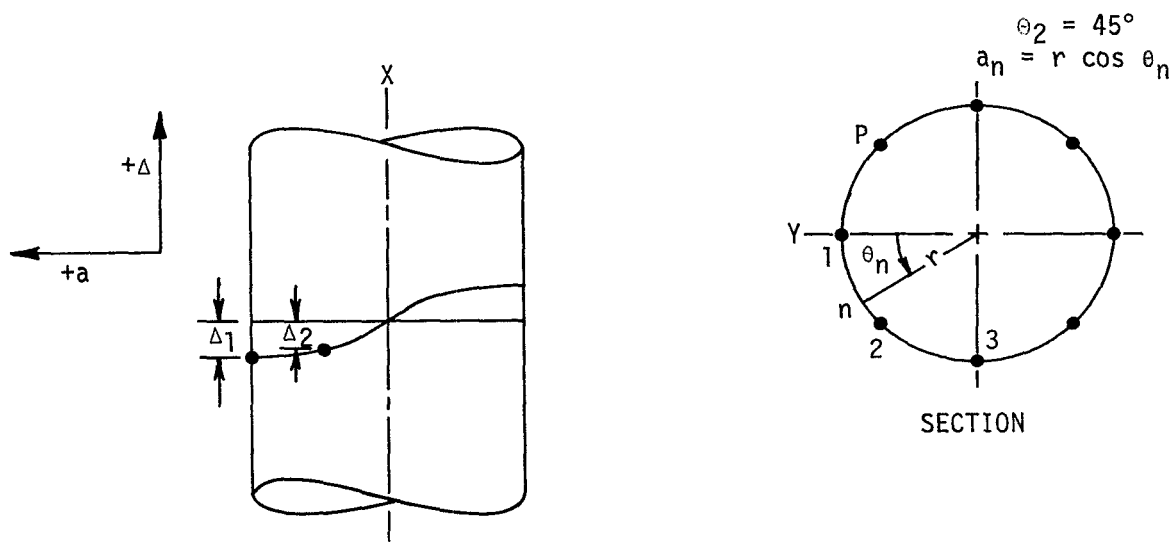


FIGURE 4-28 WARPED SECTION OF CYLINDRICAL MODEL

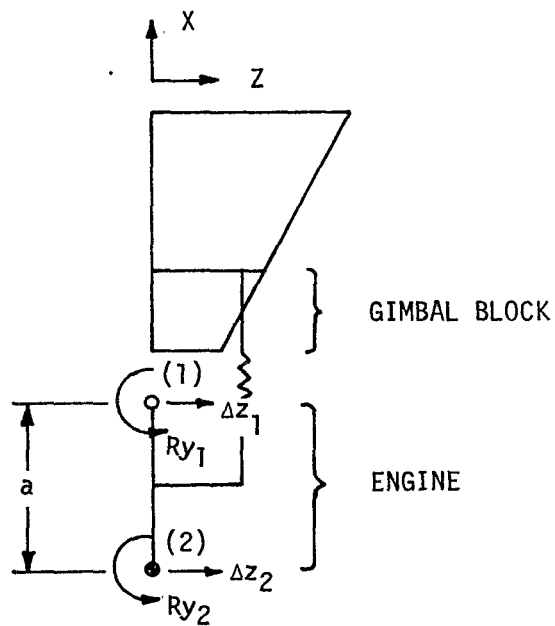


FIGURE 4-29 S-IVB ENGINE MODEL

4.4.6 (Continued)

$$\begin{Bmatrix} \Delta z_1 \\ Ry_1 \\ \Delta z_2 \\ Ry_2 \end{Bmatrix} = \begin{bmatrix} 1 & 0 & 0 \\ 0 & 1 & 0 \\ 0 & 0 & 1 \\ -\frac{1}{a} & 0 & \frac{1}{a} \end{bmatrix} \begin{Bmatrix} \Delta z_1 \\ Ry_1 \\ \Delta z_2 \end{Bmatrix} \quad (4.48)$$

This transformation was used to transform the engine mass matrix.

4.5 VIBRATION ANALYSIS AND MODAL SYNTHESIS

4.5.1 General

This section discusses how the math models of stiffness and inertia characteristics are combined to form a dynamic model of the vehicle. It also covers special techniques, such as modal synthesis, used to simplify this model. Additional material is presented on damping considerations used in modeling.

4.5.2 Eigenfunction Solutions and Modal Orthogonality

Once the stiffness and mass matrices are generated, the system can be solved for its characteristic roots and vectors. The undamped system equation of free vibration is:

$$\begin{matrix} [M_{ij}] \ddot{\{q\}} + [K_{ij}] \{q_j\} = \{0\} & (4.49) \\ \text{NxN} & \text{Nx1} & \text{NxN} & \text{Nx1} & \text{Nx1} \end{matrix}$$

There are N independent solutions to this homogeneous system of equations.

Because of the speed and the accuracy of the matrix transformation technique, it is numerically and economically feasible to obtain all of the eigenvalues from even large order matrices. As a result, a direct formulation of the eigenvalue problem can be made. In general, the inertia matrix will be nonsingular, even for a free-free system. Consequently, Equation (4.49) can be premultiplied by the inverse of the inertia matrix to give

$$[M_{ij}]^{-1} [K_{ij}] \{\phi_{jn}\} = \omega_n^2 \{\phi_{jn}\} \quad (4.50)$$

4.5.2 (Continued)

If the equation above is rooted, the eigenvalue routines will converge to the highest frequency solutions first. This means that the roots of greatest interest, the low frequency solutions, cannot be obtained until after all the higher frequency solutions have been converged to and eliminated. However, the matrix transformation technique can rapidly and accurately obtain all the modes involved. It is not necessary to eliminate the rigid body modes prior to rooting the matrix, as it is when matrix iteration methods are used. If rigid body (zero frequency) solutions are included in the system, these will also be solved for by this technique.

A modified Householder routine is used to obtain the eigenvalues and eigenvectors of the Saturn V vehicle. This routine is programmed for the IBM 360 computer using double precision arithmetic (Reference 4-10). The routine will obtain all the roots of a 300th order system in 75 minutes of computer time. This includes calculation of natural frequencies, mode shapes, generalized masses, and generation of the plot tapes.

Another method used to obtain the mode shapes and frequencies of systems up to 130th order is the iterative QR transformation scheme derived in References 4-11 and 4-12. The dynamic matrix is first converted to the upper Hessenberg form (zero in all positions i, j for $i > j + 1$) using elementary row and column manipulations. A sequence of mathematical transformations are then applied to the dynamic matrix which causes the diagonal elements to converge to the desired eigenvalues. The largest eigenvalue, which occupies the Nth diagonal position in an Nth order matrix, will converge the most rapidly. If the formulation of Equation (4.50) is rooted, the first eigenvalue will correspond to the largest value of ω_n^2 which will be the highest frequency root. This routine will obtain mode shapes, frequencies, generalized masses and generate the plot tape for a 130th order system in 15 minutes of computer time.

The requirements for a composite structural dynamic model and a corresponding vibration analysis arise from the necessity to ensure the integrity of the vehicle. The natural and induced environment to which the structure is subjected contain some vibrational power content versus frequency. The fundamental task of the dynamicist is to ensure that vehicle response to these environments does not become catastrophic. A detailed knowledge of the structural dynamic characteristics is thus necessary to define frequency separation and/or isolation required to eliminate near-resonancy failures.

Structural dynamic characteristics perform a second useful function: that of providing a generalized coordinate system within which the dynamic problem complexity is reduced. This normal mode method can be visualized as a process of representing the loaded deflection shape (static and dynamic) by use of a truncated series. The similarity transformation from structural to generalized coordinates decouples the equations of motion, which greatly facilitates their solution. Additionally, the order of the system of

4.5.2 (Continued)

differential equations can be substantially reduced by retaining only those modes that contribute to the response problem being solved.

The number of modes which are required to simulate the dynamic behavior of the structure depends on three major factors.

1. The frequency content of the imposed forcing function; all modes within the frequency spectrum must be candidates for inclusion in the problem.
2. The quasi-steady deflected shape of the vehicle may dictate that similar appearing modes be included in the problem to obtain the proper static solutions.
3. Particular modes may be required in the analysis simply because these modes, although lightly excited, produce unusually large loads and/or acceleration at particular vehicle stations.

Examples of this last case did occur on the Saturn V. The liquid and structure coupling in the propellant tanks produces a characteristic tank breathing or bulging mode, which obviously contributes significantly to local bulkhead and Y-ring loads. Inclusion of this mode in the liftoff and rebound response analysis is thus mandatory if bulkhead pressures are required; however, this mode contributes little to accelerations in the payload of the vehicle.

Determining which modes can produce large local effects is accomplished by inspection of modal gain characteristics. Modal gain is obtained directly from the dynamic characteristics and is by definition the (static) ratio of output to input. Depending on the nature of the problem, output can be an acceleration, internal load or liquid pressure; input may be a generalized force or displacement.

During the Saturn V program several types of gain were used to identify dynamic modes of interest; these included the instrument unit control system attitude/attitude rate gyroscope gains (modal slope per control thrust force), the command/service module interface load gains (modal bending moment per unit thrust) and lower bulkhead pressure gains for thrust oscillations. Calculation of these types of gain factors is incorporated directly in the computer routine for vibration analysis. Frequency response plots are a convenient way to evaluate the composite modal gain characteristics.

Early in the Saturn V program, it was judged advantageous to include the propellant slosh behavior in the structural dynamic analysis. Subsequent eigensolutions of the system revealed slosh modes which were simply linear combinations of rigid body and flexible modes. Defining slosh stability margins was extremely difficult using modes from the structural dynamic analysis. Consequently, in the latter stages of Saturn V design

4.5.2 (Continued)

assurance studies, slosh masses were treated as a frozen solid in the structural model. Spring-mass slosh models were then included in the dynamic response and stability analyses.

The slosh modes of the six Saturn V mainstage tanks are obtained from the digital computer routine described in Reference 4-13. This program was developed from variational principles. It is based on using the sum of shallow tank and deep tank model solutions as a set of velocity potentials. The unknown coefficients associated with these modal functions are solved for by a Rayleigh-Ritz procedure. The tanks are assumed to be rigid, which is valid for the Saturn V, since the ring mode frequencies are two orders of magnitude higher than the slosh frequencies. For each slosh mode retained in the analysis, an equivalent spring mass system is constructed. The mass, m_n , and attach station x_n , for each of these mechanical oscillators is obtained by equating the total force and moment of the mechanical and liquid systems. Step-by-step procedures for developing the parameters associated with the spring-mass analogy are presented in Reference 4-14.

The entire operation of the dynamic characteristics analysis hinges on the usage of the results. Requisite accuracy in sensitive areas must be defined as early in the development as feasible: for the Saturn V program, these sensitive regions included thrust structure/gimbal block areas; IU local deformations; and precise definition of modal bending moment and shear contributions in the forward portions of the vehicle. Synthesis of the dynamic model is accomplished within the framework of these requirements.

4.5.3 Modal Synthesis

Modal synthesis is a process whereby a complex structure is divided into sections and the dynamic properties of each section represented by selected modes from that section. The modes from each section must be chosen carefully to make sure that they can represent deformations produced by reactions from the adjoining sections. The following example illustrates the importance of these reaction effects.

One of the prime goals of the Saturn V test program was to develop mathematical models which could accurately predict the structural gain required to perform control system analysis. One of the essential parameters required was the local modal slope at the flight control gyro which is located in the Saturn V instrument unit. The gyro location is shown on Figure 4-30. A detailed math model was developed for the short-stack, consisting of the S-IVB forward skirt, IU, and SLA (see Figure 4-11). A free-free modal analysis of this model was made. Modes up to 45 Hz in frequency were used to represent this model in the analysis of the total vehicle. This model accurately predicted the vehicle centerline slope, but failed to predict the local control gyro slope obtained from test (see Figure 4-31). An investigation showed the difference in centerline and control gyro slopes was due to local deformations in the IU. These

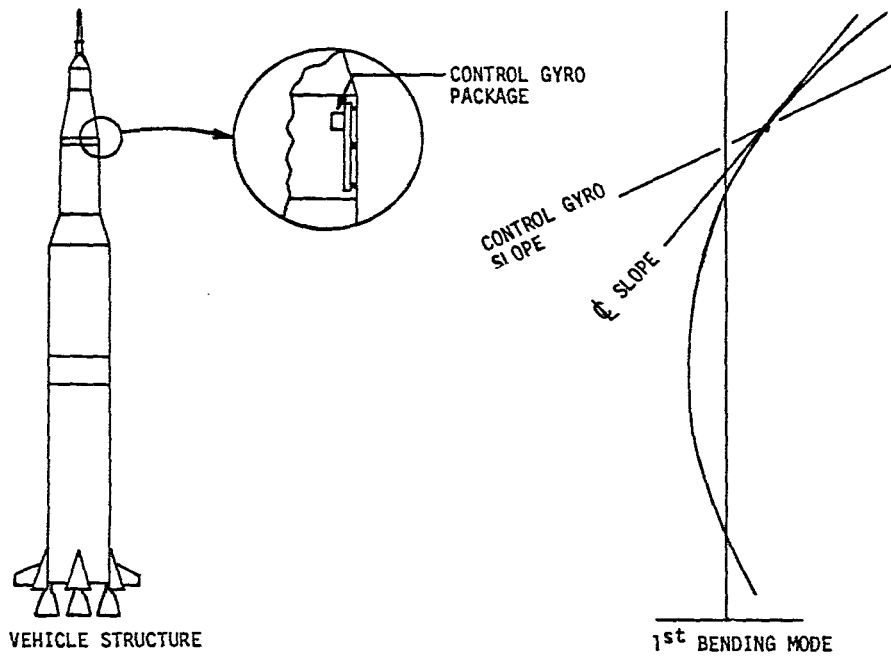


FIGURE 4-30 CONTROL GYRO LOCATION

4.5.3 (Continued)

deformations were caused by the way loads from the CSM and LM were conducted through the IU. When a modal analysis was made of the IU and SLA with the CSM removed, these local deformations did not appear in the modes below 45 Hz. Consequently, the modal synthesis solution effectively eliminated the local effects being sought. An interim solution for the local deformations was obtained by:

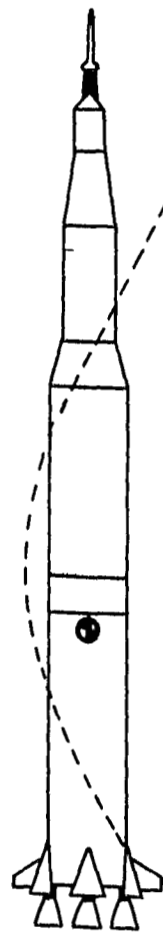
1. Obtaining the modal displacements at the top of the SLA and at the bottom of the S-IVB forward skirt from the dynamic model of the total vehicle.
2. Determining the inertia loads for the short stack model, using the accelerations from the total model.
3. Applying the boundary displacements and inertia loads from steps 1 and 2 to the short stack stiffness model.
4. Solving the static deformation problem to obtain the local deformations of the IU.

The modal synthesis solution was later used successfully by cantilevering the shortstack model at the bottom of the S-IVB forward skirt and accounting for the CSM reactions at the top of the SLA. This approach produced the desired local deformations in all modes of interest. Cantilever modes are better than free-free modes for most modal synthesis applications.

When using modal synthesis, the modes must be chosen carefully so that deformations produced by the attaching structure are represented. The modal models should be loaded with static forces at the interface to make sure the resulting deflections are nearly identical to the original model.

When the size of the dynamic model exceeds the capability of available eigenvalue routines, modal synthesis techniques can be used to obtain a solution. Given an eigenvalue routine which can solve an "n" degree of freedom problem, the structure can be divided into sections which contain less than n degrees of freedom as illustrated in Figure 4-31. The flexible cantilevered and appropriate rigid body modes are then determined. In determining the flexible modes of the cantilevered sections, all of the inertia effects of the system above the cantilevered location should be included in that section. For example, the inertia effects of Sections 2 and 3 should be lumped at the top node of Section 1, before the cantilevered modes of Section 1 are determined. Also, the inertia effects of Section 3 should be lumped into the top node of Section 2 before the cantilevered modes of that section are determined. This enables the modes of interest of the total coupled structure to be obtained using a small number of cantilevered modes. Before the mass matrices are coupled together the inertia effects that were added to the top nodes of sections 1 and 2 should be accounted for. The generalized mass and

FREE-FREE SYSTEM



SECTION
3

SECTION
2

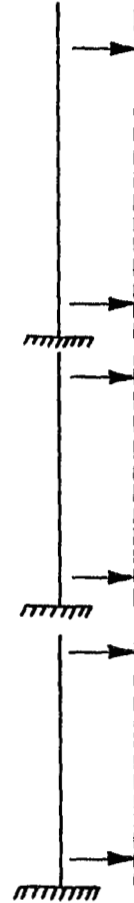
SECTION
1

FLEXIBLE MODES

CANTILEVERED SYSTEMS



RIGID BODY
ROTATION



RIGID BODY
TRANSLATION

FIGURE 4-31 ILLUSTRATION OF MODAL STACKING TECHNIQUES

4.5.3 (Continued)

stiffness matrices are determined, the cantilevered constraints removed from the stiffness matrices and the sections coupled together using modal synthesis. If the number of modes used to couple the three sections together is less than n , one coupling is required.

Present Saturn V analyses do not require the use of modal synthesis techniques because accurate large order eigenfunction routines have been developed to handle the total vehicle coupled dynamic matrix.

4.5.4 Evaluation

Evaluation of the analysis results relies heavily on experience and judgement. Rough calculations to determine approximately the first modal frequency for each axis analyzed and for large components should be made before the analysis starts.

These frequencies help in evaluating the results of the analysis. If the structure is unrestrained, the numerical accuracy of the solutions can be partially checked by evaluating the system dynamic shear and moment closure. With no external forces on the system or any grounded springs, both the shear and moment values should sum to zero in each mode if the structure is in equilibrium. If closure is not achieved the problem will be either a poor eigenvalue solution or an incorrect matrix.

A lumped parameter model will give resonances which are not realistic but arise solely from the lumping procedure. The analysis results must be evaluated to be sure that these lumping resonances either lie above the frequency range of interest or their presence does not adversely affect the dynamic characteristics being sought.

The eigenvalue solution is checked by the orthogonality condition of the modes. This is accomplished by checking the off-diagonal terms of the generalized mass $[\phi]^T[M][\phi]$ and stiffness $[\phi]^T[K][\phi]$. The off-diagonal terms are theoretically zero when the modes are orthogonal. In reality the off-diagonal terms are never zero because of numerical error. A good rule of thumb is that six orders of magnitude difference between diagonal and off-diagonal terms should be a minimum objective for the mass matrix, with three orders of magnitude required for the stiffness matrix. Plots of the mode shapes are necessary for evaluating whether the modes satisfy physical considerations.

The eigenvalue solution of a large free-free system can produce small negative eigenvalues for the rigid body (zero frequency) modes. This is caused by numerical errors associated with the large number of operations required to develop the stiffness matrix and to solve the eigenvalue problem. The eigenvectors associated with these rigid body modes should be examined to make sure they are acceptable rigid body displacement vectors. The off-diagonal terms in the rigid body rows of the generalized mass matrix should be at least six orders of magnitude smaller than the diagonal terms in those same rows. Normally, if the absolute value of the negative eigen-

4.5.4 (Continued)

values in frequency (ω) units is less than 10^{-6} radians/second, the eigenvectors should be valid rigid body modes.

4.5.5 Establish Tolerance

Tolerances are determined for two parameters of the analytical data, frequency and gain. The frequency tolerances for the Saturn V flight vehicles are assumed to be the same as the percent difference between the analysis and full scale test data. The gain tolerances are obtained by determining the differences between the analytical and test gains and expressing them as percents of the maximum analytical gain. For example:

$$GT = \frac{G_t - G_a}{G_{\max_a}} \quad (4.53)$$

where

GT = Gain tolerance

G_t = Gain from test data

G_a = Gain from analytical data

G_{\max_a} = Maximum gain from analytical data

Gain is defined in Section 4.4.2.

4.5.6 Damping Considerations

On the Saturn V program the damping was assumed to be proportional. This allowed the damping to be introduced as an equivalent viscous damping factor applied to each mode. These equivalent modal damping factors were obtained from full scale tests.

Damping is not only dependent on component construction, it is also strongly influenced by load, reference Section 5.2.4. In the Saturn V vehicle, typical equivalent viscous damping ranges from 0.4 percent in the S-II tanks to three percent in the spacecraft and to 70 percent in the engine servoactuator system. Where local damping differences of this magnitude exist, the normal assumption of modal (uniform) damping is invalid. In this case local amplitude and phase characteristics predicted by modal damping techniques will not give acceptable accuracy. Readily usable techniques need to be developed for estimating and including nonproportional damping in structural dynamic analyses.

Math modeling of the S-II crossbeam and LOX tank is not accurate enough to support Pogo analyses. Much of the prediction tolerance is associated with the damping uncertainty. There is no advantage to developing

4.5.6 (Continued)

techniques for predicting structural gains to 10 percent accuracy when damping is handled by a gross estimate that may be in error by 1000 percent. Structural damping characteristics need to be investigated to where material properties, geometry, type of joints, loads, and temperatures could be the input that would allow a damping matrix to be generated in much the same way a stiffness matrix is generated now.

4.6 SATURN V MODEL EVOLUTION

Early in the Saturn V dynamic analysis program, it was decided that local structural and inertial effects could have a significant effect on the response of control instrumentation. This decision precluded the use of beam type mathematical models which would give centerline motions but would not be able to predict motions on the surface of the structure where the control instrumentation was to be located. The importance of local effects set the requirement for a three-dimensional shell representation of the Saturn V structure. Initially, it was not possible to model the structure in three-dimensional shell detail throughout because the computer computational capacity was not available. Therefore, the original models were a combination of beams and three-dimensional shells which were intended to model both overall dynamic effects and local effects at the flight sensor locations.

As the program progressed, both the engineers and the computer programs were updated through experience and the model evolved accordingly. All the math models used in the pre-test analysis were coplanar models (with the exception of a full shell S-IVB/IU/spacecraft model which incorporated pitch-longitudinal coupling capability). Available data in the early stages of the program indicated that the vehicle was symmetrical in both mass and stiffness. This meant that the structure could be represented by modeling one quadrant of the shell and imposing symmetrical-antisymmetrical boundary conditions to represent the effect of the other three quadrants. These boundary conditions did not allow any cross plane coupling and the vehicle was effectively constrained to planar motions.

As more and more information became available and as testing progressed, it became apparent that significant asymmetries did exist in the Saturn V structure. These asymmetries caused coupling between all planes of motion which could not be predicted by the quarter shell models then in use. The AS-501 and AS-502 flights brought to light strong pitch and longitudinal coupling with the lunar module acting as the primary coupling mechanism. As a result of these two flights, along with the introduction of a heavier and more flexible payload on AS-503 and subsequent vehicles, it was decided to develop a math model with freedom in all six planes which could fully incorporate cross plane coupling capability. When the first coupled model was initiated the eigenvalue capability was limited to 130th order problems so it was necessary to use the modal synthesis approach discussed in Section 4.5.

4.6 (Continued)

The AS-503 and AS-504 vehicles were analyzed using modal synthesis techniques. The effective model size was 291st order. Development of a 300th order eigenvalue capability was completed prior to the AS-505 analysis. This capability proved to be more efficient and less subject to engineering error so it was adopted and is the tool presently being used for Saturn V dynamic analysis. Figure 4-32 shows the evolution of these models. Advantages and disadvantages of each model are shown in Table 4-I.

4.7 COST AND ACCURACY

4.7.1 Cost

Cost and flow time are prime considerations in model development. As an aide for future Government and Industry engineering groups involved in math modeling of complex structures, an estimate has been made of the costs of developing the presently used Saturn V model. In forming this estimate, the following assumptions have been made:

1. Adequate software and hardware program capability exists.
2. The current three-dimensional model is the baseline.
3. No iterations have been considered due to idealization errors.
4. Structural drawings are available.
5. No evaluation of data is involved except the mechanical checks.
6. Mass data breakdowns of each stage and payload module are available, but mass data requires redistribution to nodal network.
7. No allowance has been made for the learning curve.
8. Computer hours are based on the IBM-360 system.
9. No documentation of data has been included.
10. Manpower does not include any allowance for clerical work or supervision.

The planning estimate is shown in Table 4-II. Computer hours, manpower resources in manmonths, and flow time are shown for the stiffness matrix development, the merge of component modules and the generation of dynamic characteristics for one time. As previously stated, this cost

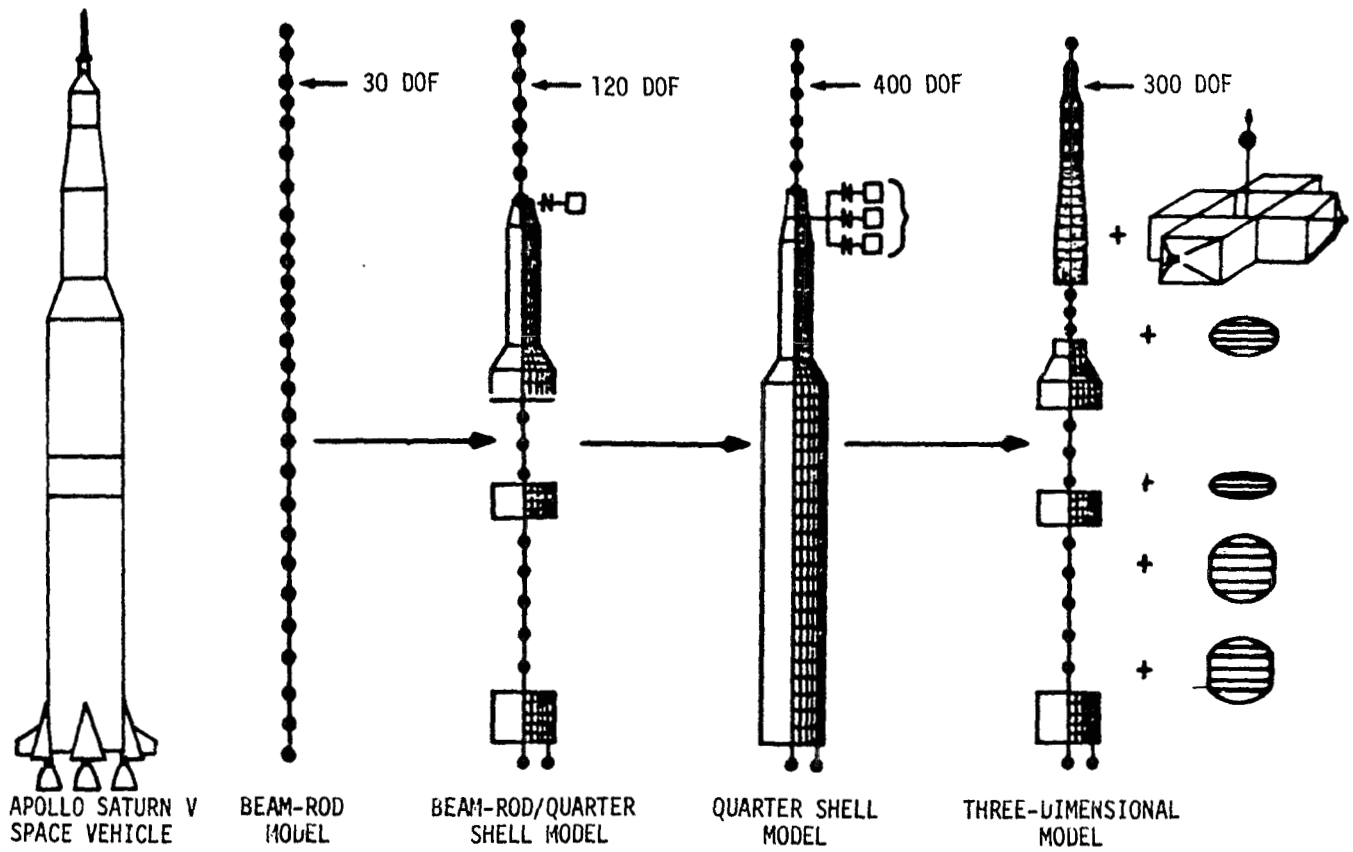


FIGURE 4-32 MATH MODEL EVOLUTION

MODEL	ADVANTAGE	DISADVANTAGE
Beam-Rod Model	Good centerline characteristics, through first four modes.	No interplane coupling allowed. Inaccurate slopes at Flight Gyro Locations. Poor dynamic characteristics above 5 Hz.
Beam-Rod/Quarter Shell Model	Simplicity	Different model required for each flight sensor location.
Quarter Shell Model	Good centerline, component characteristics to 10 Hz, efficient use of freedoms, minimum cost, good representation of instrument unit region.	Model limited due to payload representation, no interplane coupling representation. Different models required for pitch, yaw, longitudinal, and torsional analysis.
Three-Dimensional Model	Good characteristics to 20 Hz, interplane coupling represented, efficient use of degrees of freedoms, good payload representation, good representation of instrument unit region. Coupled pitch, yaw, longitudinal, and torsional characteristics obtained from single analysis.	Configuration changes are costly to make due to large size.

TABLE 4-I ASSESSMENT OF SATURN V MATH MODELS

SATURN V MODULE	COMPUTER HOURS	MANMONTHS	FLOW TIME (MO.)
Launch Escape System	1.0	1.0	1.0
Command Module	2.0	2.0	2.0
Service Module	4.0	6.0	3.0
Saturn LM Adapter Instrument Unit	20.0	30.0	6.0
Lunar Module	6.0	12.0	4.0
S-IVB Stage	5.0	4.0	2.0
S-II Stage	6.0	5.0	2.5
S-IC Stage	6.0	5.0	2.5
TOTAL	50.0	65.0	13.0 *
System Merge	2.0	0.5	0.5
Mass Distribution	6.0	8.0	4.0
Dynamic Characteristics Analysis (1 case)	3.0	0.5	0.5

* Considering work done in series

TABLE 4-II MATH MODEL DEVELOPMENT PLANNING ESTIMATE

4.7.1 (Continued)

breakdown is based on experienced personnel and with the provision that the model nodal network is defined. For the engineering group with average talent faced with a new program such as the Saturn V, factors should be applied to the estimates shown. It is suggested that a factor of 2.0 be applied to manpower, computer hours and flow time to bring an organization up to the plateau of the learning curve. Even experienced engineers in this type of analysis must iterate solutions many times to determine the proper structural idealization with a practical number of degrees of freedom. A factor 2.5 is recommended to be applied to account for the formulation of the optimum nodal network. Checkout of new computer programs is not normally a large expense, however, the flow time is considerable even with comparatively minor program changes.

4.7.2 Accuracy

The math model was accurate in predicting the overall modal properties of the full scale test vehicle for the modes of interest. The frequencies of the first 4 pitch modes were predicted within four percent, and the mode shapes were predicted with equal accuracy. A correlation of the full scale analysis and test results of the first four pitch modes for 100 percent propellant condition is presented in Figures 4-33 and 4-34. The first three longitudinal modes for 100 percent propellant condition were predicted with the same accuracy as the pitch modes. A correlation of these modes are shown in Figures 4-35 and 4-36. The predicted frequency of the fourth longitudinal mode was seven percent lower than that from the full scale test. The correlation of the mode shapes was not very good for this mode. The correlation is shown in Figure 4-36. The fourth longitudinal mode is extremely weak and has little effect on the response characteristics of the vehicle. A frequency response plot of the S-IC outboard gimbal is shown in Figure 4-37. The fourth mode contribution is shown by the small peak near 7.5 Hz. An extensive correlation of pretest analysis and test results is contained in Reference 4-15.

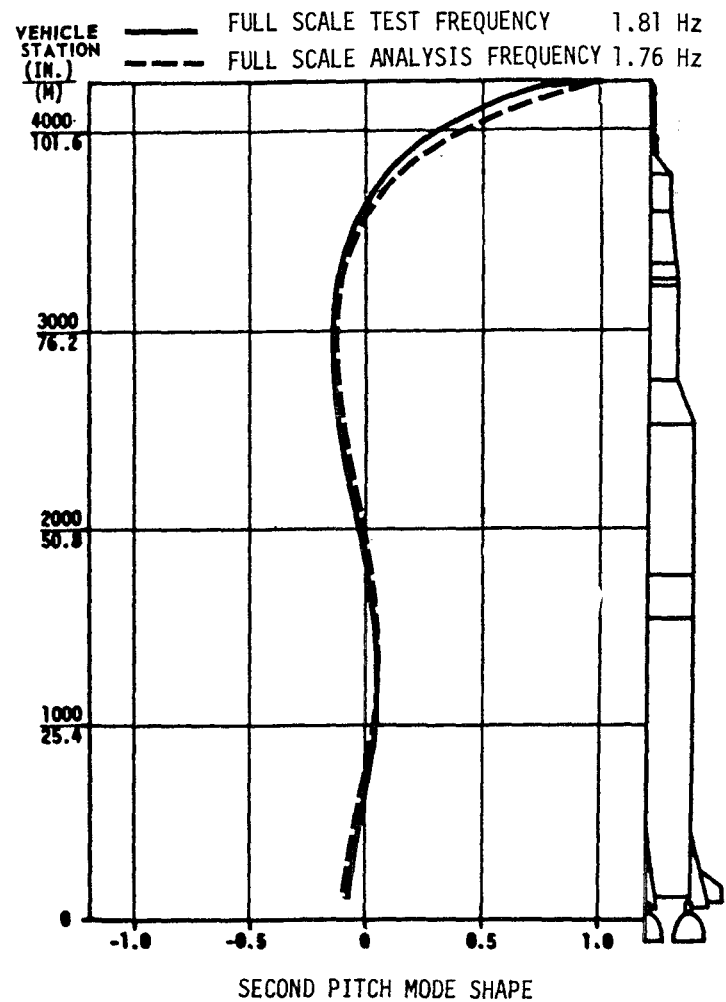
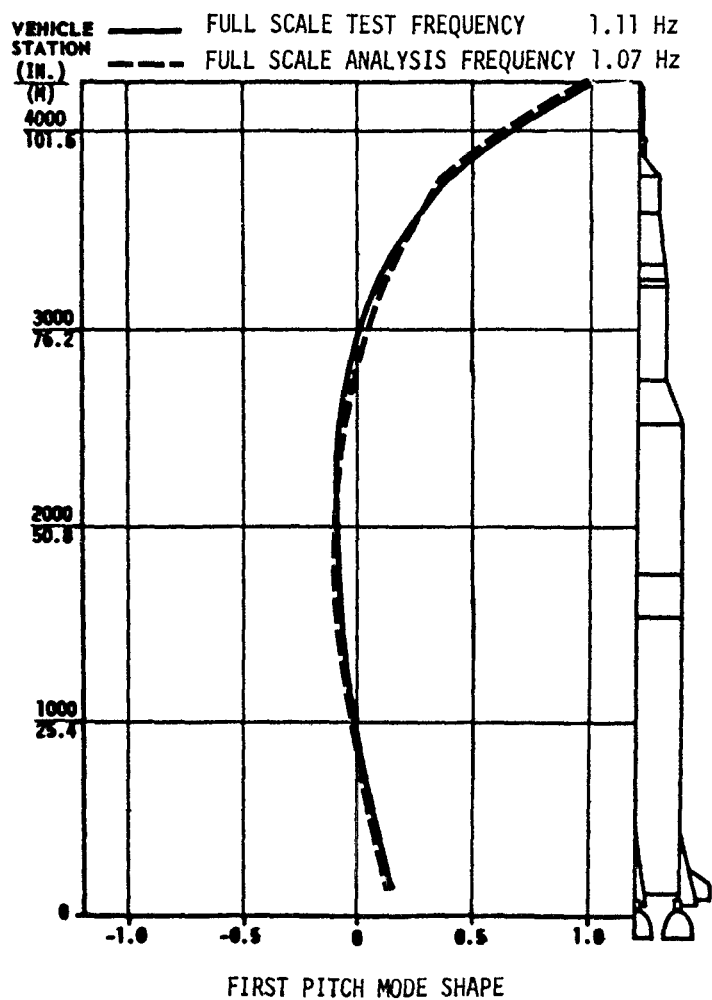
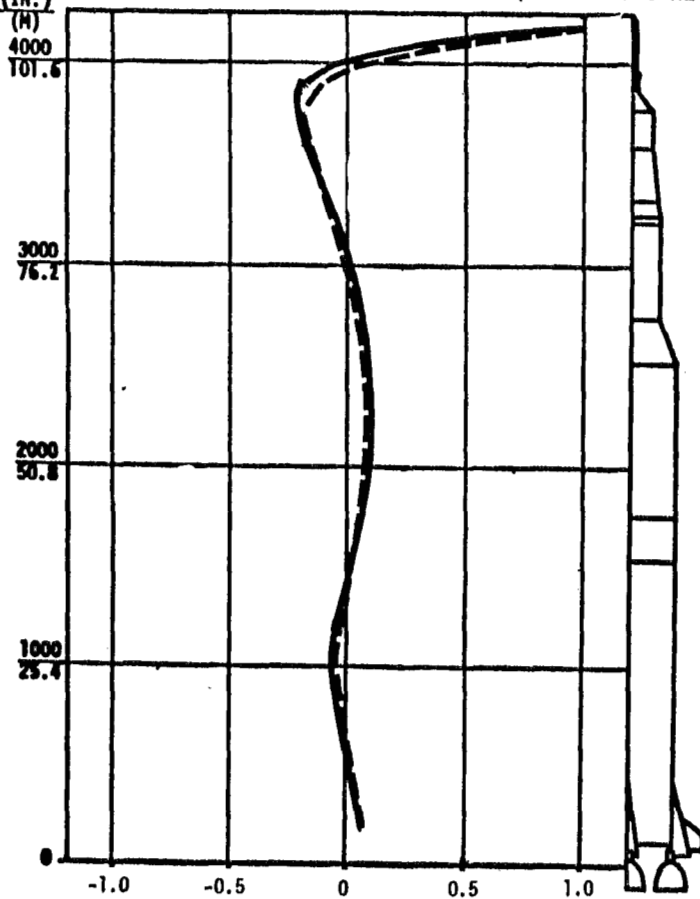


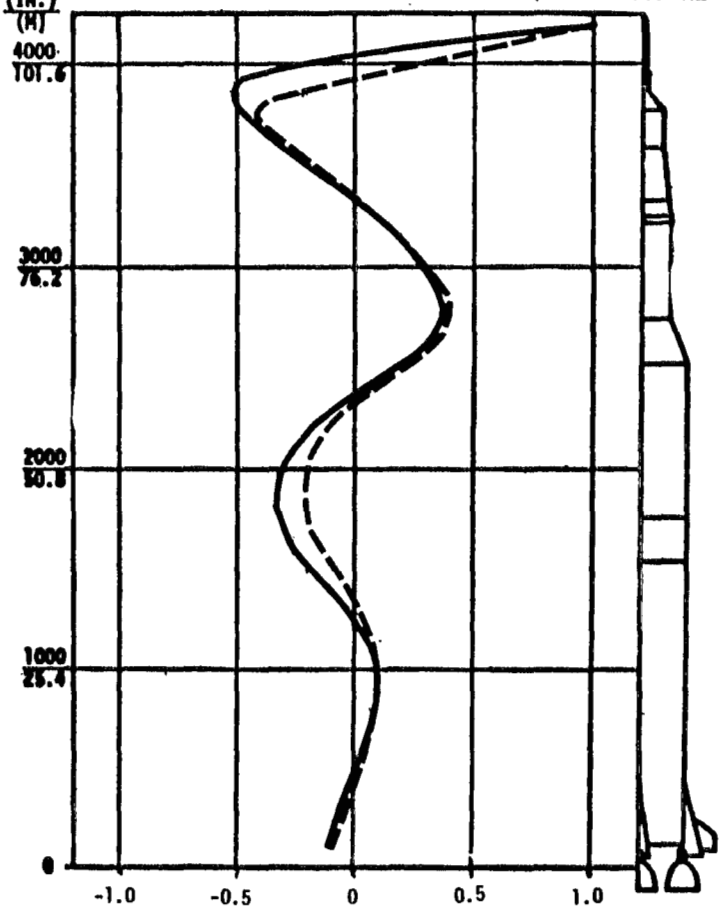
FIGURE 4-33 COMPARISON OF FULL SCALE PITCH TEST AND ANALYSIS RESULTS
 MODES 1 AND 2 - 100 PERCENT PROPELLANT

VEHICLE STATION (IN.)
 ——— FULL SCALE TEST FREQUENCY 2.55 Hz
 - - - FULL SCALE ANALYSIS FREQUENCY 2.65 Hz



THIRD PITCH MODE SHAPE

VEHICLE STATION (IN.)
 ——— FULL SCALE TEST FREQUENCY 3.43 Hz
 - - - FULL SCALE ANALYSIS FREQUENCY 3.32 Hz



FOURTH PITCH MODE SHAPE

FIGURE 4-34 COMPARISON OF FULL SCALE PITCH TEST AND ANALYSIS RESULTS -
 MODES 3 AND 4 - 100 PERCENT PROPELLANT

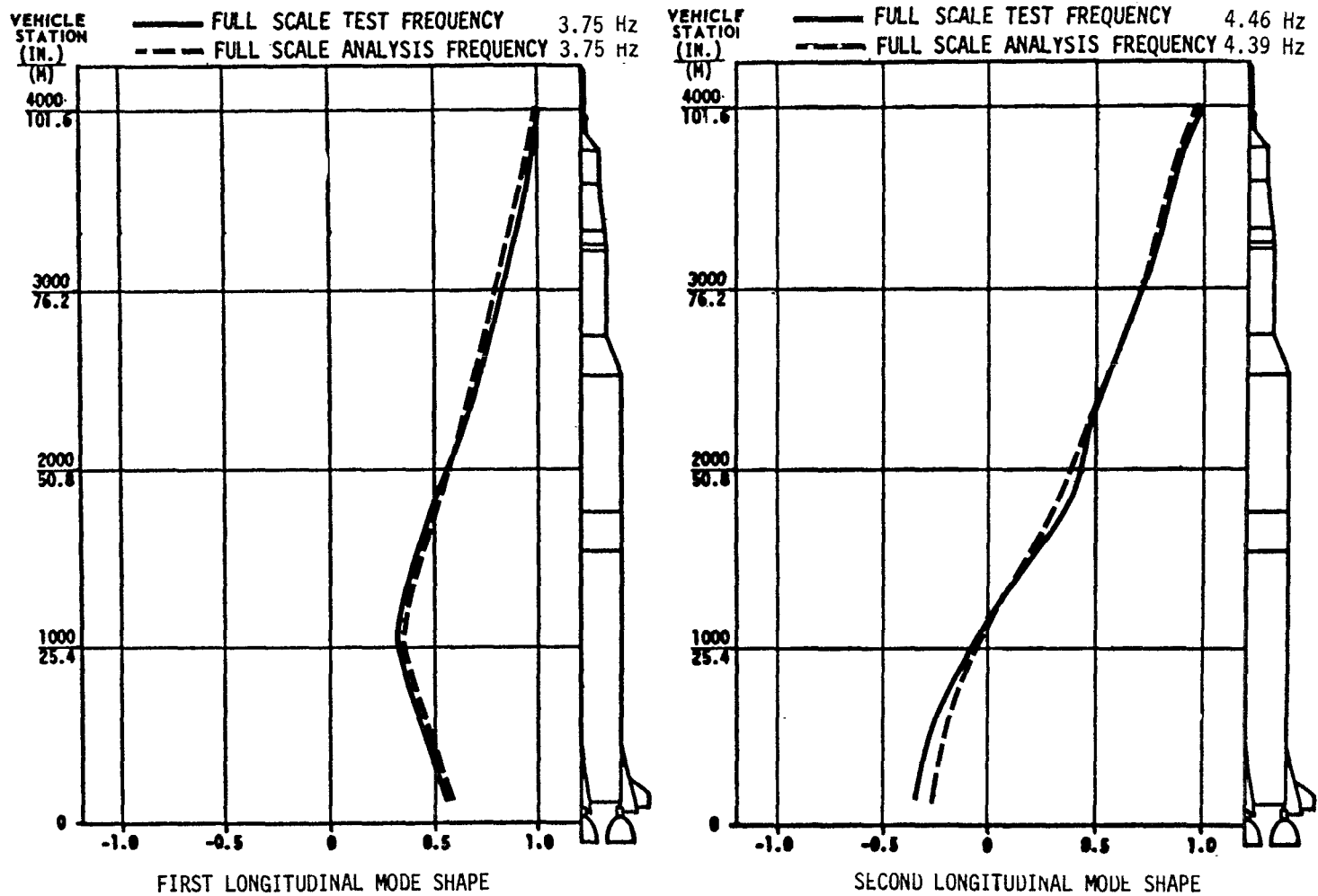
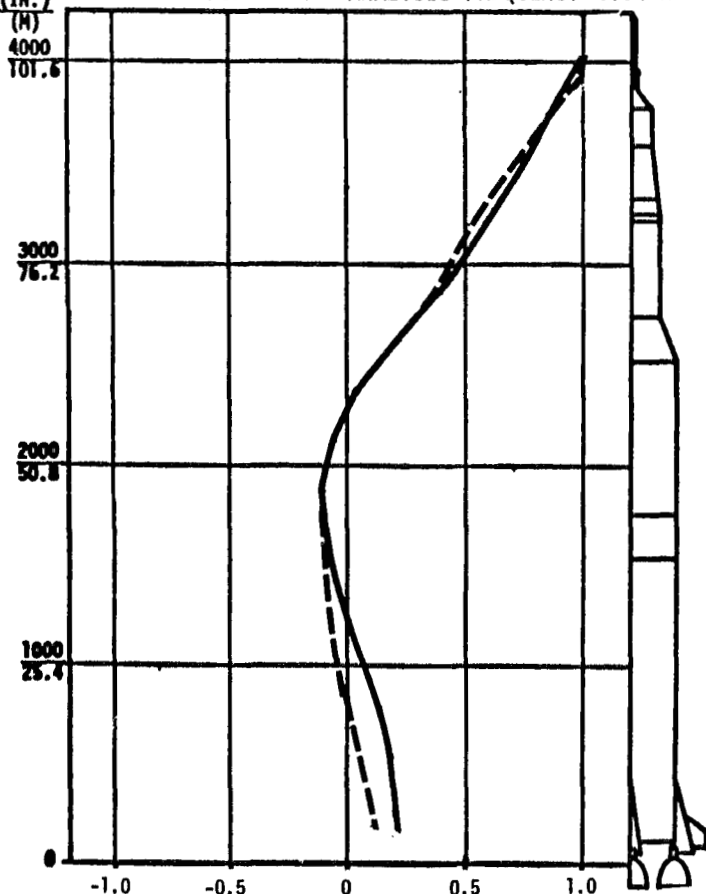


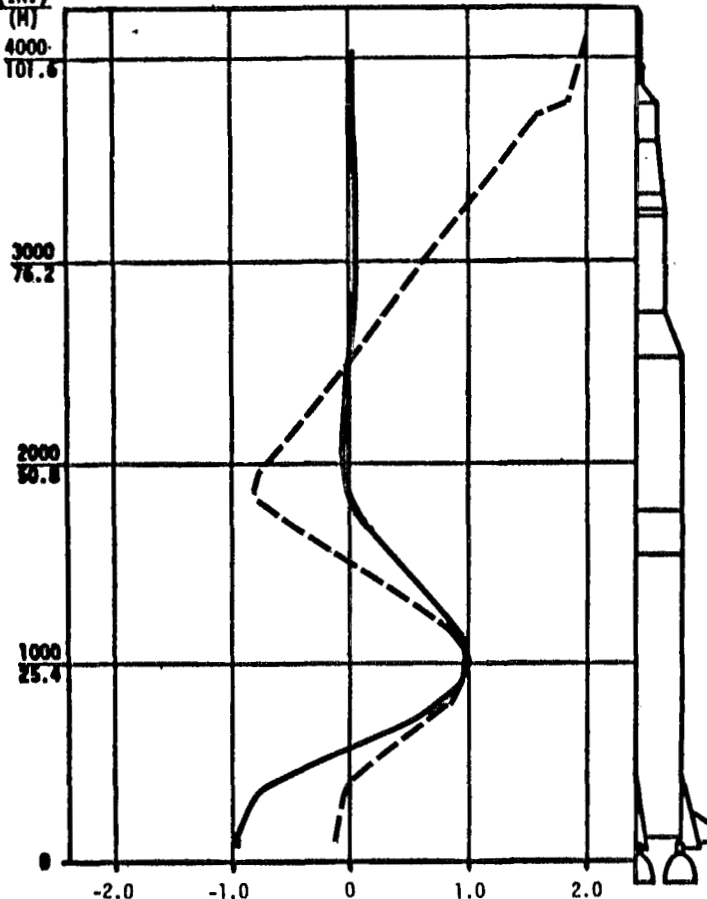
FIGURE 4-35 COMPARISON OF FULL SCALE LONGITUDINAL TEST AND ANALYSIS RESULTS - MODES 1 AND 2 - 100 PERCENT PROPELLANT

VEHICLE STATION (IN.)
 ——— FULL SCALE TEST FREQUENCY 6.51 Hz
 - - - FULL SCALE ANALYSIS FREQUENCY 6.34 Hz



THIRD LONGITUDINAL MODE SHAPE

VEHICLE STATION (IN.)
 ——— FULL SCALE TEST FREQUENCY 7.57 Hz
 - - - FULL SCALE ANALYSIS FREQUENCY 7.04 Hz



FOURTH LONGITUDINAL MODE SHAPE

FIGURE 4-36 COMPARISON OF FULL SCALE LONGITUDINAL TEST AND ANALYSIS
 RESULTS - MODES 3 AND 4 - 100 PERCENT PROPELLANT

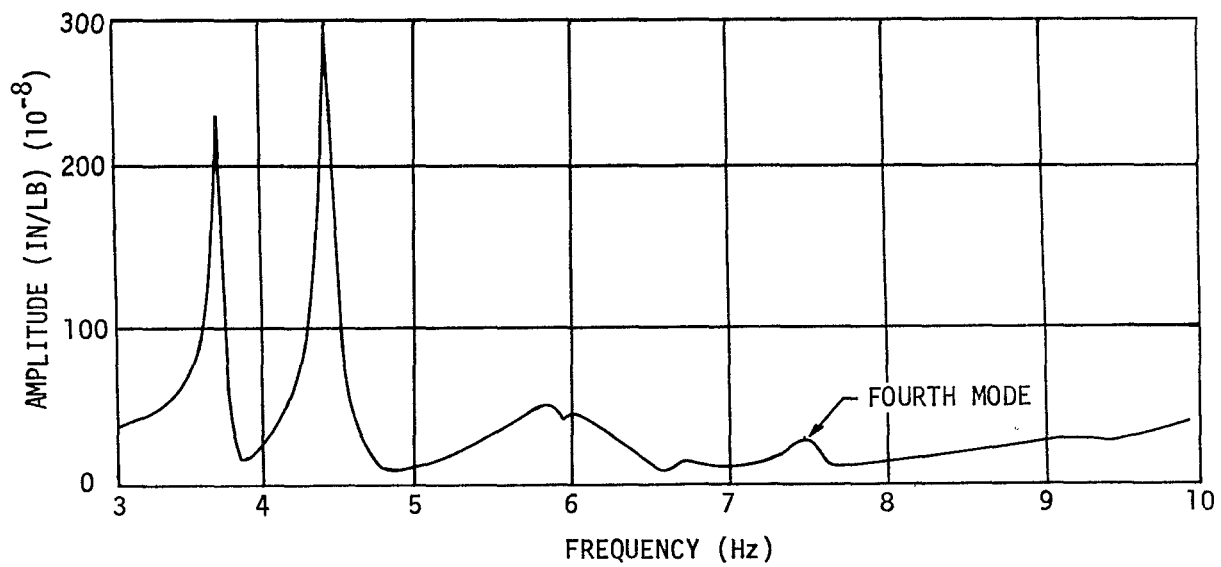


FIGURE 4-37 LONGITUDINAL FREQUENCY RESPONSE OF OUTBOARD GIMBAL -
100 PERCENT PROPELLANT

REFERENCES

- 4-1 Document D5-15204, Saturn V DTV Pre-Test Analysis Methods, The Boeing Company, Huntsville, Alabama, February 26, 1965.
- 4-2 Martin, H., Introduction to Matrix Methods of Structural Analysis, McGraw-Hill, New York, 1966.
- 4-3 Greene, B., Strome, D., and Weikel, R., Application of the Stiffness Method to the Analysis of Shell Structures, Paper presented at the Aviation Conference, American Society of Mechanical Engineers, January, 1961.
- 4-4 Guyan, R. J., Reduction of Stiffness and Mass Matrices, AIAA Journal, Vol. III, P. 380, 1965.
- 4-5 Archer, J., Consistent Mass Matrix for Distributed Mass Systems, Journal of the Structural Division, American Society of Civil Engineers, Volume 89, August, 1963.
- 4-6 Przemieniecki, J., Theory of Matrix Structural Analysis, McGraw-Hill, New York, 1968.
- 4-7 Pestel, E. and Leckie, F., Matrix Methods in Elastomechanics, McGraw-Hill, New York, 1963.
- 4-8 Hurty, W. and Rubinstein, M., Dynamics of Structures, Prentice-Hall, Inc., Englewood Cliffs, New Jersey, 1965.
- 4-9 Palmer, J., and Asher, G., Calculation of Axisymmetric Longitudinal Modes for Fluid-Elastic Tank-Ullage Gas Systems and Comparison with Model Test Results, AIAA Symposium on Structural Dynamics and Aeroelasticity, Boston, September 1, 1965.
- 4-10 Wilkinson, J. H., Householder's Method for the Solution of the Algebraic Eigenproblem, Computer Journal, Vol. 3, 1960.
- 4-11 Francis, J., The QR Transformation -- A Unitary Analogue to the LR Transformation -- Part 1, The Computer Journal, Volume IV, October, 1961.
- 4-12 Francis, J., The QR Transformation -- Part 2, The Computer Journal, Volume IV, January, 1962.
- 4-13 Lomen, D., Digital Analysis of Liquid Propellant Sloshing in Mobile Tanks with Rotational Symmetry. NASA CR-230, 1965.
- 4-14 Lomen, D., Liquid Propellant Sloshing in Mobile Tanks of Arbitrary Shape. NASA CR-222, 1965.

REFERENCES (CONTINUED)

- 4-15 Document D5-15722, Dynamic Test Vehicle Test-Analysis Correlation,
The Boeing Company, Huntsville, Alabama, November 22, 1967.

SECTION 5 DYNAMIC TEST TECHNOLOGY

5.0 GENERAL

The purpose of this section is to present the experience and knowledge gained from the Saturn V full scale dynamic test program on the technology of dynamic testing. Beginning with the establishment of test requirements, the material presented includes a discussion of digital data reduction techniques and concludes with test data evaluation procedures.

The major objective of the dynamic test program was to verify Saturn V math models. These math models were then used to predict characteristics of each flight vehicle with a high degree of confidence. This test-analysis correlation cycle is illustrated in Figure 5-1. This figure is a flow chart showing that the full scale math model was developed using the 1/10 scale analysis and test results. This model was used to predict the dynamic characteristics of the full scale test vehicle. The dynamic characteristics were correlated with test results and the math model revised until good correlation was achieved. The math model was then considered test verified. This verified model then became the baseline model for the Saturn V family of flight vehicles. Tolerances were derived from the correlation. The various structural and mass differences between the test and flight article were then included in the flight model and the test system restraints removed. Since the differences noted above represented a change in input data rather than a math model change, the flight article model could also be considered test verified. The basic criterion was that as long as the article being tested could be described analytically, then defined deviations from the flight article would be allowed.

However, the differences between pretest analysis and flight analysis must be kept to a minimum. A considerable technical judgment is required to determine what differences can be bridged analytically. This judgment must be tempered with the practical aspects of cost and schedule. For example, the localized response that occurred in the IU during full scale testing showed that the flight configuration IU should have been simulated as closely as possible. This is due to the extreme sensitivity of the dynamics at the flight control gyro location to local mass and stiffness changes. The IU simulation on the full scale test vehicle proved to be adequate for the job. However, the simulated LM (which represented the mass and C.G. locations, but not the dynamics of the LM) proved to be an inadequate simulation of flight hardware. Using this simulator, the bridge between the full scale test and analysis correlation math models and flight models was too great. As a result the required confidence level of the flight analysis was degraded where LM activity was significant.

5.1 TEST REQUIREMENTS

A most important item in any major dynamic test is the definition of the test requirements. Test requirements are not a pattern copied from another similar test, but must be carefully considered in light of the objectives. Every facet must be considered to determine whether the objec-

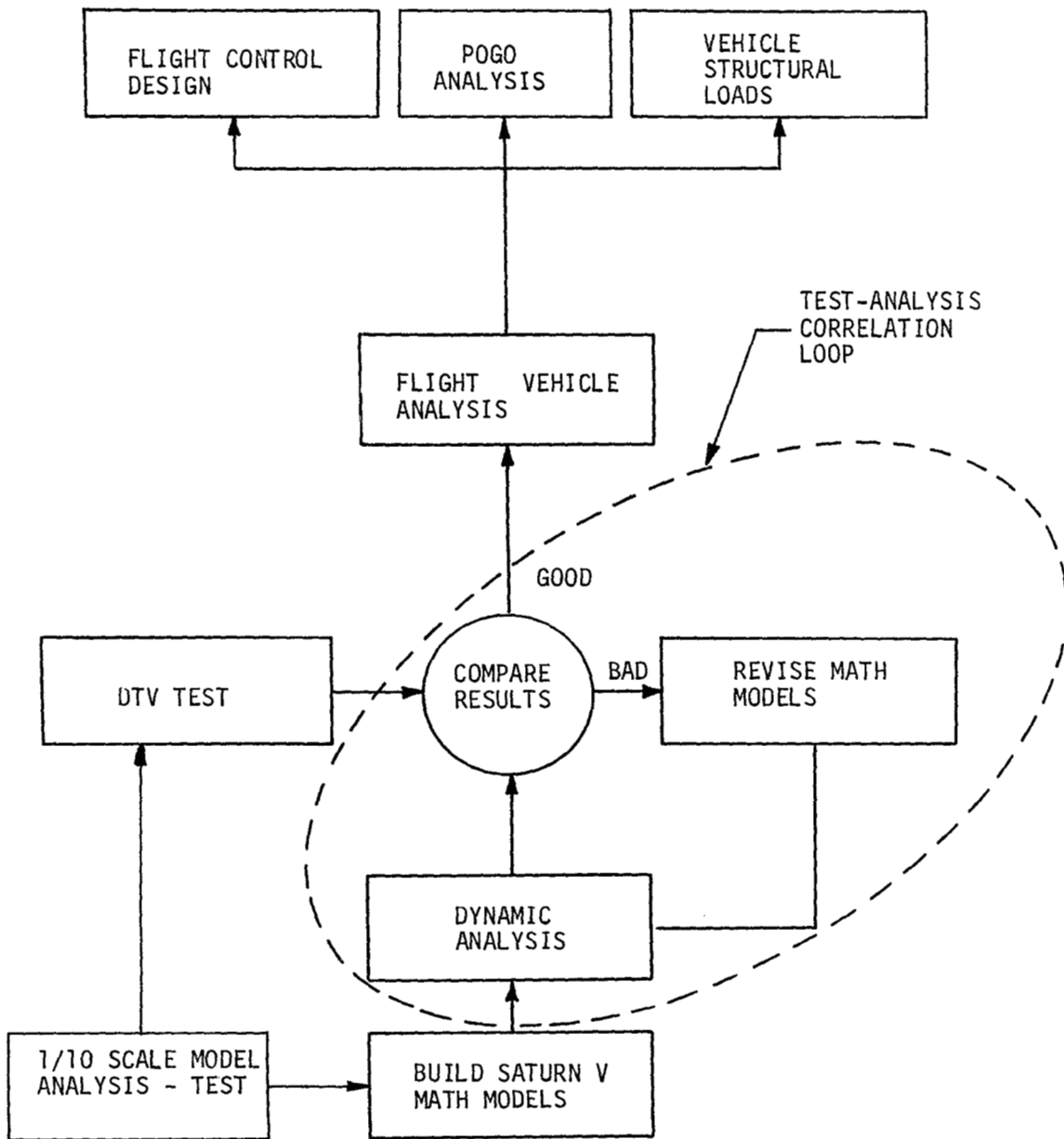


FIGURE 5-1 TEST ANALYSIS PHILOSOPHY

5.1 (Continued)

tives will be met, considering adequate technical output, cost, schedule and volume of data collected. Experience with the full scale test indicates that the user organization must be responsible for certifying the technical adequacy of the test in terms of quality and quantity of data. User requirements must be clearly defined and understood before test requirements can be written. In particular, the dynamic parameters that are important to each user must be identified, and allowable tolerances specified. The sensitive parameters for the Saturn V vehicle are listed in Table 5-I for Pogo, loads, and flight control studies. The user organization must specify the accuracy with which each of these parameters must be determined before requirements for math models and dynamic testing can be defined. For example, if all accuracy requirements fall within the math model confidence band, there is no requirement for dynamic test. All affected organizations must have insight into the requirements and be able to critique requirements that have been initiated by the prime organization. This is a basic consideration in insuring that the test will satisfy all affected organizations.

Test requirements should be a top level control of every important aspect of the test. The full scale test requirements covered test objectives, test configuration, test facility, data acquisition and reduction systems, tests that were to be conducted, pretest analysis, data correlation, and reporting of test results. All of these requirements were merged into a single source document that controlled the test program (Reference 5-1). Requirements could not be changed without a revision to this document being made. Consequently, only the major items were included in this single source document. This document was also the basis for contractual actions in determining the negotiated cost of the total test.

Program level requirements must be identified early in the program. If a program covers several contractors and/or government agencies, a mechanism for maintaining rapid data flow needs to be established at the program management level. One of the major problems encountered initially on the full scale program was the difficulty of getting spacecraft structural drawings. Normal data acquisition channels from one NASA center to another required supplemental action to support the required schedule.

5.1.1 Test Objectives

The basic objective of the full scale test program was to verify mathematical models. These mathematical models could then be used to obtain structural dynamic source data for use in flight control system analyses, flight and ground loads analyses, and Pogo stability analyses. Some secondary objectives were required to support the mathematical model. These objectives included:

1. Determination of dynamic characteristics for major components such as engines, first stage engine fins and fairings, and the first stage propellant lines.

TABLE 5-I SATURN V SENSITIVE PARAMETERS

POGO	LOADS	FLIGHT CONTROL
1. Frequency Range	1. Frequency Range	1. Frequency Range
2. Longitudinal Mode Frequencies	2. Pitch (Yaw) Mode Frequencies	2. Pitch/Yaw/Torsional Mode Frequencies
3. Propellant Line Fluid Mode Frequencies	3. Bending Mode Slopes	3. Pitch/Yaw/Torsional Mode Damping
4. Longitudinal Mode Shapes	4. Bending Mode Shapes	4. Frequency Resp. of the following to a Unit Pitch/Yaw/Torsional Force Applied at the Engine Thrust Pad:
5. Modal Damping	5. Modal Damping	a. Pitch/Yaw/Torsional Slope at Control Gyro Brackets
6. Frequency Response of the Following to a Unit Longitudinal Force Applied at the Engine Thrust Pad:	6. Frequency Response of the following to a Unit Pitch (Yaw) Force Applied at the Engine Thrust Pad:	b. Pitch/Yaw/Torsional Accelerations at Thrust Pad
a. Thrust Pad Longitudinal Acceleration	a. Pitch (Yaw) Bending Moment at Key Vehicle Stations	5. Slosh Mode Frequency
b. Tank Pressure at Propellant Line Outlet	b. Pitch (Yaw) Slope at Thrust Pad	6. Slosh Mode Damping
c. Pump Inlet Longitudinal Acceleration	c. Reactions at Major Component Attach Points	
d. Pump Inlet Pressure	7. Pitch/Yaw/Torsional Response at Key Vehicle Stations Produced by Unit Longitudinal Force Applied at Thrust Pad	

5.1.1 (Continued)

2. Definition of the thrust vector control system dynamics using live hydraulics with proper feedbacks in the actuator system.
3. Determination of modal damping factors to support the flight control and Pogo stability analyses.

At the time of the full scale test, the objectives were considered to be essentially satisfied if the characteristics through the first four vehicle modes (0 to 10 Hz) were adequately defined. As the Saturn V program evolved, the number of modes required to support the problems of the flight vehicles increased. For example on the second stage, a strong Pogo instability occurred at 18 Hz when the frequencies of the LOX tank mode and center engine crossbeam mode coalesced. This local mode corresponds to the 56th elastic mode obtained from the math model.

Bending test results were obtained to 11 Hz and longitudinal test results were obtained to 30 Hz on the full scale vehicle. Since there were no well defined user organization requirements above 10 Hz, the longitudinal data were not extensively reduced and correlated. If a user organization required that all high gain modes be explored to obtain flight control and Pogo parameters, the second stage Pogo modes could have been identified prior to the first flight. This illustrates the importance of identifying in the requirements all parameters that are of importance to the user organizations and following through in the measurement and correlation phases.

5.1.2 Vehicle Configuration

There are two basic vehicle configuration guidelines which the full scale experience indicates are essential requirements for successful test-analysis correlation. The first is to know completely and accurately the configuration at all times. The second is to exercise a stringent technical review of each and every configuration deviation. These are ordinary configuration control functions on any test, but they take on added significance in a dynamic test and analysis task. The following paragraphs will discuss configuration requirements in two parts, structure and ballast.

The basis for configuration decisions include the following considerations:

1. Will a special test article be built?
2. If not, on what schedule will a flight article be available?
3. What restraints does the schedule impose on the tests?
4. Are simulations technically acceptable?

The philosophy of the full scale test program was to have as few structural differences as possible between the test specimen and the flight

5.1.2 (Continued)

vehicle. In general, it is unrealistic to require 100 percent flight hardware since the ground test objectives are to support flight tests rather than to be parallel effort. The deviations which are allowed should be assessed mathematically to insure that they can be modeled accurately. The full scale test requirements placed the following controls on deviations:

1. All deviations from flight hardware where the item weight is more than 20 pounds (9.1 KG) shall be simulated.
2. Simulation of flight hardware for weight, stiffness, and moment of inertia shall be within 5 percent.
3. Simulated components must be mounted on their respective flight specification brackets.

The above requirements were found to be unrealistically stringent. It would have been better to establish a review system for those deviations from flight hardware which exceeded the allowable mass or stiffness changes. For example, a mass change of 1,000 pounds (453.6 KG) in the first stage tank might not have any effect on the ability to meet the test objectives. However, a mass change of 50 pounds (22.7 KG) in the region of the IU flight gyros would have a considerable effect on the flight gyro response and would be a serious detriment to meeting the test objectives. These decisions should be based on engineering judgment and math simulation. They require an advanced knowledge of user accuracy requirements.

A good example of the importance of using actual hardware or accurately simulated hardware was the LM. An excellent LM simulator, fabricated largely from flight article hardware, was originally slated for use on the full scale test. However, as the production of LM hardware fell behind schedule, substitutions had to be made to keep the total program moving. A simple mass simulator was constructed using flight article hardware only in the bracketry that attached the simulator to the vehicle. This simulator was designed to be easy to model and to introduce no unaccountable dynamic characteristics into test results.

The cost of this substitution was not recognized until after the second Saturn V flight. A first stage Pogo instability developed in a strongly coupled longitudinal and pitch mode. The predominant coupling mechanism was traced to stiffness asymmetry in the LM. A special dynamic test had to be conducted to establish confidence in the math models developed to represent this coupling and to provide verification of Pogo suppression hardware.

It is essential to know the configuration being tested to the extent of being able to define at any time what the structure of the various stages is, know what deviations have been made, and be able to

5.1.2 (Continued)

describe the deviations in the pre-test analyses such that the math model being analyzed and the test vehicle are identical. This is a normal configuration control task on most tests, but in dynamic testing it is essential that the configuration does not change from the flight configuration unless the requirements permit this change. Therefore, every deviation from flight hardware that exceeds allowable tolerances in certain areas of the vehicle must be passed through the technical organization for approval before the configuration change is allowed.

The vehicle propellants were simulated in all areas of the vehicle for the testing. Simulants were used because of the logistics problems and cost associated with storing liquid cryogenics (LH₂ and LOX) for long periods of time, and the potential hazard to personnel working near the vehicle during testing.

A study to determine a propellant simulant considered densities, viscosity, homogeneity, flammability, compatibility, contamination, corrosion, along with handling facilities, storage facilities, dumping facilities and cleaning facilities. The results of the study indicated a solution of water and sodium dichromate would fulfill most requirements for a fluid simulant. This solution was used in all cases to simulate the LOX and RP-1. A separate analysis determined that for bending tests the LH₂ tanks could remain empty with no degradation of results and for longitudinal tests the LH₂ could be simulated by an equal weight of the water solution.

To minimize corrosion, the tanks of the first stage were filled with water containing 100 parts per million by weight of sodium dichromate. Since the second stage would be used for other testing and could not be contaminated, deionized water with a minimum of 100 parts per million by weight of sodium dichromate was used as ballast. Third stage and payload propellant masses were also simulated with a ballast of deionized water and sodium dichromate.

In all cases where there was liquid propellant, the ballast was simulated by weight as opposed to a volume simulation. Where there was solid propellant, the ballast was simulated by lead rings. In the oxidizer (LOX) tanks, the water levels extended further up into the bulkheads than in the normal flight condition. Therefore, special hardware was required to extend the LOX vent valves above their flight level. No hardware changes were necessary on the S-IC fuel (RP-1) tank since the water level was lower than the normal flight condition.

Another study was performed to determine the tolerance required in establishing the levels of propellants in the tanks. The following tolerances resulted: first and second stage tank tolerances were $\pm 2,000$ pounds (907.2 KG) per tank; third stage tank tolerance was $\pm 1,000$ pounds (453.6 KG) per tank. A sight gage was used to indicate fill level and the quoted tolerances came from the maximum resolution obtainable from the vertical sight gage coupled with the tank calibration error. The

5.1.2 (Continued)

study indicated that the obtainable tolerances using the sight gages were acceptable. The SM and LM tank tolerances were one-tenth of one percent. These tolerances were a combination of the allowable error in tank calibration and the allowable error in measurement. Propellant levels were prescribed in the requirements document, and then established in test within the prescribed tolerances. The liquid levels were recorded in test and used in the post-test analysis (when any significant changes occurred). The requirement for propellant levels was supported by math analysis. Both the actual condition and the equivalent weight water simulation were analyzed. The results were similar.

Gaseous nitrogen (GN₂) was used to simulate the ullage pressure in all stage tanks. The ullage pressure used on the launch vehicle stages was 10 psi (68,948 N/M²) (about one-third of the flight pressure). Positive pressure in all stage propellant tanks was maintained at all times, but ullage pressure was not used in payload propellant tanks. The requirement for the reduced ullage pressure was based on:

1. Flight pressures could not be used since safety requirements would have barred all personnel from the test area and this was not acceptable.
2. Some ullage pressure was necessary to eliminate local bulk-head resonances.
3. Ten psi was shown to be satisfactory on the 1/10 scale model test and compatibility between the two tests was desirable.
4. The possibility of negative pressures due to temperature changes needed to be eliminated.

Pretest analysis and early 1/10 scale model tests results indicated that the reduced ullage pressure would not significantly affect modal characteristics of the vehicle structure.

5.1.3 Test Facilities Requirements

The major items considered in defining requirements for the full scale facility were the housing structure, suspension system, stabilization system, excitation system, hydraulic system and propellant ballast system. The experience gained with these items on the full scale test program led to the establishment of the following general guidelines for defining test facility requirements:

1. The effects of the suspension system on the dynamic characteristics of the test article must be assessed analytically before the suspension system requirements can be defined.

5.1.3 (Continued)

2. When research and development items are required for a test program the schedule must include adequate time for acceptance tests and modification. Design criteria for such items must be stringently evaluated to determine compatibility with test objectives, structural capabilities, and overall test requirements.
3. In a test program involving large pressure vessels or tanks such as the Saturn V vehicle, it should be a test requirement that a fail-safe system be installed to prevent negative pressures occurring in these tanks. The Saturn V tanks are such that draining the tank with no open vents will buckle the upper bulkheads.
4. The stabilization system must provide static stability and protect the vehicle from damage during test. Stabilization system effects on test article dynamic characteristics must be assessed analytically in order to define final requirements.
5. Test facility components designed to commercial criteria must be thoroughly evaluated to insure that their performance meets the established stage criteria.

The major components comprising the test facility are discussed independently in the following paragraphs.

A. Housing structure

The test tower structure was designed prior to the establishment of the test requirements due to the very long lead time required. The test tower was also designed to handle possible growth vehicles such as the Nova, which was considered as a continuation of the Saturn family at that time. The test tower protected the vehicle from the environment, such as wind and rain, allowed access by means of platforms adjacent to the vehicle at various levels, carried and supported the propellant transfer lines, instrumentation cables and pneumatic pressurization and control system lines that go to different stages on the vehicle, and provided a means of attachment of the stabilization and suspension systems. The tower included a mobile, overhead crane for lifting the vehicle stages inside the building and stacking them on the support facility.

B. Suspension system

The requirement for simulating a free-free condition in the vertical position posed a major vehicle suspension system design problem due to the physical size of the test specimen. Prior to designing the suspension system, the test tower had been constructed; therefore, the suspension system designed would have to fit into the existing structure without creating major

5.1.3 (Continued)

rework. Both the cable and hydrodynamic support systems were developed in parallel. The cable system, being based on a proven design, was the primary support system.

The cable system supported the vehicle as a giant pendulum within the tower. The cables were attached to the tower through coil springs to give the vehicle as little vertical and rotational restraint as possible. This system turned out to be bulky, with large effective masses near the gimbal plane of the vehicle. The cable vibration modes would have added effective damping to the test system. The more revolutionary hydrodynamic system was to be checked out during the program to determine its application to future dynamic testing. The original concept devised by George Von Pragenau of NASA is described in Reference 5-2. Fortunately, the hydrodynamic suspension system proved to be highly successful and the spring cable concept was abandoned.

The hydrodynamic support system was a tremendous asset to the full scale program. Its effects on the dynamic characteristics of the vehicle were minimal due to a very low effective mass and very low damping. For example, rigid body rocking tests were performed by two men hand exciting the system by pushing on the first stage fins until the 6,000,000 pound (2,721,600 kg) system reached two inch (5.1 cm) amplitudes. The development and successful application of this design concept represented a significant advancement in the field of dynamic support systems.

The hydrodynamic support system was a combination of oil bearings and vertical gas springs which gave the vehicle essentially no restraint in the horizontal direction and a very soft spring support in the vertical direction. A major advantage of the oil/gas support system over the cable/spring system was the relatively little mass added to the vehicle structure. This system was much more compact than the cable/spring system and did not share the inherent cable dynamic problems. Figure 5-2 is an illustration of one of the four hydrodynamic (oil/gas) supports. The upper plate, upon which the vehicle rides, has a milled spherical surface on its underside which floats on an oil film pumped through in continuous high pressure flow. The upper plate is free to rotate and offers no local rotational restraint to the vehicle. The upper plate in turn rides on a second plate with a flat undersurface supported by a high pressure oil film. This flat surface provides the lateral freedom to the vehicle. The lower plate is supported by a cylinder/piston assembly which entraps a preset volume of nitrogen gas used to give the soft vertical spring support to the vehicle. Raising and lowering the vehicle is accomplished by changing the level of oil upon which the entrapped nitrogen rides within the piston. The vertical spring rate is set by controlling the initial nitrogen precharge volume.

After installation in the test tower the system was checked out using the first stage vehicle and operated very satisfactorily, passing all of the specification requirements. There were two major concerns with this system. The first was whether there would be any metal-to-metal

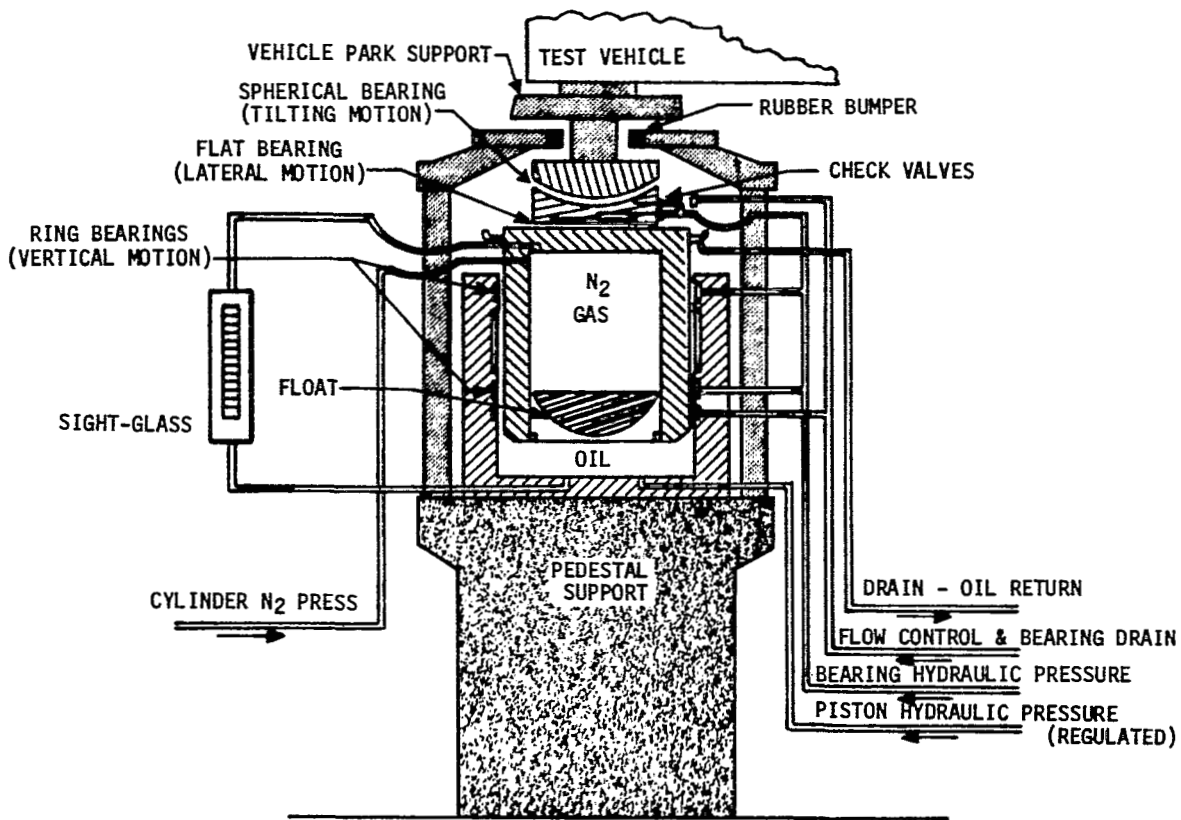


FIGURE 5-2 HYDRODYNAMIC SUPPORT

5.1.3 (Continued)

contact of the bearings during test, how this could be identified, and what the effects on test results would be. The second was whether the system was a fail-safe mechanism, i.e., what would happen if one of the pressure lines should fail and one of the supports should drop from the vehicle. Testing proved that neither concern was warranted. However, a failure analysis was performed to determine what structural damage to the vehicle would result from hydrodynamic support failure. This analysis indicated possible catastrophic damage to the vehicle if one support failed while the system was operating at the planned test height of 1.5 inches (3.8 cm) above the parked position. Rather than redesign the support system to prevent this catastrophic failure, analysis showed that changes in operation methods could effectively eliminate the problem. Operating height was reduced to 0.7 inch (1.8 cm) above the parked position and shims were installed under the support system to lower deceleration loading that would occur if one support failed.

C. Stabilization system

The stabilization system accomplished the following two objectives:

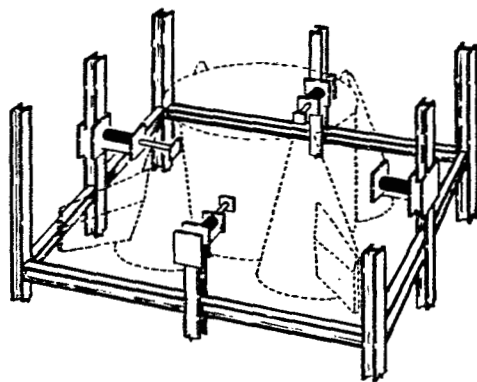
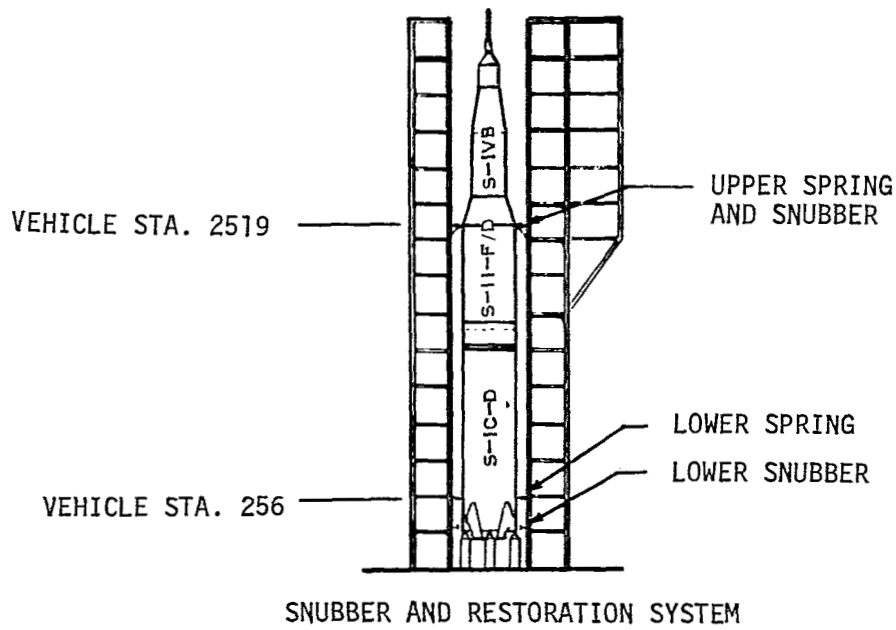
1. Maintained static stability of the vehicle.
2. Kept the vehicle centered on the support system during test.

The vehicle under some propellant loading conditions was statically unstable. The criterion for stability was that the stability ratio (the restoring moment divided by the overturning moment) must be equal to or greater than 1.5. As the hydrodynamic support system itself provided no lateral restraint, the vehicle also had a translational instability. To eliminate these kinematic instabilities, an elastic restoring system was added. Lightweight collars were used to attach coil springs to the vehicle at the S-IC thrust structure and at the top of the second stage. Figure 5-3 is a schematic of the stabilization system.

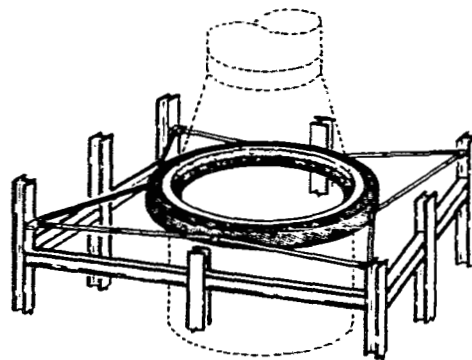
An upper and lower snubber system shown in Figure 5-3 was designed to restrain the vehicle in the event of excessive tilt resulting from a failure of the restoration system, hydrodynamic support system, vehicle structure or force excitation system.

The design of the restoration system had to satisfy the following dynamic criteria:

1. The rigid body lateral or rotational frequency was limited to one-sixth of the fundamental vehicle bending frequency.
2. The rigid body torsional frequency was limited to one-sixth of the fundamental vehicle torsional frequency.
3. The system was required to have small damping.



LOWER SPRING
(STATION 256)



UPPER SPRING
AND SNUBBER (STATION 2519)

FIGURE 5-3 STABILIZATION SYSTEM

5.1.3 (Continued)

4. The location of the restoration system attachment to the vehicle should result in negligible effects on the mode shapes and frequencies.
5. The restoration system itself was not allowed to have a resonant frequency in the test range of frequencies (0.1 to 30.0 Hz).

A parameter study was initiated to determine the effects of the suspension on the flexible mode shapes and frequencies. Results indicated that the upper and lower systems could be positioned at points that were near the nodal points for the first four flexible vehicle modes. Beam analyses were conducted to compare the dynamic characteristics with and without the restoration system. The results of the study showed negligible differences in the modal characteristics.

All of the restoration springs were pretensioned to allow a residual tension stress in all springs when the vehicle was at its limit of travel, i.e., all springs were always fully effective up to maximum excursion of the vehicle. The fatigue life of the system was designed for 10^7 cycles.

The snubber system was required to restrain the vehicle in such a manner that no structural failure would occur at the points of snubber contact and that the vehicle would not tilt sufficiently to contact the work platforms or tower structure. The snubber system was equipped with micro-switches to sense excessive vehicle motion and turn off the thrusters as quickly as possible such that:

1. The oscillations would be reduced before the snubber loads become excessive.
2. Time was available to take corrective action to right the vehicle in event of excessive tilt.
3. The test data would not be affected by undetected snubber contact.

D. Excitation system

As was the case for the suspension system, the excitation system was a project requiring research and development. Based on a preliminary projection of requirements, NASA decided that the thruster systems then on the market would not be sufficient to do the job. Consequently specifications were developed to procure a thruster system with a capability of four-inch (10.2 cm) single amplitude linear stroke with a 20,000 pound (88,965 N) force output. An independent study was made to determine requirements for an excitation system. These studies generally concurred with the NASA requirements for the four-inch (10.2 cm) stroke.

5.1.3 (Continued)

This stroking requirement was based on an excitation of sufficient amplitude at the sensor points to allow an accurate determination of mode shape using the available instrumentation. It was determined subsequently that the four-inch (10.2 cm) stroke was not a requirement and that a 0.5 inch (1.2 cm) stroke would have been sufficient. This difference was due to improvements in instrumentation sensitivity and to modal damping that was near 0.5 percent rather than the estimated 2 percent. Also, the limited structural capability at the CSM interface and at the upper Y rings of the S-IVB stage restricted the excitation force and stroke.

Acceptance testing showed that the initially procured thrusters were totally unacceptable. The sine wave was distorted, and a large amount of third harmonic content was evident in the signal. It appeared for some time that the thrusters would have to be rejected and the test schedule extended. However, modification to the equipment and changes in the operating procedures produced acceptable thruster characteristics. The major problems encountered and their solutions are:

1. The output of the thruster was unstable and tended to enter a divergent 120 Hz oscillation that was driven by noise in the power amplifier. It was found that the armature and stinger connecting it to the vehicle had a 120 Hz component resonance. The amplifier feedback circuit coupling the output signal back to the amplifier input had a large enough gain at 120 Hz to induce the instability. The stinger was redesigned to eliminate the 120 Hz resonance, and a notch filter was added to the feedback circuit to reduce gain at 120 Hz.
2. Harmonic distortion in the thruster force output was caused by back e.m.f. generated by the thruster. The distortion was eliminated by operating with maximum armature current and minimum field current necessary to obtain the desired force level.

The thrusters were connected to the vehicle by stinger assemblies that consisted of flexures, a load cell, and a piece of pipe. Dynamic analysis was performed on the assemblies to insure that no resonances occurred in the test frequency range. The primary purpose of the flexures was to limit the moment and shear loads imposed on the thrusters. At the beginning of testing a large number of flexures and load cells failed. Analytical study indicated that the flexures were inadequate from a fatigue standpoint. This problem was eliminated by using flexures from a different manufacturer.

5.1.3 (Continued)

E. Hydraulic systems

A ground hydraulic system was provided to support the frequency and transient response testing of the first stage thrust vector control (TVC) servoactuators. These servoactuators control the thrust alignment by gimbaling the four outboard engines. The ground hydraulic system was designed to commercial system criteria. The supplied filtration proved inadequate to maintain the combined ground-stage system at the cleanliness levels required by the stage. These requirements were necessary to obtain representative performance from the servovalves. The addition of a filter solved this problem. System cleanliness was checked by particle counts of supply and return fluid samples prior to test and every four hours during test. Evidence of servovalve silting was checked for by examining servoactuator static stability as evidenced by limit cycling. A pretest analysis of the stage TVC system and ground hydraulic unit was accomplished to predict system performance during test and to determine ground system accumulator design requirements.

5.1.4 Data Acquisition and Reduction System

The experience from previous dynamic tests indicated that a program of the magnitude of the full scale test would require a completely automated system for data acquisition and reduction. The volume of data to be acquired and reduced was such that the more completely automated the system could be, the more engineering time could be spent on data validation and evaluation. The system used for the full scale test was completely automated. This allowed the data to be evaluated to a high level of confidence within 24 hours of when the data were obtained. Also, rapid dissemination of reduced data to user organizations was possible.

The following guidelines pertain to the establishment of requirements for the data acquisition and reduction systems:

1. Large scale tests with extensive instrumentation require that the data acquisition and reduction systems be automated. Automatic control increases consistency and decreases error incidence. In addition, automatic data reduction techniques increase the amount of data that can be effectively reduced. Further, it is important to reduce, validate and evaluate all test data. Acquiring more data than can be effectively reduced and properly evaluated is an expensive waste of equipment and manpower.

5.1.4 (Continued)

2. The end item accuracy of the instrumentation train required to meet the objectives must be determined. This will permit accuracy tolerances to be assigned to each instrumentation component, such as accelerometers and amplifiers.
3. Acceptance test requirements for test equipment must be rigorous enough to detect any deviation from specifications. Also, the requirements for acceptance test should be defined in light of the test objectives rather than the theoretically possible performance of the equipment.
4. The reputation of the vendor is of equal importance to the specification in the selection of critical instrumentation.
5. Data acquisition system requirements must be closely matched to those of the data reduction system to insure total system compatibility.
6. Graphic display systems should be considered when establishing data reduction system requirements for future tests. Especially valuable for on-site evaluation, such systems can provide real-time visibility of test parameters. Graphic displays are also valuable tools for final data validation and editing functions. It should be a test requirement that graphical records be made of all test data, and that these records be displayed on-site as the data are obtained.

A. Data acquisition system

The basic component of any dynamic test data acquisition system is the sensor instrument. Requirements for the sensing instruments used on DTV were based on the available accuracy and sensitivity in the frequency and amplitude ranges of interest. Stringent accuracy requirements were imposed on the full scale test instrumentation because the test data would be used to force the mathematical model to conform to the measured structural dynamic response of the test article. The end item accuracy of the entire instrumentation train is governed by the test objectives. From the overall accuracy required to satisfy test objectives, individual component accuracies can be determined. Allowable percentage error can be allotted to the sensor, the signal train, the data reduction equipment, etc. The dynamicist has to be concerned with the amplitude and phase characteristics of his instrumentation system over the amplitude and frequency range of the test. An instrumentation specialist has to convert these requirements into the specifications to be used in the selection of particular instruments.

5.1.4 (Continued)

Full scale test data were collected in the form of digitized data on magnetic tape (128 channels) and analog signals on oscillograph chart recorders (64 channels). The fact that only one-half the total channels could be displayed on oscillograph recorders was a disadvantage for on-site review. For example, the automatic gain control system increased or decreased the gain by a factor of 10. During initial testing it was noted that in isolated instances the gain was really a random number for some channels. This gain change error was very difficult to identify since the change normally occurred approaching a resonant peak where a factor of 10 change would not be noticed except on the oscillograph records. Future data acquisition system requirements should include on-line display of all recorded data.

Automation of the acquisition system required that the data collection and recording functions be computer controlled. This imposed a requirement for significant amounts of software development or preprogramming of the computer system. This was illustrated on the full scale test by the automatic frequency interval selection and steady-state amplitude determination features of the acquisition system. The acquisition computer varied the thruster frequency increments such that relatively large increments were produced at the low response portions where definition was non-critical while increments as small as 0.002 Hz were chosen at the peaks for maximum definition of resonant frequencies and response peaks. The steady-state amplitude feature allowed the computer to automatically decide when the vehicle had settled out at each test frequency and the data collection would commence.

A minor disadvantage to automatic computer control of the data acquisition system is the total dependence upon the state of the equipment. Failure of the computer core or peripheral equipment can cause considerable down time while waiting replacements. A preliminary requirement that the responsible vendor have replacements available on short notice would reduce this problem significantly.

B. Data reduction

The purpose of the data reduction system is to reduce the data acquired and present it in the form required for proper analysis and evaluation. On-site reduction of data is necessary to permit a quick evaluation of whether the test can proceed to the next condition. In addition, real time data reduction and display are essential to insure that response levels detrimental to the test article are not produced during test.

Considerable advance planning of how the data will be processed is required for these reasons:

1. Validation of a large volume of data is a time consuming task without automated data reduction techniques.

5.1.4 (Continued)

2. Data must be reduced and presented in the format required by the user organizations in order to be of maximum benefit to them.
3. The data reduction methods must be selected; complex reduction techniques such as the Levy curve fit procedure are especially tailored to automated processes.

The on-site mode shape display concept employed on the full scale test would be of singular value to exploratory testing. In this system a Fourier analysis was made on up to 30 significant sensors. The normalized output was displayed on an oscilloscope with the vehicle outline sketched on the screen. The mode shape characteristics were monitored on site and were also recorded on film to obtain a permanent record of mode shape development.

Central control should be exercised over all structural testing and data from a major program such as the Saturn V. Several different Government agencies and their contractors will be involved in structural dynamic testing of program hardware. For example, on Saturn V, MSFC was responsible for dynamic tests of the Saturn V performed by Chrysler and Boeing, of major component tests performed by North American, and of an S-II mini-stage test performed internally. On the same program, MSC was responsible for a spacecraft test performed internally, a spacecraft test performed by Wyle Labs, and tests of the LM performed by Grumman. LRC was responsible for testing the 1/10 scale model.

In each case, different data acquisition and reduction techniques were used. Where contractors were involved, they were each given responsibility for setting up and maintaining the library of their test data. Each agency established its own system with varying degrees of rigorous documentation. The end result is a collection of data in different formats that impedes flow of information across a program and insures that carryover from one program to the next will be negligible.

An integrated technical test plan should be developed for all structural testing within a program. Part of this plan should be the development of a single structural dynamic data reduction program having various output options that are all in consistent format. This program should be used by the Government and their contractors. General criteria should be developed to insure consistency in the data obtained from the various tests. A central library of test experience should be established and maintained. Data from this library should be readily accessible to any agency having a legitimate need-to-know. This will promote data cross flow and insure preservation of data for future programs.

C. Calibration

There are four basic calibrations that each sensor should be subjected to:

5.1.4 (Continued)

1. Acceptance test
2. Pretest calibration
3. On-site calibration
4. Post-test calibration

The acceptance test is nothing more than a check on the vendors product to insure that it meets specifications. The importance of this step is illustrated by the servo-force-balance accelerometers initially procured for the full scale test. Eighty-five percent of these accelerometers were rejected as received from the vendor because they did not pass the acceptance test. The primary problem was that the bearings in the accelerometer would malfunction and cause a considerable shift in the sensor output. This was of real concern since the test schedule was impacted considerably and obtaining special purpose accelerometers requires a long lead time. The problem was resolved by going to another vendor who, at considerable extra program cost, produced sufficient accelerometers to maintain the full scale test schedule. This experience not only points out the importance of the acceptance test but also emphasizes the importance of the vendor's reputation.

The second calibration required for each instrument is the pre-test calibration. This is a sophisticated calibration that determines DC output factors, amplitude and phase output deviations as a function of frequency and linearity. The linearity characteristics are determined by performing the calibration at several different levels, i.e., 10 percent full scale, 50 percent full scale, and 100 percent full scale. In addition to verifying the vendors calibration, the pretest calibration also:

1. Provides the correction factor that must be used in data reduction. For example, 1.0 g may equal 9.985 volts as opposed to 10 volts nominal.
2. Provides the scale factors for use in the on-site calibrations.
3. Provides the phase and amplitude deviations as a function of frequency to be used in the data reduction program for sensor output correction. This correction is combined with the phase and amplitude deviations of other elements in the acquisition system.
4. Provides the baseline calibration to be used to spot check calibrations after individual tests.

The on-site calibration performs two basic functions. It corrects amplifier settings to assure that no drift has occurred in the system. Secondly, it provides verification that none of the instruments have become

5.1.4 (Continued)

invalid during the test. On the full scale test this calibration was performed every four hours by an automatic procedure programmed through the control computer.

D. Error analysis

An error analysis was performed to include the effects of the complete signal train, beginning with the transducer and terminating with the processed data. This was accomplished in three steps. First, the transducer error was determined; second, the error of the transducer plus the linear amplifier was determined; and third, the error of the total system was determined.

No attempt was made to perform a purely theoretical error analysis because a large amount of test data was available to work with. This processed data contained the actual errors which had accumulated as the data passed through the various analog and digital systems used during the full scale program. Figure 5-4 shows the typical data signal path with the type of errors introduced in the data as it changed from raw analog signals to processed data. Each block of the Figure 5-4 diagram represents a separate component function in the signal train.

In addition a rigid body error analysis was made in order to check the results obtained by a statistical and probability analysis. Rigid body mode shapes offer a unique method of determining relative errors of a large number of transducers simultaneously. Rigid body frequency is defined as that resonance at which the dynamic test vehicle is vibrating as a single mass with the suspension system acting as the effective spring and with no flexible deformation of the vehicle introduced. The rigid body frequencies on the full scale test were an order of magnitude lower than the lowest flexible body modes.

The acceleration rigid body mode shape is characterized by a straight line and the rate gyro rigid body mode slope is characterized by a constant rate throughout the vehicle. Longitudinal rigid body mode shapes should consist of vertical line displaced from the origin by an amount equal to the g-level; pitch or yaw rigid body mode shapes should consist of an inclined straight line intercepting the zero g-axis at the center of rotation of the vehicle. The error is defined as the difference between the best straight line fit between all the accelerometer readings at the rigid body frequency and the deviation from this line of an individual accelerometer. For a rate gyro, the error is defined as the difference between the calculated mode slope (from the accelerometer mode shape) and the indicated slope.

The chief advantages in using this technique to determine relative errors between transducers are that many instruments can be compared simultaneously and that the highest acceleration magnitudes, which are

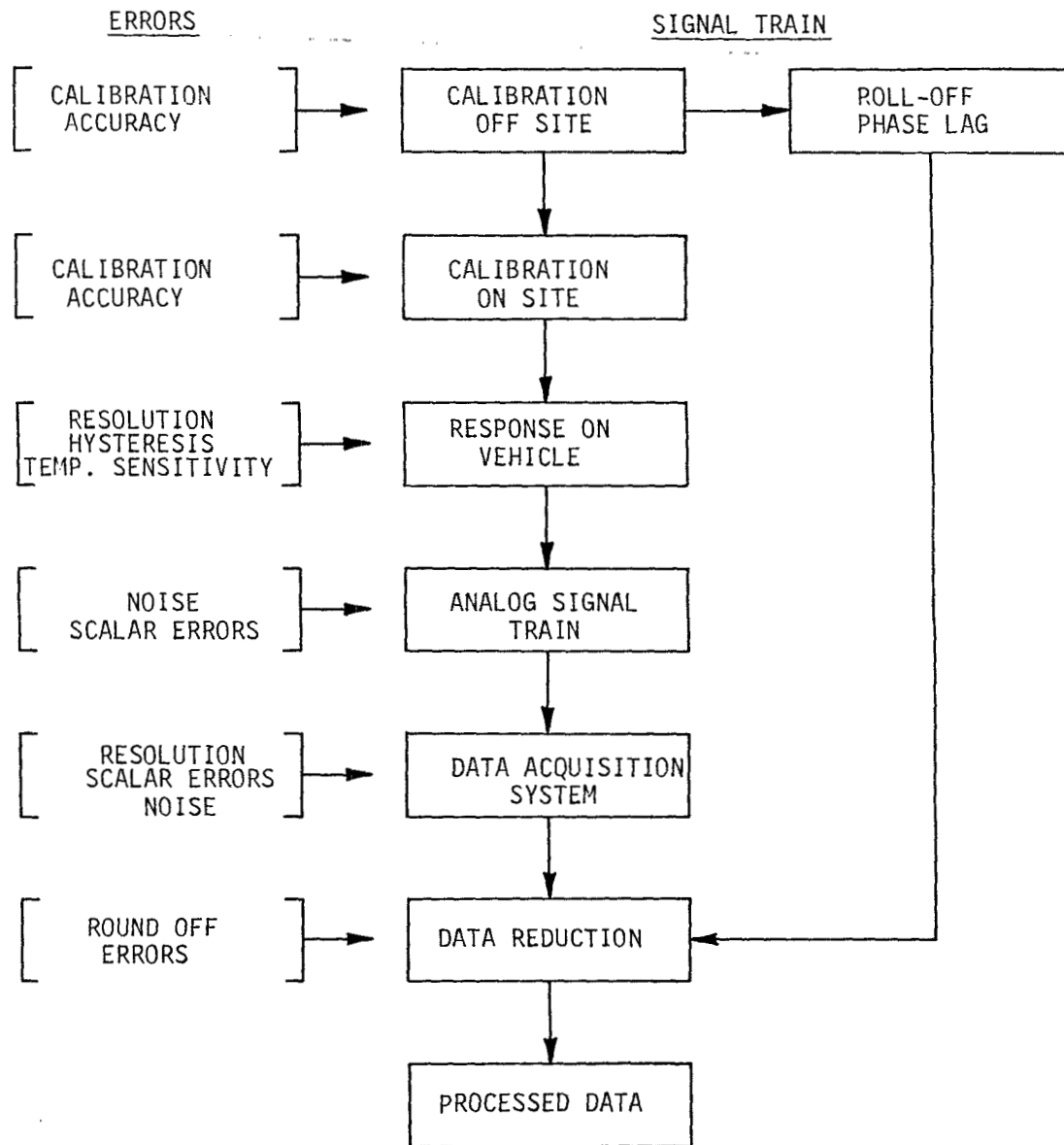


FIGURE 5-4 FULL SCALE DATA ACQUISITION AND REDUCTION SYSTEM SIGNAL TRAIN

5.1.4 (Continued)

generally the most accurate, can be used to set the rigid body mode shape line. The rigid body accelerations at the top of the vehicle are significantly higher than at other vehicle stations.

Although the rigid body error check offered a relatively quick method of determining the error band of the full scale test accelerometers and rate gyros, the maximum response amplitudes were usually only five percent of full scale. Because of the extremely low natural frequency of the suspension system, a two inch displacement produced only 0.01 g accelerations. In order to overcome these limitations, a technique was developed to compare the output of two sets of accelerometers and rate gyros located at the same station on the test vehicle. When comparing these sensor outputs two factors must be included in order to buildup an error curve:

1. Any errors in two samples, if assumed random and non-scalar, will have an equal chance of occurring simultaneously as either positive, or negative or of the same sign.
2. The standard deviation of the difference between two samples from the same population is equal to the standard deviation of that population (from statistical theory).

At least 100 data points were used at each test time point incremental frequency sweep. In all cases sensor comparisons were made at exactly the same frequency. Figure 5-5 shows the error measured by the rigid body comparison method. The dashed line represents the \pm one sigma deviations from the average error distribution represented by the solid line.

The error curves in Figure 5-5 have been extrapolated from 10 percent to 100 percent full scale by assuming that the error values are dependent only on the data acquisition system input signal level. The gain change of a factor of 10 has therefore been assumed to reproduce the same error curve between 10 and 100 percent full scale as was found between one and 10 percent full scale. This figure shows the percent error is reduced when the amplification factor is increased. The ability to change the amplification factor enabled the system to receive data one magnitude lower and maintain the same accuracy.

The effectivity of the Fourier analysis, in removing noise and harmonic distortion from the data, can be seen by the relatively low average errors contained within the test data. At signal levels of 0.1 percent full scale the analog signal to noise ratio is 1:1, whereas the average error is only \pm 22 percent. The Fourier analysis enabled the signal level to reduce to 0.01 percent full scale before the signal to noise ratio became 1:1.

5.1.5 Test Conduct

Experience with test programs prior to the full scale test pointed out the importance of having detailed test procedures written prior to actual testing. This guideline was adhered to on the full scale program and resulted

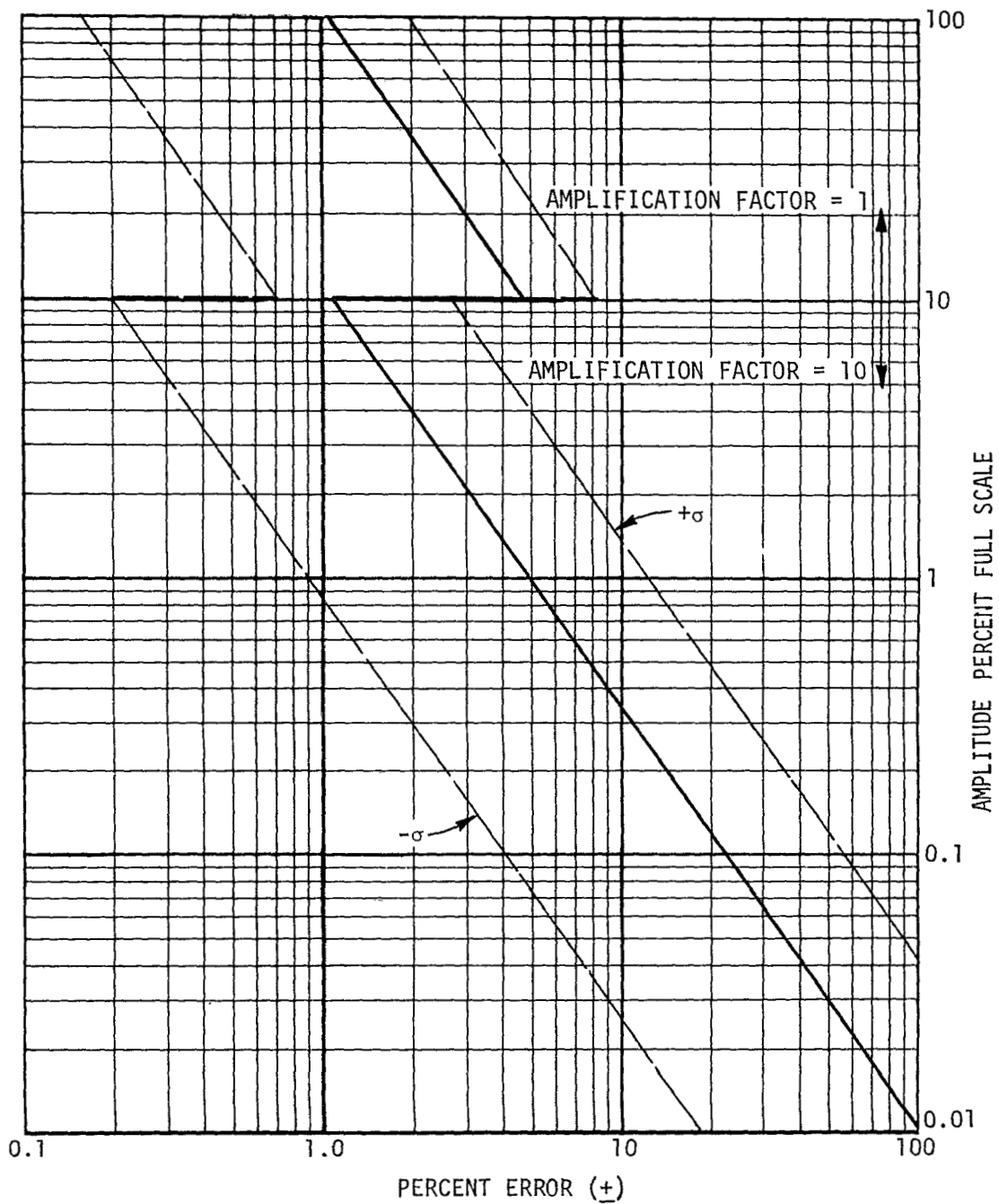


FIGURE 5-5 FULL SCALE TEST ACCELEROMETER DATA ERROR

5.1.5 (Continued)

in a minimum of test conduct problems. The test procedures delineated the vehicle and test support conditions necessary to satisfy the established test requirements. Included in the test procedures were the ballast and pressure levels, restoration system preload, shaker orientation and a detailed step-by-step operational procedure to follow in the conducting of tests. An additional factor in the successful accomplishment of the tests was the test readiness review. Immediately prior to the start of each test a meeting was held between all responsible test engineers and technicians to review the test procedures and to ascertain that all representatives were cognizant of and in agreement with any deviations from the procedures. The foregoing steps are considered essential in conducting a smooth and orderly dynamic test.

The actual test sequence began with a manual excitation test which consisted of two technicians manually shaking the vehicle at each rigid body resonant frequency. This was performed to check the phasing of the out-of-plane instruments to verify that each sensor was aligned properly and connected to a specific channel. Then a manually controlled vibration sweep was performed to gain advance knowledge of the vehicle resonances and maximum force levels that could be used during test. During the resonance search the in-phase sensors were checked for both amplitude and phasing at the rigid body resonance. Once the resonant frequencies were known, a frequency sweep program was made for the control computer which contained the minimum and maximum frequency increments to be taken throughout the test frequency range. The dynamic testing was begun with the pre-programmed control computer providing the incremental frequency sweep to the excitation system and recording the output data.

Additional tests performed included the force linearity test, ring-out damping test and ring mode test. The force linearity test consisted of exciting the vehicle at three different force levels at each resonant frequency to determine the nonlinear characteristics of the vehicle. The ring-out damping test consisted of exciting the vehicle at each of the first four flexible mode resonant frequencies and measuring the logarithmic decay of the response to determine the damping at each sensor when the force was suddenly removed. The ring mode test consisted of an incremental frequency sweep to determine IU ring mode activity.

In the beginning of the test program twenty-three (23) men per shift were required to conduct the test previously outlined. As the test program progressed fewer personnel were required due to constant review and streamlining of procedures and increased efficiency. The required manning level was reduced to fifteen (15) men per shift in the latter stages of testing.

5.2 DIGITAL DATA REDUCTION TECHNIQUES

The following paragraphs review the techniques used in the full scale digital data reduction program and place particular emphasis on the

5.2 (Continued)

methods used to curve fit the test data and compute the vehicle modal parameters. The actual data reduction problems encountered will be presented along with the necessary workarounds used. A critical evaluation of the accuracy and limitations of the techniques used on the full scale program will also be given.

A chart showing the general operations of the digital data acquisition and data reduction system is given in Figure 5-6. The data acquisition system was designed to digitize and record on magnetic tape 900 data points per second per channel for 128 channels of data. The principal operations of the digital data reduction program were to:

1. Read raw data tapes and check gain settings,
2. Perform a Fourier analysis for each channel of sinusoidal data,
3. Calculate a transfer function by dividing each instrument response by the forcing function of each incremental frequency,
4. Convert selected instrument responses to displacement units prior to curve-fitting,
5. Curve-fit the frequency response data using a modified Levy complex curve-fit routine,
6. Reduce the equations obtained from the Levy routine by a partial fractions scheme to represent each modal resonant peak as a single degree of freedom system for computation of modal parameters,
7. Plot frequency response transfer functions, curve-fit transfer functions, mode shapes, and mode slopes.

The automated data reduction techniques used on the full scale test proved highly successful in:

1. Obtaining modal parameters from test data.
2. Providing analytical expressions for test results that could be compared directly with mathematical predictions.
3. Eliminating noise and harmonic distortion from the excitation and response signals.
4. Providing rapid display and evaluation of large volumes of data and rapid distribution to user organizations.

Similar procedures are highly recommended for future programs.

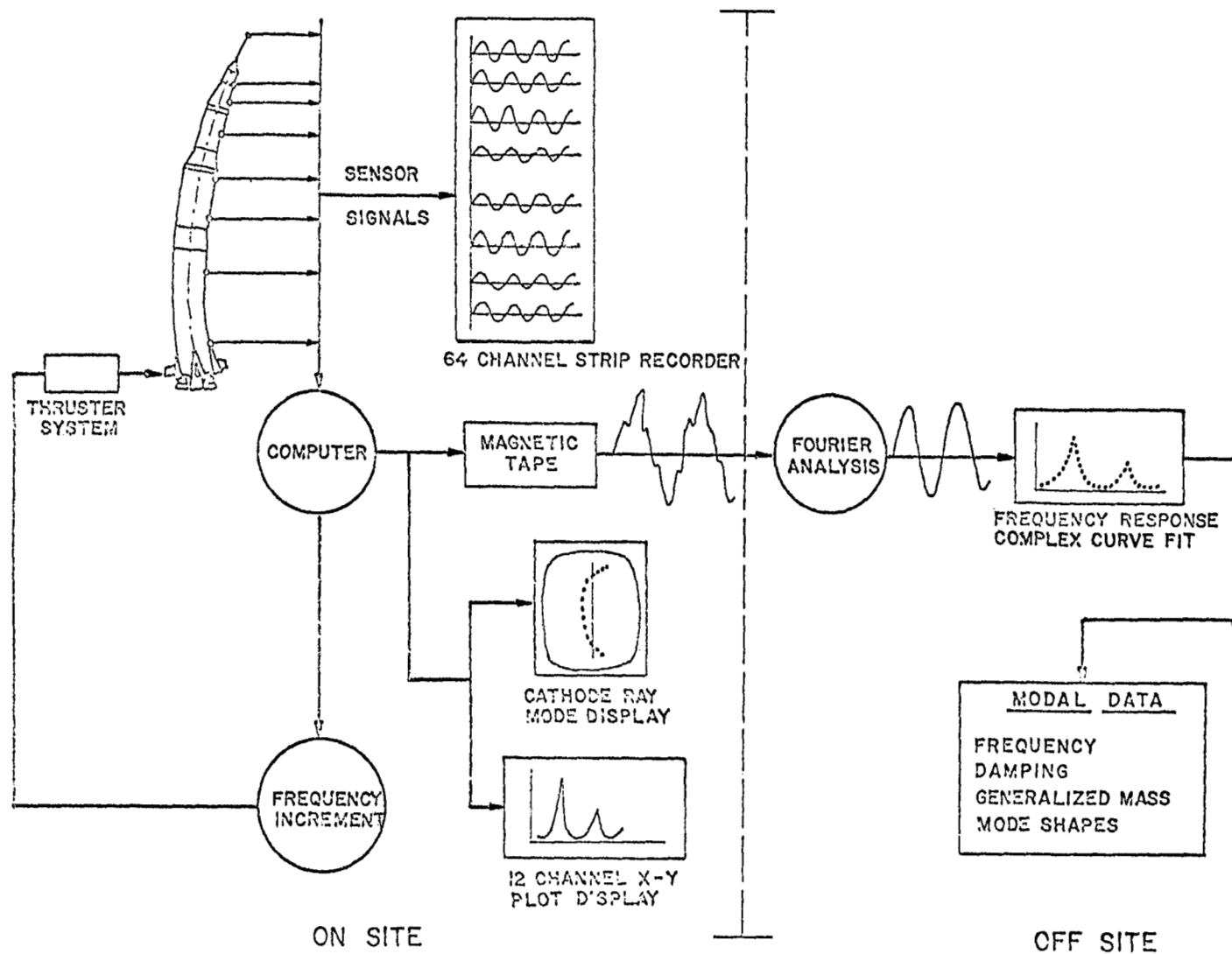


FIGURE 5-6 FULL SCALE TEST DATA REDUCTION FLOW CHART

5.2.1 Fourier Analysis

For sinusoidal dwell excitation, the response measured by each instrument is the sum of a periodic function plus noise. This type of data is conveniently reduced by Fourier analysis. Three significant advantages are realized from a Fourier analysis:

1. It is an effective narrow band filter to remove the effects of thruster wave distortion,
2. It permits analysis of the harmonic content of the output wave,
3. It represents each cycle of data by only two numbers, thereby simplifying calibration corrections.

Using the correct procedure for determining the sampling rate will result in accuracy and more efficient computation. This was a basic deficiency in the full scale test data reduction system. The data acquisition system was limited to a fixed rate of 900 data points per second. This would provide only 20 samples per cycle for 45 Hz ring modes, but would provide many more samples per cycle than necessary for the basic vehicle modes, which were in the 1-10 Hz range. This caused extra expense for the low frequency Fourier analysis program since each cycle of data had to be analyzed in segments. Also, the full scale test constant sampling rate never produced cycles of data that started and ended on data points, thus requiring that linear interpolation be employed to yield exactly one cycle of data.

To circumvent these problems, it is recommended that the sampling rate be made an exact multiple of the excitation frequency. The multiplier would be the number of data points per cycle required to attain the desired accuracy. By always dividing each cycle into exactly N equal parts the sine and cosine sample functions are numerically orthogonal. This orthogonality reduces the least squares solution for the Fourier coefficients to the following simple form:

$$\begin{Bmatrix} a_0 \\ a_1 \\ b_1 \end{Bmatrix} = \begin{bmatrix} \frac{1}{N+1} & \frac{1}{N+1} & \frac{1}{N+1} & \dots & \frac{1}{N+1} \\ 1 & \cos \frac{2\pi}{N} & \cos \frac{4\pi}{N} & \dots & 1 \\ 0 & \sin \frac{2\pi}{N} & \sin \frac{4\pi}{N} & \dots & 0 \end{bmatrix} \begin{Bmatrix} y_0 \\ y_1 \\ \vdots \\ y_n \end{Bmatrix} \quad (5.1)$$

where

a_0 = constant term
 a_1 = coefficient of fundamental cosine term
 b_1 = coefficient of fundamental sine term
 $N+1$ = number of samples per cycle of data
 y_0, y_1, \dots, y_n = sampled response function

5.2.1 (Continued)

This method is readily extendable to include higher harmonics. Calculations of this type can be performed rapidly on a digital computer. The method conserves both tape storage and computer time.

If the sampling rate is frequency dependent, the sine and cosine Fourier coefficients for each cycle of data are automatically orthogonal and the orthogonality is not affected by the use of a numerical integration routine. Thus, a significant computational advantage is achieved by eliminating cycle interpolation and by reducing the sampling rate.

The fixed sampling rate of 900 samples per second used on the full scale program made calculation of higher harmonics unacceptably expensive. Studies made using DTV data show that twelve samples per cycle would have been sufficient to analyze the data accurately through the third harmonic.

5.2.2 Point Transfer Functions

The next step in data reduction is to determine the amplitude and phase of each sensor on the test article relative to the input force. Before this can be done, however, each channel of data must have certain corrections incorporated and have the voltages converted to engineering units. The corrections include curves of phase lag and rolloff characteristics for each instrument and similar data for the data acquisition system. Full scale test data reduction equations were obtained for each correction curve through the use of a curve fit routine and then these curves were applied to each channel of data after completion of the Fourier analysis.

The transfer function for each data channel is the ratio (acceleration per unit force) of the corrected response divided by the forcing function. The transfer function and the corresponding phase angle of each instrument relative to that of the forcing function was computed throughout the test frequency range.

5.2.3 Transfer Function Equations

The structural response of a system is the sum of the responses in several modes. Separation of the test data into modal components is recognized to require special techniques; some of these techniques are cited in References 5-3 and 5-4. The solution chosen for separation of full scale test data into modal components was a modification (Reference 5-5) to a complex curve fitting method developed by E. C. Levy in Reference 5-6. The complex curve fit technique used is explained in detail in Reference 5-7.

5.2.3 (Continued)

The technique expresses the measured response per unit force as a ratio of two frequency-dependent complex polynomials.

$$G(j\omega)_k^* = \frac{a_0 + (j\omega)a_1 + (j\omega)^2 a_2 + \dots + (j\omega)^{2n-2} a_{2n-2}}{b_0 + (j\omega)b_1 + (j\omega)^2 b_2 + \dots + (j\omega)^{2n} b_{2n}} \quad (5.2)$$

where $G(j\omega)_k^*$ = Curve fit transfer function

k = The k^{th} sensor transfer function

ω = Excitation frequency

$a_0, a_1, \dots, b_0, b_1, \dots$ are constants to be determined

n = Number of modes being curve fit

The error at each discrete excitation frequency is the difference between the absolute magnitudes of the actual transfer function and the polynomial ratio.

$$e(j\omega)_k = G(j\omega)_k - G(j\omega)_k^* \quad (5.3)$$

where $G(j\omega)_k$ = transfer function measured during test

$e(j\omega)_k$ = error

The polynomial coefficients are evaluated as the result of minimizing the sum of the squares of the above error at the experimental points. The least squares solution is carried out by an iterative procedure.

To isolate the modal parameters the partial fractions expansion of the transfer function Equation (5.2) is carried out by well known techniques. The resulting expression is:

$$G(j\omega)_k^* = \sum_{u=1}^n \frac{A_u [1 + j\omega B_u]}{(j\omega)^2 + j\omega C_u + D_u} \quad (5.4)$$

where u = an index

n = the total number of modes in the transfer function

k = the k^{th} transfer function

$A_u, B_u, C_u, \& D_u$ are constants determined from partial fractions expansion.

5.2.3 (Continued)

The procedure for evaluating these parameters is explained in detail in Reference 5.7.

An example of the curve fit achieved on full scale test data is shown in Figure 5-7. The solid line represents results of the curve fitting routine for both the amplitude and phase plots. The dashed line shows the weak mode that was not obtained by the curve fit routine. The points plotted are the test transfer function data which were always plotted with the curve fit results to evaluate the accuracy of the curve fit.

The quality of the curve-fit was found to be dependent on the following:

1. Relative peak amplitudes
2. The units of the data
3. The distribution of the data points
4. The frequency range
5. Closeness of the modal resonant frequencies

The preceding factors affected the resulting curve-fit to such an extent that the curve fit for a transfer function could not be obtained in a single computer run. Instead, it was required that an engineer evaluate the transfer function data considering the above parameters and submit the routine for fitting. Then the resulting curve fit was evaluated and changes were made in the parameters to improve the fit. The computer time associated with curve fitting decreases with experience. This is particularly true when, as in full scale testing, several tests are to be run which produce data having similar characteristics. The addition of an engineering graphics computational system for evaluation of the curve fit while the data is in the computer would greatly shorten both flow and computational time required for curve fitting.

The relative peak amplitudes for each peak curve fitted within a selected frequency range should be fairly consistent since the nature of a the curve fit routine gives more accuracy to the larger peaks in the data, while some smaller peaks may not be fit. This is evident in Figure 5-7. The peak amplitudes obtained for the suspension system modes in full scale testing were much larger than amplitudes obtained in the flexible modes. To obtain satisfactory solutions for flexible body resonances, it was necessary to eliminate the low frequency range containing the suspension modes. As a rule of thumb, modes whose peak amplitudes are at least one fifth of the amplitude of the strongest mode in the array should be curve fit accurately. Most of the modes of interest occur in the low frequency range (above the frequency range of the suspension modes). Displacement units emphasize the low frequency peaks, thus improving the accuracy with which these peaks are curve fit.

The accuracy of the curve fit is affected significantly by the distribution of the data points over each resonant peak. Smaller frequency increments should be used around the resonances. Full scale test experience

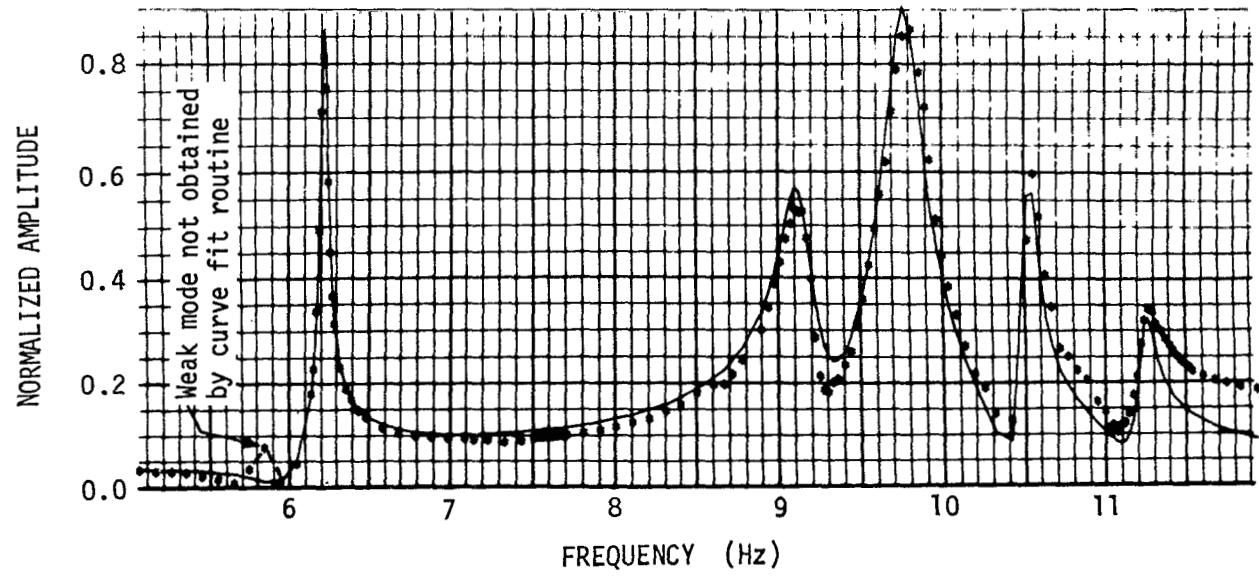
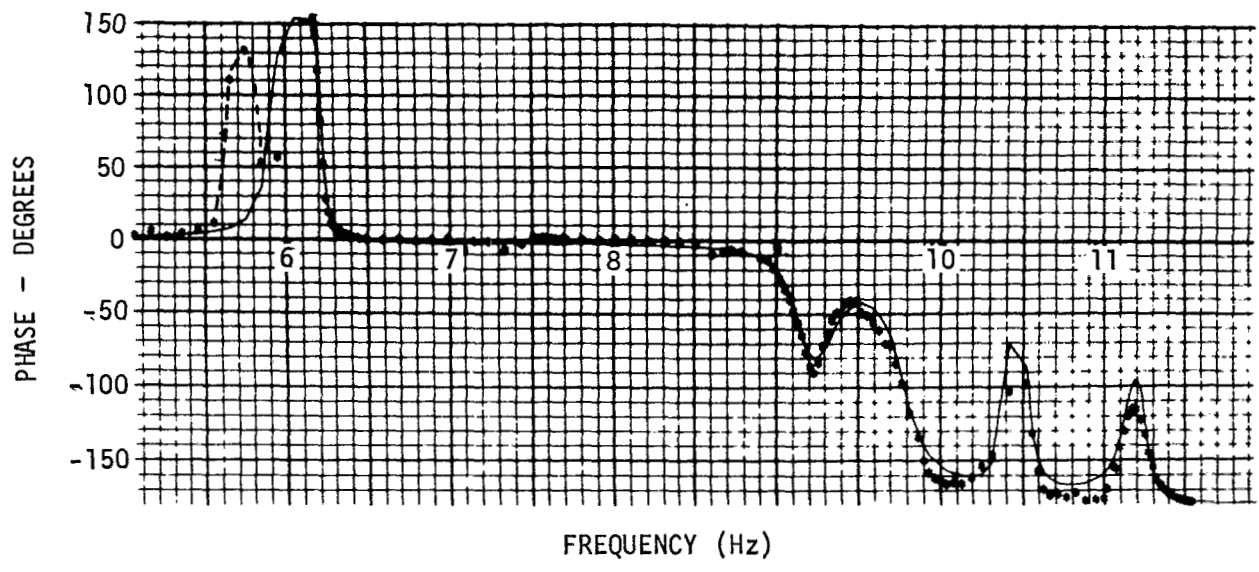


FIGURE 5-7 TYPICAL CURVE FIT OF FULL SCALE TEST DATA

5.2.3 (Continued)

has shown that 8-10 frequency increments are sufficient to define a resonance above its half amplitude point; the accuracy of the curve fit will not be greatly increased by adding more points.

Limiting the frequency range also increases the accuracy. This is because the equations that have to be solved to obtain the curve fit contain powers of the frequency. The highest power is equal to the number of terms retained in the denominator of Equation (5.2). As the frequency range is extended, the magnitude spread between terms in the coefficient matrix rapidly diverges for two reasons. First, increasing the frequency range increases the number of modes included and requires higher order terms in the least squares solution. Second, ω itself gets bigger. Experience has shown that the order of the polynomial can be as high as 12 (6 resonances) and cover a frequency range of $20\omega_0$, where ω_0 is the lowest sample frequency, provided double precision is used. If more modes, or a larger frequency range must be covered, the curve fit can be carried out in segments.

Two modes of nearly identical frequency are difficult to curve fit. For example, double resonant peaks occurred in some pitch and yaw data. These nearly identical resonances were produced by the small pitch and yaw asymmetries in the test article. An example of a double peak obtained during the test is shown in Figure 5-8. In this case the peaks are nearly equal in amplitude. Usually one of the peaks was larger than the other. These peaks were fitted as one mode (Figure 5-8 shows a typical fit) because of the small frequency difference in the modes. Although the curve fit did not separate the two modes, the single mode approximation did represent the composite response characteristics of the two modes accurately. Modal resonances closer than one percent in frequency could not be separated successfully. However, modes as close as two percent in frequency could be separated accurately if they were of nearly equal strength.

5.2.4 Computation of Modal Parameters

The partial fraction expansion form of the transfer function equation (Paragraph 5.2.3) is recognized to have the general form of the equation for the transfer function of a linear viscously damped system, which is represented by:

$$G(j\omega)_k = \sum_{u=1}^n \frac{(\phi_{1u} \phi_{ku})/\bar{m}_u}{(j\omega)^2 + 2(j\omega) \zeta_u \omega_u + \omega_u^2} \quad (5.5)$$

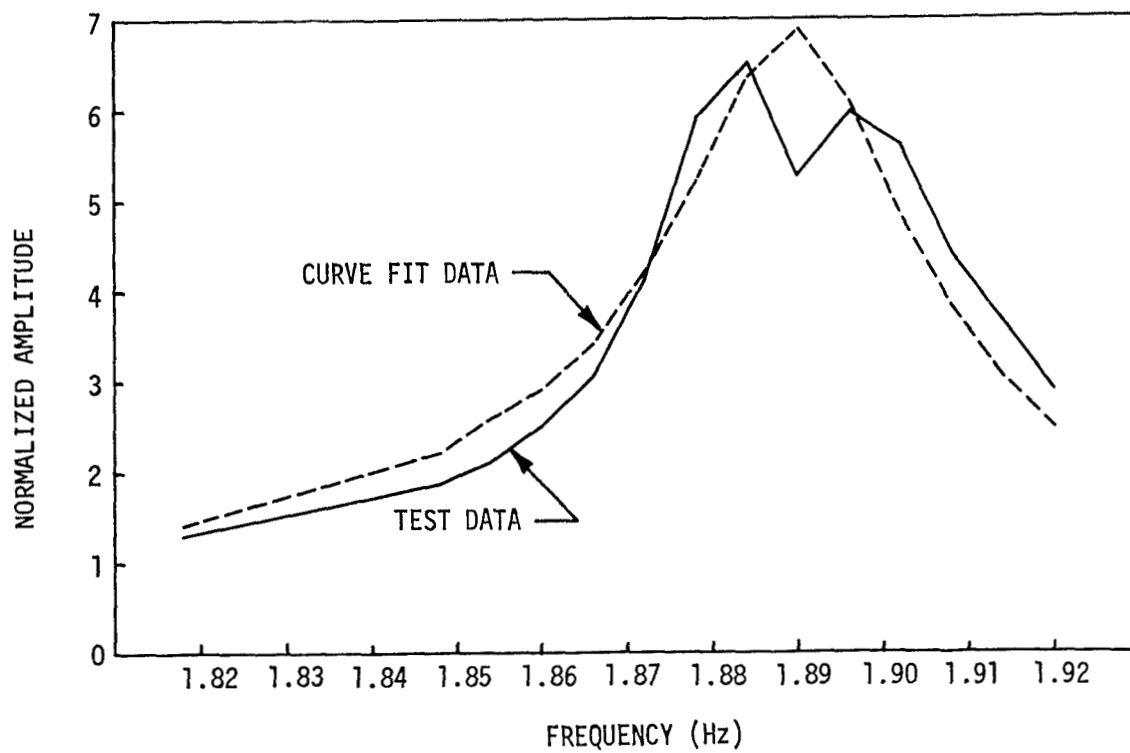


FIGURE 5-8 TYPICAL CURVE FIT OF DOUBLE PEAK RESONANCE

5.2.4 (Continued)

where

- ϕ_{1u} = Normalized modal displacement at the forcing points
- ϕ_{ku} = Normalized modal displacement at the k^{th} sensor station
- \bar{m}_u = Generalized mass for the u^{th} mode
- ω_u = Frequency of the u^{th} mode
- $G(j\omega)_k$ = Transfer function (displacement per unit force)
- ζ = Modal damping factor

This equation was used for full scale test data to compute for each mode (u) and mode shape sensor transfer function (k), the modal frequency and damping, the gain of the mode, and the generalized mass. The workable techniques developed to extract these data from test results are discussed in the following paragraphs. A more detailed description of these techniques is given in Reference 5-7. Experience indicates that a close evaluation of the partial fractions is required to assure that they represent the actual data to an acceptable degree of accuracy before proceeding into the computation of modal parameters.

A. Modal frequency

The modal frequency was calculated for each mode (u) of each sensor transfer function (k). It was determined by extracting the square root of $(\omega_u)^2$ from Equation (5.5). The natural frequency values derived from the various sensors was amazingly consistent. The values seldom deviated by as much as 1/2 percent between sensors showing well defined response.

For modes too weak to curve fit, the frequency at which the imaginary component of response peaked was taken as the modal resonant frequency.

B. Modal damping

The modal damping was determined from the transfer function equation by equating like terms in Equations (5.4) and (5.5).

$$\zeta_u = \frac{C_u}{2\omega_u} \quad (5.6)$$

5.2.4 (Continued)

The degree of linearity of the test article is of prime importance in accurately defining the system damping. Generally in full scale test data, it was observed that the response per pound did not remain constant but tended to decrease with an increase in force. This nonlinear response is illustrated in Figure 5-9. This figure presents the frequency response data of the LES for three different force levels. This non-linearity made it essential to excite the test article to levels expected during flight. Linearized damping estimates obtained from the sensors seldom differed by more than five percent. This established a high confidence that the damping values were valid.

C. Mode shape determination

Originally, it was intended to obtain mode shapes by normalizing like mode components from the curve fit routine. A computer subroutine was written to calculate the single mode amplitudes of selected sensors at the modal frequencies. This subroutine used the partial fractions (one for each mode). Some of the problems encountered here were:

1. Some of the mode shape sensors would not have a peak of sufficient amplitude to curve-fit.
2. In the case of a double peak it was difficult to display a mode shape because the curve-fit equations gave one peak for some sensors and two peaks for other sensors. This distorted the mode shapes in sections of the vehicle.

Generally the amplitude subroutine was of insufficient accuracy to present a good plot of the mode shape, and another run was required to eliminate the erroneous values after evaluation by the engineer. For this reason the point transfer function data of the mode shape instruments were used to hand plot the mode shape. It was found that the normalized accelerometer readings produced mode shapes of acceptable accuracy, although the phase angle was difficult to interpret for sensors showing small response. Usually the sign was determined by establishing a band of phase such as 0 degrees to 180 degrees as positive and 0 degrees to -180 degrees as negative.

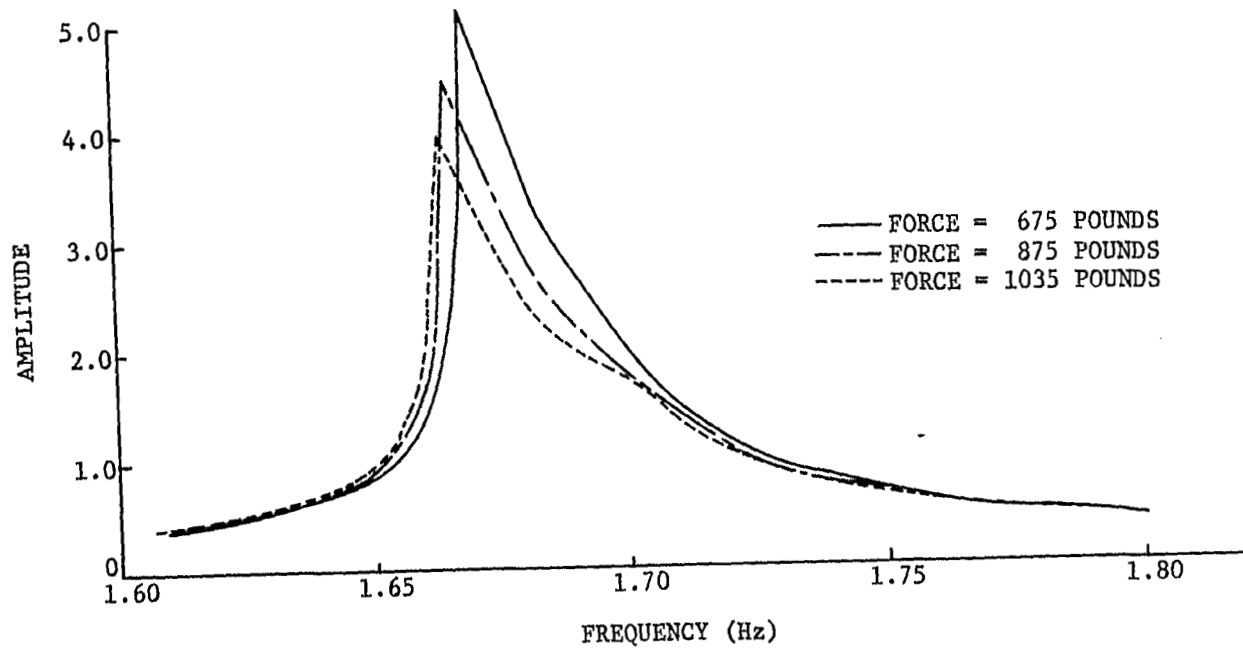


FIGURE 5-9 TYPICAL EFFECT OF FORCE LEVEL ON FREQUENCY RESPONSE

5.2.4 (Continued)

D. Mode slope determination

The mode slope is defined as the rate of change of the mode shape with vehicle length. Two methods were used to determine the mode slopes for the full scale test. The first was direct measurement by rate gyros. The other method of determining the mode slope involved using a polynomial to curve fit the mode shape data (Reference 5-7). The mode slope was obtained by differentiating this polynomial solution. This technique has the advantage of determining the slope of any specific station along the vehicle. In using this technique, considerable error may occur if the slope changes appreciably from interval to interval or if the intervals are too large. These limitations must be recognized in spacing the accelerometers along the vehicle.

E. Generalized mass

The generalized mass values were also obtained from curve fit results. In practice the coefficient B_u of the first order term in the numerator proved to be negligible. Consequently, B_u was set to zero so that a direct comparison of theoretical and test results could be made.

$$A_u = \frac{\phi_{1u} \phi_{ku}}{\bar{m}_u} \quad (5.7)$$

Rearranging, the expression for generalized mass is:

$$\bar{m}_u = \frac{\phi_{1u} \phi_{ku}}{A_u} \quad (5.8)$$

Generalized mass values obtained from the sensors that could be curve fitted accurately, normally agreed within 10 percent.

5.3 TEST DATA EVALUATION PROCEDURES

5.3.1 On-Site Data Evaluation

A qualified structural dynamicist was on-site at all times to evaluate data as it was taken. This is an essential requirement. During each test sweep, the raw data as provided from the "quick-look" system was compared with the pretest analysis to ensure that all the predicted

5.3.1 (Continued)

modes had been excited and that sufficient data had been recorded to analyze the structure completely at the test time point. The output signal of each transducer was examined at the rigid body resonant frequency to ensure that the sensors were phased properly and that the signal level was in agreement with the vehicle response. All sensors were monitored for noise content and wave shape distortion by use of an analog chart recorder. Oscilloscopes were used to determine if transducer output was becoming erratic or faulty.

In addition to monitoring the individual sensor output signals, the overall vehicle response as portrayed by the mode display, and 12 channels of transfer plots were closely watched in order to insure that the test data was realistic and that no anomalies were present.

If data correlation was good between the pretest analysis and raw test data, the vehicle was then made ready for the next time point and the thrusters repositioned for excitation in a different axis. If data correlation was not good, then an overall check was performed on those instruments which deviated to the greatest extent from the predicted response. Furthermore, a manually controlled frequency sweep was made for excessively weak modes until the structural dynamicists were satisfied that the pretest analysis was in error. If the on-site evaluation indicated no problems, it was considered that there was an 80 percent confidence level in the data validation. The value of a rigorous pretest analysis to on-site evaluation cannot be overemphasized.

5.3.2 Test Data Validation

While the test data were being processed, the analog recordings were being annotated. The processing of the 128 channels of digital data usually took about eight hours. After the printouts and plots were received, the modal frequencies were approximately determined from the plots and then accurately determined from the printout. Data from the mode shape sensors were recorded and normalized to the same stations used in the pre-test analysis. The comparison of test and analytical mode shapes and frequencies was the first step in data validation. The second step in validation was extracting data for all flight sensors. This data was compared at the rigid body frequency to insure that all amplitudes were within instrumentation tolerances. Slopes of flight gyros at flexible frequencies were also compared with the mode shapes and with the non-flight backup instrumentation.

The rest of the instrumentation was then checked by scanning the transfer function plots to determine if any unexplainable activity was evident. Where sensor output was questioned, a comparison was made with the analog recorder data and the transfer function plots.

5.3.2 (Continued)

This validation effort normally took four engineers about six hours. When sufficient data were acquired to allow a satisfactory definition of the dynamic characteristics of the vehicle, a phone call was made to test site indicating a "go" decision on validation, and testing proceeded to the next time point.

5.3.3 Test Data Evaluation

The validated data were then evaluated more carefully by experienced structural dynamicists before the data were considered acceptable for release in the test report. This evaluation consisted of a detailed examination of each sensor output to determine whether it was consistent with other sensors and represented a condition that was physically possible. Component characteristics and out-of-plane motion were examined in the evaluation. Results of this evaluation are contained in the discussion section of all test reports. A common mistake which should be avoided is the recording of such a volume of data that complete evaluation is impractical.

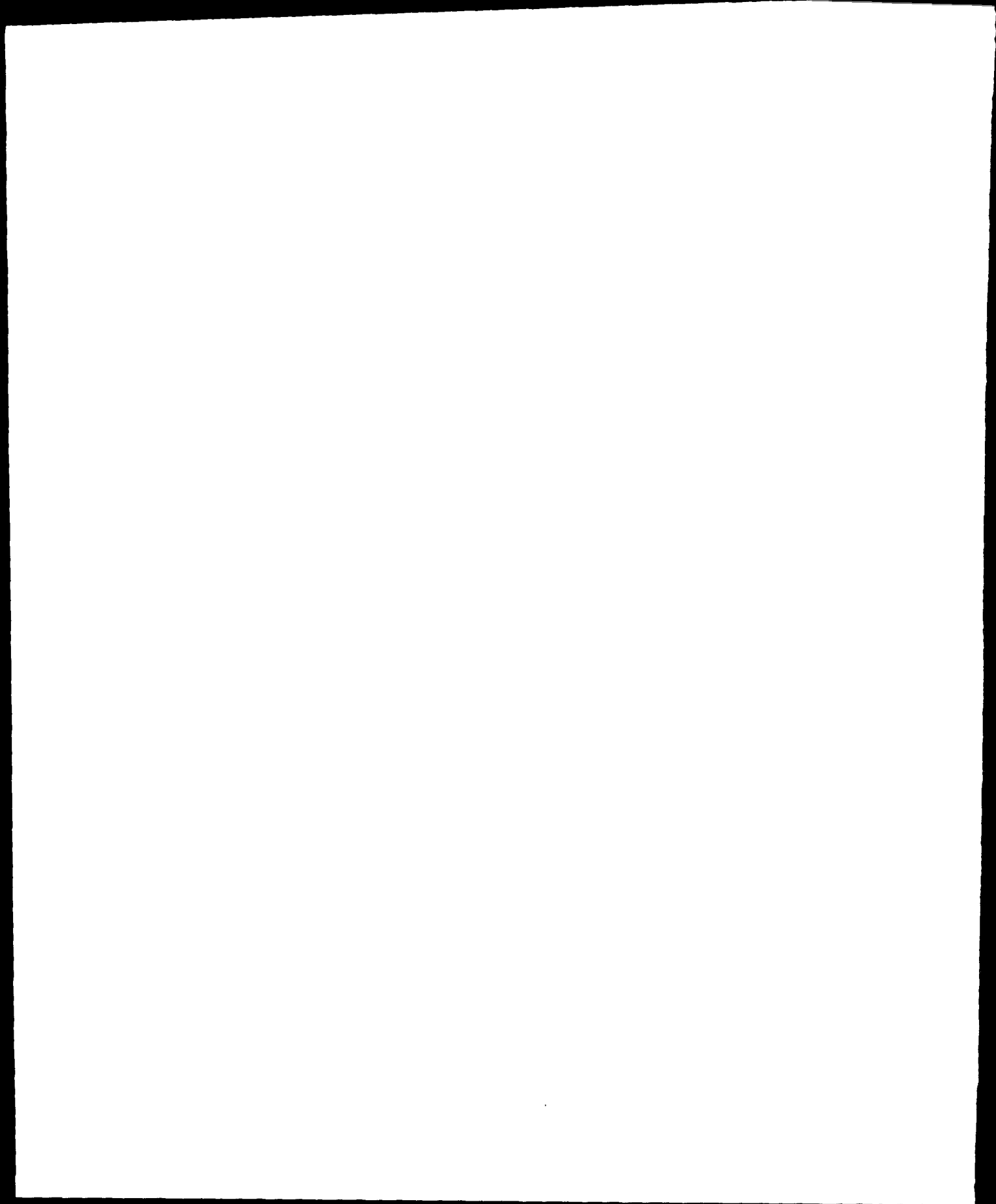
5.3.4 Test Data Reporting

The data reporting for the full scale test program consisted of two reports: Flash Report and Test Data Report. A Flash Report was submitted for each time point tested and contained the reduced data obtained from the "quick-look" analysis. These data included modal frequencies, mode shapes, excitation forces, modal damping values, transfer functions, and flight gyro response. These reports were released within two days after the conclusion of each test.

A Test Data Report was submitted after the completion of each configuration tested. Each report contained a description of the test objectives, configuration, support equipment, data acquisition system, instrumentation, data reduction techniques, pretest analysis and models, and data evaluation. The report also contained transfer functions, mode shapes, frequencies, and damping values.

SECTION 5 - REFERENCES

- 5-1 Document D5-11093, Saturn V Dynamic Test Program Requirements, The Boeing Company, Huntsville, Alabama, October 26, 1967.
- 5-2 Von Pragenau, G., A Hydraulic Support for Free-Flight Simulation with the Saturn V Apollo Vehicle, AIAA/JACC Guidance and Control Conference, Seattle, August, 1966.
- 5-3 Woodcock, D., On the Interpretation of the Vector Plots of Forced Vibrations of a Linear System with Viscous Damping, The Aeronautical Quarterly, February, 1963.
- 5-4 Kennedy, C. and Pancu, C., Use of Vectors in Vibration Measurement and Analysis, Journal of the Aeronautical Sciences, Vol. 14, p. 603, 1947.
- 5-5 Sanathanan, C. and Koerner, J., Transfer Function Synthesis as A Ratio of Two Complex Polynomials, IEEE Transactions on Automatic Control, January, 1963.
- 5-6 Levy, E., Complex Curve Fittings, IRE, Professional Group Transactions on Automatic Control, Vol. AC-4, May, 1959.
- 5-7 Document D5-15210C, Saturn V Dynamic Test Vehicle Data Reduction Techniques, The Boeing Company, Huntsville, Alabama, October 26, 1967.



SECTION 6 CONCLUSIONS

This document has presented practical guidelines for accomplishing structural dynamic analysis, dynamic test, and data reduction that were established during the successful Apollo Saturn V programs. These guidelines and recommended practices were presented so major pitfalls and problems encountered during this program could be avoided in future programs. The material presented in this document is oriented towards the technical managers of future structural dynamic programs.

The following points are emphasized based on the experience gained during the Saturn V programs:

1. Replica models can be an effective tool to pilot structural dynamic programs of future space vehicles,
2. Math models can be used to predict the overall vehicle dynamic characteristics accurately, provided the guidelines presented in this document are followed,
3. Local deformations and major component dynamics can be predicted with limited confidence; static or dynamic testing of major assemblies or stages is required to guide math model development,
4. Automated data acquisition and reduction systems should be used on all major dynamic test programs.
5. A single technical test plan should be developed for each space program. Consistent data acquisition, data reduction, and data library procedures should be used for all major dynamic tests within a program.